REPOR

1. AGENCY USE ONLY (Lea	7-22-93	IRT TYPE AND DATES COVERED Final Report

4. TITLE AND SUBTITLE

Optical Studies of glasses embedded with inorganic ions and organic dyes

5. FUNDING NUMBERS

Project-task 3484/RS

6. AUTHOR(S)

B.R. Reddy

7. PERFORMING ORGANIZATION NAME(S) AND ADDRESS(ES)

Alabama A&M University
PO Box 254
Normal, AL 35762-0254

8. PERFORMING ORGANIZATION REPORT NUMBER

9. SPONSORING/MONITORING AGENCY NAME(S) AND ADDRESS(ES)

AFOSR/NC
Building 410, Bolling AFB DC
20332-6448

10. SPONSORING/MONITORING AGENCY REPORT NUMBER

AFOSR-90-0160

11. SUPPLEMENTARY NOTES

Final Report covering the period February 15, 1990- May 31, 1993

12a. DISTRIBUTION/AVAILABILITY STATEMENT

APPROVED FOR PUBLIC RELEASE; DISTRIBUTION IS UNLIMITED.

12b. DISTRIBUTION CODE

13. ABSTRACT *(Maximum 200 words)*

Abstract is on the reverse

14. SUBJECT TERMS

Energy Upconversion Studies, Nonlinear Optics, OPtical Phase Conjugate Studies, Optical studies of glasses doped with inorganic ions and organic dyes.

15. NUMBER OF PAGES 100

16. PRICE CODE

17. SECURITY CLASSIFICATION OF REPORT	18. SECURITY CLASSIFICATION OF THIS PAGE	19. SECURITY CLASSIFICATION OF ABSTRACT	20. LIMITATION OF ABSTRACT
UNCLASSIFIED	UNCLASSIFIED	UNCLASSIFIED	unlimited(sar)

DISCLAIMER NOTICE

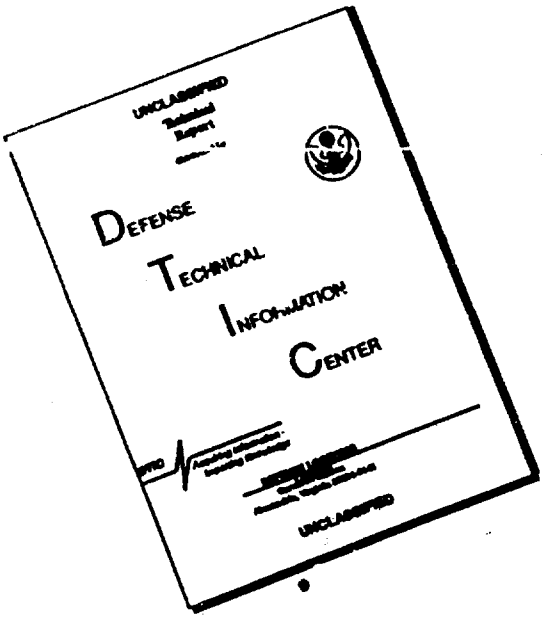

THIS DOCUMENT IS BEST QUALITY AVAILABLE. THE COPY FURNISHED TO DTIC CONTAINED A SIGNIFICANT NUMBER OF PAGES WHICH DO NOT REPRODUCE LEGIBLY.

Abstract

13 We performed optical studies of organic dye doped glasses and rare earth ion doped glasses. We doped several organic dyes in boric acid, sucrose and polycarbonate hosts and detected phase conjugate signals from all these samples. Sucrose samples are hygroscopic and hence are useful for characterizing dyes only. Boric acid samples were damaged even at moderate laser powers. On the other hand polycarbonate samples could withstand high input powers and hence will be useful in device applications. Styryl 7 doped boric acid sample exhibited several interesting nonlinear optical phenomena and was also found to be useful for long-term/permanent information storage due to photochemical effects undergone by the excited molecules. PC signals in Pyridine 1 dye doped samples exhibited oscillations (period ~hour) which was found to be due to thermal effects/large Stokes shift in the emission. DCM and R110 doped boric acid samples are found to be chemically stable even after three years. We measured third order susceptibilities of DCF, DCM, R110, AY and R6G doped samples. We experimentally demonstrated that excited state absorption alters the transmission/saturation characteristics of the dyes in condensed media. These results have been published in three journal papers.

We made different glasses like Sulfates, borates, silicates, borosilicates and multicomponent oxide glasses doped with rare earth ions. Sulfate glasses were hygroscopic, binary and ternary borate glasses tried by us were found to be brittle and silicate glasses required very high temperatures. We investigated borosilicates and multicomponent oxide glasses doped with Nd^{3+} and Er^{3+} ions. In borosilicate host, we detected very weak violet emission from the L levels of Nd^{3+} in the region 380-460 nm at liquid nitrogen temperature, when its E levels were resonantly excited with 514.5 nm. In Er^{3+} doped borosilicate we detected very weak green emission from the E levels, at room temperature, when its B levels were resonantly excited with ~797 nm. However in a multicomponent oxide glass doped with Er^{3+} we detected intense green emission at room temperature from the E levels of Er^{3+} when its B levels were excited with a near infrared laser beam. When the D state (or phonon coupled levels of B state) of Ho^{3+} in LaF_3 were resonantly excited with 636 nm (or 800 nm) we detected green and blue upconverted emission from the $F(^5S_2)$ and $F(^5F_3)$ levels at 546 and 485 nm and at 416 nm from the $J(^5G_5)$ levels. When the LaF_3:Pr^{3+} was irradiated with 805 nm we detected very strong green emission at 540 nm and broad emission at 491 and 521 nm. When either the D or S levels of Nd^{3+} were resonantly excited with a 580 nm or 800 nm, we detected upconverted violet emission from the L levels in CaF_2, SrF_2, BaF_2 and LaF_3. Some of the results are in the process of communication and work is in progress on some systems. We are expecting at least four journal pares from our work on rare earth materials.

OPTICAL STUDIES OF GLASSES EMBEDDED WITH INORGANIC IONS AND ORGANIC DYES

Final Report

Grant Number: AFOSR-90-0160

B.R. REDDY
Department of Physics, P.O. Box 1268
Alabama A&M University
Normal, AL 35762

Funding Agency
AIR FORCE OFFICE OF SCIENTIFIC RESEARCH
DIRECTORATE OF CHEMISTRY AND MATERIALS SCIENCE
BOLLING AIR FORCE BASE, DC 20332-6448
Attn: Thomas E. Erstfeld, Major, USAF
Program Manager

Table of Contents **page #**

1. Personnel 1

2. Objective 2

3. Abstract 2

4. Introduction to rare earth spectra 3

5. Preparation of Inorganic glasses 5

(a) Sodium borosilicate glass preparation 5

(b) Preparation of a Multicomponent Oxide glass 5

(c) Preparation of a borate glass 6

(d) Preparation of a Sulfate glass 6

6. Glass polishing technique 6

7. Summary of glasses 7

8. Energy upconversion studies in rare earth ion doped oxide glasses 8

9. Energy upconversion in $LaF_3:Ho^{3+}$ 9

10. Energy upconversion in $LaF_3:Pr^{3+}$ 9

11. Energy upconversion in $MF_2:Nd^{3+}$ (M=La, Ca, Sr, Ba) 9

12. Third order nonlinearity of Organic dyes 9

13. Organic dye doped systems 10

14. Preparation of boric acid glass doped with dyes 11

15. Preparation of Sucrose samples doped with dyes 11

16. Preparation of Polycarbonate doped with dyes 12

17. Excited state absorption studies 12

18. Estimation of third order susceptibilities, $\chi^{(3)}$ 14

19. Optical Phase-conjugate Studies (Degenerate four-wave mixing) 14

20. Research personnel 15

21. Students participation 15

22. Major Equipment purchased 15

23. Miscellaneous supplies 16

24. Summary and Conclusions 17

25. References 18

25. Appendix: Reprints 19

(1) Reprint of "Laser induced gratings in a Styryl dye". 20

(2) Reprint of "Optical Phase Conjugate Studies of Organic Dyes doped in a boric acid host". 25

(3) Preprint of "Optical Phase conjugation in a polycarbonate resin doped with Coumarin 314 dye". 33

(4) Manuscript of "Infrared to visible upconversion in Er^{3+} doped Oxide glass". 36

(5) Abstract of "Energy Upconversion in LaF_3:Ho^{3+}". 46

(6) Abstract of "Energy upconversion in neodymium doped sodium borosilicate glass". 47

(7) Abstract from the M.S. thesis (1991) of Mr. Anthony Ololo. 48

(8) Manuscript of "Excited state absorption cross section measurement in rhodamine 6G tetrafluoroborate". 51

(9) Manuscript of "Spectroscopic studies of Sodium borosilicate glasses doped with Pr^{3+}, Nd^{3+} and Er^{3+} ions". 64

(10) Manuscript of "Near infrared to blue energy upconversion in LaF_3:Ho^{3+}". 84

(11) Reprint of "Optogalvanic effect in neon hollow cathode discharge." 92

1. Scientific Personnel

Principal Investigators: B.R. Reddy
P. Venkateswarlu
M.C. George**

Students: Anthony Ololo (M.S.)
Andre Ellison (B.S.)
Paul Williams* (B.S.)
Shelia-Nash Stevenson* (Ph.D.)
M. Mahdi* (Ph.D.)

*Student participants/collaborators supported by other research grants in the department
**Now at the University of West Florida, Pensacola

2. Objective

The goal of the work is to synthesize glass materials with known organic and inorganic impurities and to analyze them for nonlinear optical behavior and energy upconversion.

3. Abstract

We performed optical studies of organic dye doped glasses and rare earth ion doped glasses. We doped several organic dyes in boric acid, sucrose and polycarbonate hosts and detected phase conjugate signals from all these samples. Sucrose samples are hygroscopic and hence are useful for characterizing dyes only. Boric acid samples were damaged even at moderate laser powers. On the other hand polycarbonate samples could withstand high input powers and hence will be useful in device applications. Styryl 7 doped boric acid sample exhibited several interesting nonlinear optical phenomena and was also found to be useful for long-term/permanent information storage due to photochemical effects undergone by the excited molecules. PC signals in Pyridine 1 dye doped samples exhibited oscillations (period ~hour) which was found to be due to thermal effects/large Stokes shift in the emission. DCM and R110 doped boric acid samples are found to be chemically stable even after three years. We measured third order susceptibilities of DCF, DCM, R110, AY and R6G doped samples. We experimentally demonstrated that excited state absorption alters the transmission/saturation characteristics of the dyes in condensed media. These results have been published in three journal papers.

We made different glasses like Sulfates, borates, silicates, borosilicates and multicomponent oxide glasses doped with rare earth ions. Sulfate glasses were hygroscopic, binary and ternary borate glasses tried by us were found to be brittle and silicate glasses required very high temperatures. We investigated borosilicates and multicomponent oxide glasses doped with Nd^{3+} and Er^{3+} ions. In borosilicate host, we detected very weak violet emission from the L levels of Nd^{3+} in the region 380-460 nm at liquid nitrogen temperature, when its E levels were resonantly excited with 514.5 nm. In Er^{3+} doped borosilicate we detected very weak green emission from the E levels, at room temperature, when its B levels were resonantly excited with ~797 nm. However in a multicomponent oxide

glass doped with Er^{3+} we detected intense green emission at room temperature from the E levels of Er^{3+} when its B levels were excited with a near infrared laser beam. When the D state (or phonon coupled levels of B state) of Ho^{3+} in LaF_3 were resonantly excited with 636 nm (or 800 nm) we detected green and blue upconverted emission from the E ($^5S_2$) and F($^5F_3$) levels at 546 and 485 nm and at 416 nm from the J($^5G_5$) levels. When the LaF_3:Pr^{3+} was irradiated with 805 nm we detected very strong green emission at 540 nm and broad emission at 491 and 521 nm. When either the D or S levels of Nd^{3+} were resonantly excited with a 580 nm or 800 nm, we detected upconverted violet emission from the L levels in CaF_2, SrF_2, BaF_2 and LaF_3. Some of the results are in the process of communication and work is in progress on some systems. We are expecting at least four journal pares from our work on rare earth materials.

4. Introduction to Rare Earth Spectra

Rare earth ions doped in solids are useful in the laser development and hence have been investigated thoroughly. In addition these materials are useful to upconvert energy. That is, when the materials are exposed to low energy radiation (infrared) they emit high energy radiation (visible). Rare earth ionic spectrum is the result of electronic transitions within the f^n electronic configuration[1]. These are forbidden transitions but weakly allowed due to crystal field mixing of the wave functions of $4f^n$ with those of $4f^{n-1}5d$ at noncentrosymmetric sites. The oscillator strengths of the radiative transitions are $\sim 10^{-6}$ and the energy levels have long lifetimes and hence the spectral lines are sharp. Excited ions relax radiatively and nonradiatively[2,3]. The nonradiative relaxation is of two types (1) multi-phonon relaxation and (2) ion-ion interaction. The former depends on the energy gap between the energy levels and the cut-off phonon frequency of the host lattice[2]. The latter depends on the inter ionic separation and the nature of coupling between the ions[4]. The nonradiative relaxation limits the quantum efficiency of the energy levels. Because of the dense energy level structure (Fig.1) of the rare earth ions sometimes a laser that is resonant from the ground state is also resonant from the excited state. Hence it is possible to upconvert energy through excited state absorption[5]. Also, two excited ions may undergo energy transfer interaction to produce upconverted energy[5]. The upconverted levels are also subjected to nonradiative relaxation as explained above which limits the upconversion

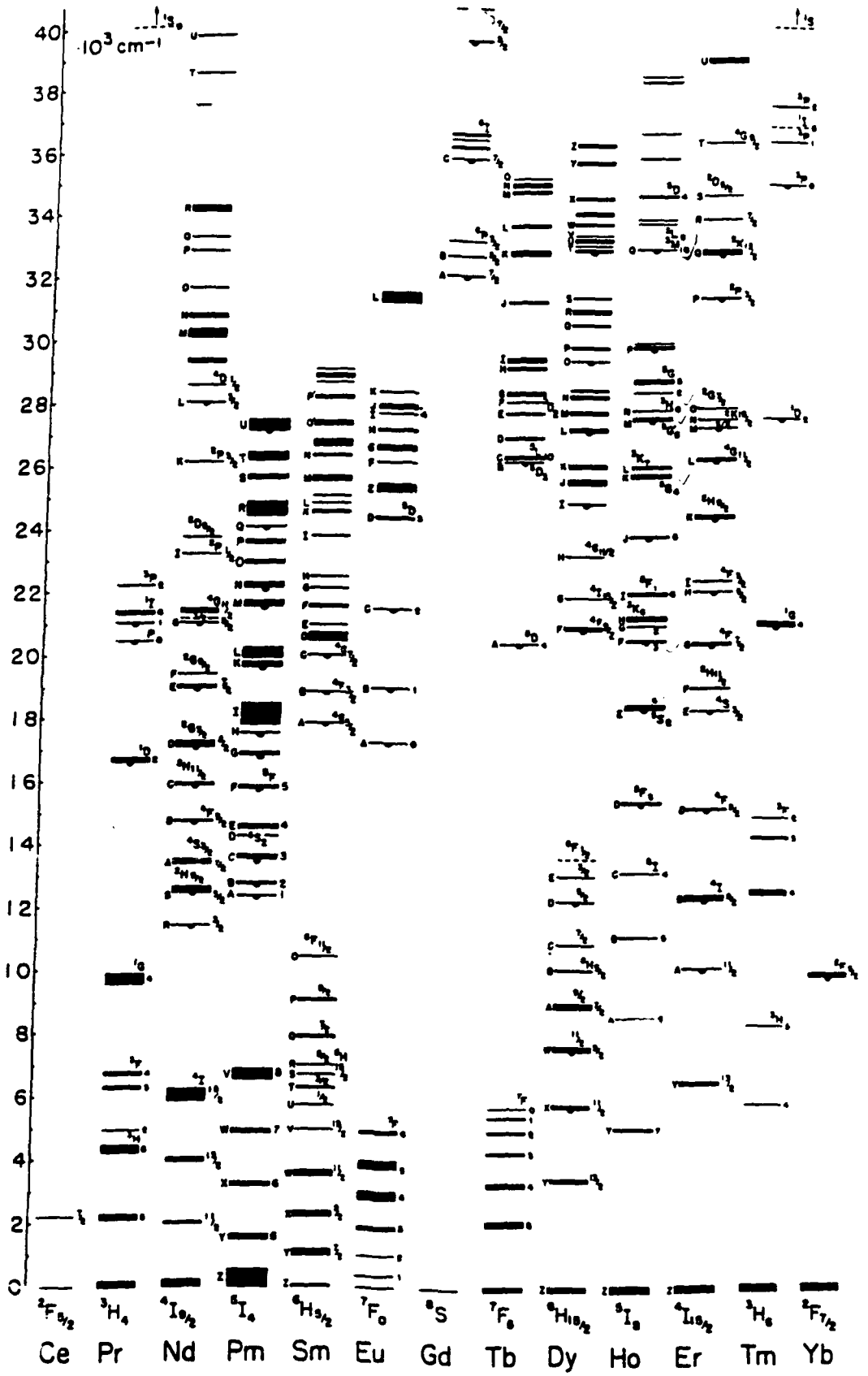

Fig.1 Energy Level Diagrams for $Ln^{3+}:LaCl_3$.

efficiency. Our aim is to make glasses doped with rare earth ions and pursue efficient upconversion phenomena in them.

5. Preparation of Inorganic Glasses

We tried to make different types of glasses like sulfates, borates, silicates, borosilicates and multicomponent oxide glasses. Each glass has certain advantages and disadvantages.

(a) Sodium borosilicate glass preparation

Because the binary silicate glasses were highly viscous, we resorted to making borosilicate glasses. For this purpose we chose a ternary component glass: Sodium borosilicate glass. We have thoroughly mixed appropriate quantities of Na_2CO_3, SiO_2, and H_3BO_3 and then poured into an aluminum crucible and heated in a box furnace at 800 °C for two hours and then at 1350 °C for another two hours in ambient atmospheric conditions. At such a high temperature these chemicals were known to oxidize. The melt was then poured into an aluminum mold and then allowed to cool naturally. Based on the amounts chosen, the glass is expected to have the following composition: Na_2O (13.6 mol%), SiO_2 (24 mol%) and B_2O_3 (62.4 mol%). However, when these samples were examined using a scanning electron microscope/energy dispersive X-ray analysis, its spectrum revealed a peak corresponding to aluminum which could have come from the crucible. The resulting glasses are extremely hard and highly transparent from violet to the infrared regions. A 60° angle prism was also made with the same glass composition and then it was used to measure the refractive index using the angle of minimum deviation technique. It's refractive index is estimated as 1.49 ± 0.01 and is found to be constant in the whole visible wavelength region. To obtain rare earth ion doped glasses appropriate quantity of rare earth compound was added to starting chemicals before they were mixed.

(b) Preparation of a multicomponent Oxide glass

Multicomponent oxide glasses are prepared to improve the efficiency of energy upconversion. With the following composition we were able to make a glass that was efficient in upconverting excitation energy from near

infrared region to the visible region[7]: La_2O_3 (2.3 mol%), PbO (13.7 mol%), TeO_2 (28.7 mol%), $MgTiO_3$ (6.3 mol%), SiO_2 (25.3 mol%), B_2O_3 (21.9 mol%), and $Ba_3Y_2WO_9$ (1.5 mol%). Appropriate amount of rare earth compound was added to the starting batch of chemicals to obtain rare earth ion doped glasses. The respective chemicals were measured, mixed thoroughly and then poured into an aluminum crucible and heated at 800°C for two hours and at 1200 °C for another two hours before pouring it out into a mold. The amount of the rare earth compound added was such that the concentration of the rare earth ion is ~10^{19} to 10^{21} /cm^3. The glass thus obtained is strong and then polished on all sides using three different grades of polishing powders as explained under glass polishing techniques.

(c) **Preparation of a borate glass**

A simple sodium borate glass was obtained by mixing sodium carbonate (1 gram) and boric acid (2 grams) and melting it at 700 C for two hours and then cooling the melt to room temperature. But it was found to be brittle. Similarly, a ternary borate glass was also prepared by mixing equal amounts of sodium carbonate, lead oxide, and boric acid and then heating the mixture at 700 C for an hour. The resulting glass was pale yellow in color.

(c) Preparation of a Sulfate glass

About 65 mol% of $ZnSO_4$ and 35 mol% of K_2SO_4 were mixed thoroughly and then heated in a box furnace at 400 °C for two hours. Then the mixture was cooled naturally. The resulting glass was transparent but was found to be hygroscopic. Hence it was not pursued anymore.

6. Glass Polishing Technique

We have used silicon carbide (grit 600), aluminum oxide (9.5 micron) and iron oxide (3.0 micron) powders in that order to polish the glasses. The polishing powder was mixed with water and the resulting paste was spread on a rotating disc covered with appropriate (grit size) polishing paper. Each glass surface was polished on the disc manually for about 20 minutes with each powder.

7. Table: Summary of glasses

Glass type	Composition	Melting point	Remarks
sulfate	K_2SO_4, $ZnSO_4$	400 °C	hygroscopic
borate	Na_2CO_3, H_3BO_3 PbO	700 °C	brittle
Silicate	Na_2CO_3, SiO_2	1600 °C	highly viscous
borosilicate	Na_2CO_3, SiO_2 H_3BO_3	1350 °C	transparent and strong
multicomponent Oxide glass	La_2O_3, $Ba_3Y_3WO_9$ PbO, SiO_2, B_2O_3 TeO_2, $MgTiO_3$	1200 °C	strong and transparent above 400 nm

8. Energy Upconversion Studies in rare earth ion doped oxide Glasses

We have investigated the rare earth ion doped glasses and crystals for energy upconversion studies. Energy level structure of the rare earth ions is shown in Fig.1. Sodium borosilicate glass was found to be transparent above 340 nm. The energy levels of Pr^{3+}, Nd^{3+} and Er^{3+} in sodium borosilicate glasses were identified from the absorption spectrum and were found to be in their expected positions. Laser excited fluorescence was recorded from these materials by exciting them with Ar^{+}, YAG:Nd^{3+}, Excimer pumped dye lasers and Ti:Sapphire lasers. When the E levels of Nd^{3+} were irradiated with 514.5 nm we have detected very weak upconversion signals at 380-460 nm at liquid nitrogen temperature. Similarly, when the B levels of Er^{3+} were resonantly excited with 797 nm, we have detected weak green emission from the E levels at 548 nm at room temperature. Such weak emission was mainly because of the large cut-off phonon frequency of the host material (sodium borosilicate). In other words, the dominant relaxation mechanism of the upconverted energy levels is nonradiative rather than radiative in this host[8]. To circumvent this problem we prepared a multicomponent oxide glass having heavy metallic elements. Because glasses are polycrystalline some of the rare earth ions may have heavier elements in their immediate surroundings. In such cases, those ions will relax radiatively. So it should be possible to detect efficient upconversion. Accordingly, we synthesized a multicomponent oxide glass containing heavier metallic elements as explained under glass preparation (section 5(b)). The resulting glass was found to be strong, nonhygroscopic and transparent above 400 nm. We investigated Er^{3+} doped glass for energy upconversion studies. When the B levels of the ion were resonantly excited with 797 nm, we have detected strong energy upconverted emission at 548 nm from the E levels at room temperature. Such signals were detected even for 50 mW of input laser power. This implies that heavy metallic glasses doped with rare earth ions are favorable for energy upconversion studies. In glasses the efficiency was limited by the nonradiative relaxation of the excited levels.

9. Energy Upconversion in $LaF_3:Ho^{3+}$

We have detected efficient energy upconverted emission at 416, 485 and 546 nm from the J, F and E levels of Ho^{3+} when its D levels were resonantly excited with a 636 nm dye laser. Intense upconverted emission was detected[9] even when the material was pumped with 30 mW dye laser beam. In this material the excited Ho^{3+} ion is relaxing to the A level and then is getting upconverted to the J levels by another photon of the pump laser. The J levels relax to the lower F and E levels which were emitting blue and green light. Their efficiency was estimated to be $\sim 10^{-4}$. When this material was excited with a near infrared laser beam of ~800 nm laser, we detected intense emission at 485 and 546 nm from the F and E levels. In this situation also, the excited ion was relaxing to the A state, that was further excited to the G level, which relaxed to the lower F and E levels causing them to emit 485 and 546 nm radiation.

10. Energy Upconversion in $LaF_3:Pr^{3+}$

When $LaF_3:Pr^{3+}$ was irradiated with 805 nm radiation we observed intense and sharp green signal at 540 nm in addition to other weak signals at 491 and 521 nm. Further work is in progress to identify the mechanism responsible for the production of green light.

11. Energy Upconversion in $MF_2:Nd^{3+}$ (M=Ca, Sr, Ba, La)

We have detected energy upconverted emission from the L levels of Nd^{3+} in the violet region (350-400 nm) when these materials were irradiated with an Ar^+ laser, a dye laser or a near infrared laser for exciting respectively the E, D or S levels of the ion. Further work is in progress.

12. Third order Nonlinearity of Organic Dyes

When a material is exposed to light its molecules are polarized and its polarizability is expressed as

$$P = \chi^{(1)}E + \chi^{(2)}E^2 + \chi^{(3)}E^3 + \ldots\ldots\ldots \quad (1)$$

where $\chi^{(1)}$, $\chi^{(2)}$ and $\chi^{(3)}$ are the first, second and third order susceptibilities.

The absorption coefficient of organic dyes obeys the relation

$$\alpha(I) = \alpha_0 / (1+ I/I_s) \quad (2)$$

where α_0 is its low power absorption coefficient and I_s is its saturation intensity for which the absorption coefficient is reduced by a factor of two.

Similarly, the susceptibility is expressed as

$$\chi(I) = \chi^0 /(1+I/I_s) = \chi^0 [1+I/I_s]^{-1} = \chi^0 [1- I/I_s + (I/I_s)^2 -.....] \quad (3)$$

The polarization of the medium becomes

$$P = \chi(I)E = [\chi^0 - \chi^0 (I/I_s) + \chi^0 (I/I_S)^2 - .....]E \quad (4)$$

$$P = \chi^0 E - \chi^0 E^3/I_s + ...; \text{ Since, } I = E^2 \quad (5)$$

A comparison of equations (1) and (5) reveals that

$$\chi^{(3)} = \text{Constant} /I_s \quad (6)$$

Hence optical saturation exhibits third order optical nonlinear effects.

13. Organic dye doped systems

Organic dyes have low melting points. Hence the host material used should also have low melting point, otherwise the dyes will decompose. Hence the number and types of host systems for dye doping are limited. We have studied the following dye doped systems.

Boric acid glass doped with organic dyes[10,11]

Sucrose doped with Dyes

Polycarbonate doped with dyes[12]

The following dyes were Investigated:

Styryl 7
DCF, DCM, R110, R6G, Pyridine 1, Acridine Yellow
Coumarin 314 and 343

14. Preparation of boric acid glass doped with dyes

Boric acid glasses doped with dyes were made earlier by other researchers also. However, we implemented a very simple method to prepare the samples. Our method is described below. The melting point of boric acid is 171°C. When boric acid melts it loses its water content and forms boron trioxide. When boron trioxide crystallizes from melt it tries to grow as microcrystallites and hence samples thicker than 100 microns exhibit cracks. A microscope slide is preheated on a hot plate to reach the melting point of the sample so that the dye does not decompose. A measured quantity of the dye and boric acid were thoroughly mixed and then spread on top of the heated glass slide. When the mixture melts another glass slide was kept on top of the sample and was sandwiched by pressing hard and simultaneously rubbing them against each other. The samples thus obtained are uniform and some samples lasted even for three years. The sample thickness was measured using a micrometer.

15. Preparation of sucrose samples doped with dyes

Sucrose melts at a temperature of about 200 °C. A measured quantity of the sample is poured into a crucible and then introduced in a preheated box furnace that was set at 200°C . After about 10 minutes a measured quantity of the dye was added, mixed well and then sandwiched between two microscope glass slides. The samples thus obtained are also in good quality[13]. However, after couple of weeks time the sample slowly transformed into fluid state/syrup state in a humid room, because, sucrose is hygroscopic. The samples lasted much longer if properly stored, when they were not in use. But sucrose turned out to be very useful in characterizing organic dyes. There is no limit on the thickness of the samples that can be made.

16. Preparation of Polycarbonate doped with dyes

Polycarbonate has been found to be one of the toughest and most durable thermoplastics known to the industrial community. It has a melting point of about 350 °C and a refractive index of 1.586. Because of their higher melting points these systems will have higher damage threshold than the boric acid glass or sucrose samples. The polycarbonate sample is available in the form small spheres ~1-2 mm and is white in color. A measured quantity is laid on top of a microscope slide and was then heated in a box furnace at ~350 °C for about 10 minutes. When it starts melting a measured quantity of the dye was spread uniformly on top of it. When the dye starts to melt another glass slide was kept on top of it and the two were pressed together by simultaneously rubbing the two together. The samples thus obtained are fairly uniform and are of good quality. A variety of Rhodamines, Coumarines and other dyes could be easily doped into the polycarbonate[12]. These samples lasted for a very long-time. When these samples are exposed to high irradiation powers, polycarbonate samples were found to possess higher damage threshold than boric acid samples. Hence, these samples may have applications in device making.

17. Excited state Absorption Studies

We also detected excited state absorption in the organic molecules and was studied using pump-probe technique as well as saturation/ transmission data. When a single weak beam irradiates the sample its transmitted intensity I_u (unpumped case) is given by

$$I_u = I_0 \exp(-\sigma_0 N l) \qquad (7)$$

where I_0 is the incident beam intensity, σ_0 is the ground state absorption cross-section, N is the concentration of the dye molecules and l is the sample thickness. However, when the sample is irradiated with a strong pump beam there will be some population in the excited state as well. In the (pumped) case the transmitted probe beam intensity is given by

$$I_p = I_0 \exp(-\sigma_0 N_0 l - \sigma_1 N_1 l) \qquad (8)$$

where σ_1 is the absorption cross section from the excited state, N_0 and N_1 are the populations in the ground and excited states when a strong pump beam is present.

$$N = N_0 + N_1 \tag{9}$$

$$N_1 = NI/(I + I_s) \tag{10}$$

At saturation intensity, $N_1=N/2$. The change in absorption coefficient of the probe beam due to excited state absorption is given by

$$\Delta\alpha = \alpha_1 - \alpha_0 = N_1(\sigma_1-\sigma_0) = \ln (I_u/I_p)/l \tag{11}$$

So, the transmitted probe beam intensity is measured with and without the pump beam. When the pump beam is turned on, the transmitted probe beam intensity decreases for $\sigma_1>\sigma_0$ and increases for $\sigma_1<\sigma_0$. Using this technique we could establish clearly the presence of excited state absorption and its relative magnitude with the ground state absorption. The transmission of the sample is measured as a function of the incident intensity. The absorption coefficients and the saturation intensity are obtained by numerically integrating

$$dI/dl = -(\alpha_1+\alpha_2)I \tag{12}$$

and fitting with the experimental data. α_1 and α_2 are the ground and excited state absorption coefficients.

$$\alpha_1 = (\alpha_0/s) \{1- \tan^{-1}\sqrt{3}s/\sqrt{3}s\} \tag{13}$$

where the saturation parameter, $s=I/I_s$ and α_0 is the low power absorption coefficient from the ground state. With this procedure we obtained unambiguous values for the ground state and excited state absorption cross sections for several organic dyes[11].

18. Estimation of third order susceptibilities, $\chi^{(3)}$

Third order susceptibilities for several organic dyes were estimated using the values obtained for α_0 and I_s from the transmission data, and by substituting in the formula,

$$\chi^{(3)} = \eta^2 c^2 \alpha_0 (d+\iota)/24\pi^2 \omega I_s \qquad (14)$$

where η is the refractive index, c is the speed of light, I_S is the line saturation intensity, α_0 is the low power absorption coefficient , δ is the normalized detuning parameter and ω is the laser frequency. The third order susceptibility has been measured for Styryl 7, R110, DCM, DCF, AY, Coumarin 314 and R6G dyes[10-13].

19. Optical Phase Conjugate Studies(Degenerate Four-Wave Mixing)

In this experiment the sample is irradiated with three input beams and the sample generates the fourth beam. In other words, two beams are used to write a grating in the material and the third beam is used to read the grating. The diffracted beam is also called the phase conjugate signal. The diffraction efficiency, the response time and durability of the material are dependent on the sample. The magnitude of nonlinearity is also found to be dependent on the structure of the molecule. In dye doped systems gratings can be formed due to modulation of electronic population in the material and thermal gratings formed due to nonradiative relaxation of the excited molecules. Hence the resulting gratings are complex and are a mixture of amplitude and phase gratings. In addition, some of the molecules may undergo photochemical changes in the excited state or may be bleached when exposed to radiation. Hence there can be efficient diffraction due to the formation of permanent gratings also. Some of the molecules may undergo excited state absorption which can change the magnitude of nonlinearity. Hence to make unambiguous estimate of its nonlinearities one has to understand all the different processes undergone by the molecules. In our studies we have detected the formation of permanent gratings due to photochemical effects in Styryl 7 and Pyridine 1 dyes, thermal gratings due to nonradiative relaxation in Pyridine 1, and population gratings due to electronic excitation in all the dyes. Phase

conjugate reflectivity is measured for all the dyes. In general these are in the range 10^{-3}-10^{-6}. In Styryl 7 doped boric acid glass we have observed self diffraction and formation of permanent gratings due to photochemical effects. The total phase conjugate reflectivity reached a value of 10%, when the gratings were written for about 30 minutes in Styryl 7. In Pyridine 1 doped sample, we have detected oscillations in the diffracted signal due to thermal effects.

20. **Research Personnel**: The principal investigator of this proposal B.R. Reddy was supported by this project.

21. **Students Participation**

The following students are either directly or indirectly supported by this project.
Mr. Anthony Ololo completed his M.S. thesis on the "Spectroscopic investigation of silicate glasses doped with certain rare earth ions" at Alabama A&M University[6]. He received financial assistance from this project.

Mr. Andre Ellison an undergraduate student also received financial assistance for sometime from this project. Mr. Andre Ellison and Mr. Paul Williams (undergraduate students) gained hands on experience in making and polishing glasses.

Ms. Shelia-Nash Stevenson (NASA employee) and M. Mahdi are working towards their Ph.D. degrees on energy upconversion studies[9] in rare earth ion doped crystals and are indirectly supported by this project by receiving guidance from Dr. Reddy who has been supported by the AFOSR- Project. They are also using the equipment purchased from this project.

22. Major Equipment Purchased

A high temperature furnace: Thermolyne, Model # F46110CM

A triple grating monochromator: Acton Research Corp., SpectraPro 500, Model# SP-405 and accessories,

A picoammeter: Keithley Model 485

A low temperature cryostat: RMC Cryosystems, Model LTS-LN_2

23. Miscellaneous Supplies

Publication charges, Art work for drawings
Inorganic Chemicals, Organic dyes, Microscope slides
Crucibles, Stationery, A filing cabinet, Optical rail and mounts
furnace supplies, miscellaneous items (hardware supplies) etc.,

24. SUMMARY AND CONCLUSIONS

(a) Energy upconversion studies useful for laser development

(1) We have developed oxide glasses doped with erbium ions which emitted intense green light[7] at room temperature when pumped with a near infrared laser beam ~800 nm.

(2) We have observed green and blue emission from $LaF_3:Ho^{3+}$ ions at room temperature[9] when pumped with a near infrared (~800 nm) or a red laser beam (~640 nm).

(3) We have detected intense green emission from $LaF_3:Pr^{3+}$ when pumped with a near infrared beam of 805 nm.

(4) We have also detected violet energy upconverted signals from Nd^{3+} doped in CaF_2, SrF_2, BaF_2 and LaF_3 crystals.

(b) Nonlinear Optical Studies

We have detected optical phase conjugate signals in the following systems:

(1) Polycarbonate doped with Coumarin dyes (first time): This is the best system known to us and has potential for practical applications[12].

(2) Sucrose doped with organic dyes: easy to make and useful in characterizing the dyes.

(3) We have detected photochemical effects in dye doped boric acid glass and are found to be useful for long term information storage[10].

(4) We have stored images in Styryl 7 doped boric acid films using an Ar^+ laser and retrieved the same using a He-Ne laser in the absence of writing beams. We think that this system will have several advantages in the demonstration of many optical effects[10].

References

1. G.H. Dieke, Spectra and energy levels of Rare Earth ions in Crystals (Wiley, N.Y., 1968).

2. M.J. Weber, Phys. Rev. 156, 231 (1967); ibid 157, 262 (1967).

3. L.A. Riseberg and H.W. Moos, Phys. Rev. 174, 429 (1968).

4. B.R. Reddy and P. Venkateswarlu, J. Chem. Phys. 77, 2862 (1982).

5. B.R. Reddy and P. Venkateswarlu, J. Chem. Phys. 79, 5845 (1983).

6. Anthony Ololo, M.S. Thesis (december 1991), "Spectroscopic Investigation of Silicate glasses doped with certain rare earth ions", Alabama A&M University, Normal, AL 35762 (unpublished).

7. B.R. Reddy and P. Venkateswarlu, "Infrared to visible energy upconversion in Er^{3+} doped Oxide glass", Appl. Phys. Letts. (submitted).

8. B.R. Reddy, A. Ololo and P. Venkateswarlu, "Spectroscopic studies of Silicate glasses doped with rare earth ions" (Manuscript).

9. B.R. Reddy, Shelia Nash-Stevenson and P. Venkateswarlu, "Energy Upconversion in LaF_3:Ho^{3+}", Interdisciplinary laser science conference IX, Toronto, Canada (October 3-8, 1993).

10. B.R. Reddy et al, Optics Commun. 84, 334 (1991); 86,555 (1991).

11. B.R. Reddy and P. Venkateswarlu, J. Opt. Soc. Am. B10, 438 (1993).

12. B.R. Reddy and P. venkareswarlu, Appl. Optics (accepted).

13. B.R. Reddy and P. Venkateswarlu, "Excited State absorption measurement in sucrose doped with R6G tetrafluoroborate" (manuscript).

Appendix

Reprints

Preprints

Manuscripts

and

Abstracts

Laser induced gratings in a styryl dye

B.R. Reddy, P. Venkateswarlu and M.C. George
Department of Physics, Alabama A&M University, Normal, AL 35762, USA

Received 17 July 1990; revised manuscript received 21 February 1991

Nonlinear optical phenomena like phase conjugation, beam coupling, self diffraction, development of permanent gratings, image storage/retrieval and photochemical effects have been demonstrated in a styryl dye doped in boric acid host. The third-order nonlinear susceptibility was estimated to be $\approx 1.7\times10^{-2}$ esu and two wave mixing gain coefficient was as high as 5. Self diffraction efficiencies into -1 image were measured as a function of laser power. Phase conjugate reflectivities were measured as a function of laser power and spatial frequency.

1. Introduction

An intense search is going on to find new optical materials that exhibit large nonlinear susceptibilities, have high damage threshold and easy to prepare high quality samples because of their possible applications in several areas [1–8]. The organic molecules exhibit large polarizabilities because excited π-bond electrons are delocalized and hence easily polarizable. Thus, organic molecules doped in amorphous materials (glasses) are turning out to be a class of useful nonlinear optical materials. In these systems optical excitation easily gets saturated at low light powers due to long lifetime of triplet states in a condensed media. Because $\chi^{(3)}$ is inversely proportional to the saturation intensity [2] these systems exhibit large third-order susceptibilities ≈ 1 esu. The order of nonlinearity and the response time that a system can exhibit depends on the structure of the organic molecules as well. So, we investigated the nonlinear optical behavior of a styryl 7 dye doped in boric acid glass which exhibited several interesting nonlinear optical phenomena and this is the most efficient system known to us in the category of organic dye doped glasses.

2. Experimental

Appropriate quantities of the boric acid and dye are mixed, melted and then sandwiched between two microscopic glass slides so that the concentration of the dye molecules is $\approx 10^{18}$–10^{20} molecule/cm^3 and typical thickness of the sample is about 100 μm. The sample has absorption in the wavelength region 300–500 nm and facilitates phase conjugate (PC) studies with Ar^+ laser. However there was no absorption at 514.5 nm when lower concentrations of the dye were used. Its fluorescence spectrum falls in the region 450–600 nm. The fluorescence lifetime was estimated to be 385 μs and there was no evidence for phosphorescence even at longer times. Nonlinear optical measurements were made in the two-wave mixing (TWM) and degenerate four-wave mixing (DFWM) configurations using Ar^+ laser. The beam size was about 4–5 mm and unfocused. The signals were detected with a PIN diode coupled to a preamplifier whose output was given to an X–Y plotter. Some of the slowly varying signals were measured with a highly sensitive power meter.

3. Results and discussion

In PC experiments the writing beams strong pump and weak probe interfere in the medium and generate a spatially periodic light intensity distribution which in turn modulates the electronic population of the dye molecules. For a typical angular separation (13°) of 488 nm (λ) writing beams the grating pe-

riod, Λ is found to be 2.15 μm. Some of the excitation energy is transferred to the host medium during nonradiative relaxation processes thus modulating the temperature and hence the refractive index of the medium. Thus in the medium a complex grating can be generated that involves changes in absorption as well as phase. The physical thickness of the sample in our case is 100 μm but its effective optical thickness [9] d is 43.6 μm for a typical transmission of 0.49 and absorption coefficient of 117 cm^{-1}. The gratings are thus inclined to thick regime because $d > 2\Lambda^2/\lambda$.

The existence of a grating can be probed in several ways. In the standard TWM configuration, in addition to the transmitted beams higher-order diffraction spots up to second order also appeared on either side. Such self diffraction effects occur when the magnitude of the nonlinearity is high. For typical pump (5.3 mW) and probe (1.8 mW) beam powers used, the transmitted probe power was 0.35 mW in the absence of the pump beam and its value increased with time as soon as the pump beam was turned on and reached a value of 1.7 mW after half an hour. This value represents a TWM gain of about 5. Such effects occur when beam coupling/energy transfer is predominant. The diffracted powers from the stronger pump beam into +1 image (which is along the transmitted probe beam direction) and +2 image are in the ratio of 1400 : 1. The +1 image and −1 image are at equal angular separations on either side of the strong pump beam. The power diffracted along the +2 image and −1 image are of the same order of magnitude. When the probe was blocked the signal showed a fast decay followed by a slow decay which revealed the presence of transient as well as permanent gratings in the medium and the signal along +1 image decayed with a time constant of about 77 min. During the initial period the grating growth was found to be nonlinear and varied quadratically with time. Diffracted signal efficiency into −1 image is plotted as a function of power and is shown in fig. 1 for two different times after the pump beam was turned on. The efficiency curves are linear at 15 min for all the laser powers used but nonlinearity sets in after 50 mW of laser power at 30 min. For normal incidence the diffraction pattern obtained with these gratings is found to be similar to that of a spectroscopic transmission grating [10] and

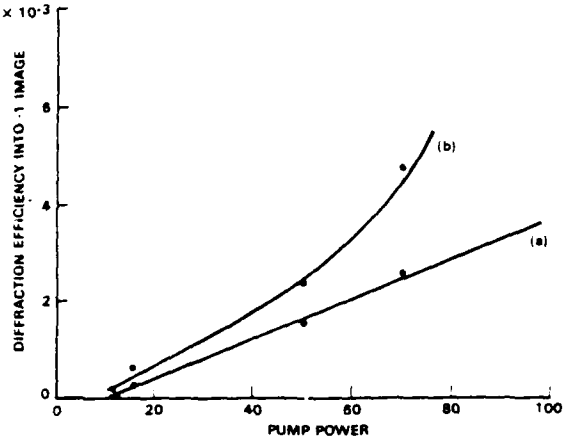

Fig. 1. Laser power dependence of diffraction efficiency into −1 image measured at (a) 15 min. (b) 30 min. after the pump beams were turned on in the TWM configuration.

the diffraction efficiency of such gratings is directly proportional to the incident power but is independent of laser wavelength. Once a grating of sufficient magnitude was developed the sample was stored for two months, and later on the same sample diffracted incident laser beams along +1 image direction. This can happen only if a permanent grating was developed because of a photochemical change undergone by the excited molecules. In that case photochemical effects should occur even when a single beam irradiates the sample. When an unexposed area of the sample was irradiated with a single laser beam of 488 nm its transmitted intensity increased by about 1% after half an hour. At 458 nm the absorption was very high and the transmitted power was very much less or absent in the beginning. But a few minutes later transmission appeared and kept on increasing. This strongly supports our idea that photochemical effects are present and the excited molecules slowly underwent a photochemical change so that they can no longer absorb light thus increasing the transmission. Such photochemical effects were found to be negligible or absent if the laser wavelength falls in the tail of the absorption spectrum or outside (e.g., at 514.5 nm). Photochemical effects were observed in other systems also [11,12] but in our system the gratings are permanent and lasted much longer than in other systems.

DFWM experiments were performed in the stan-

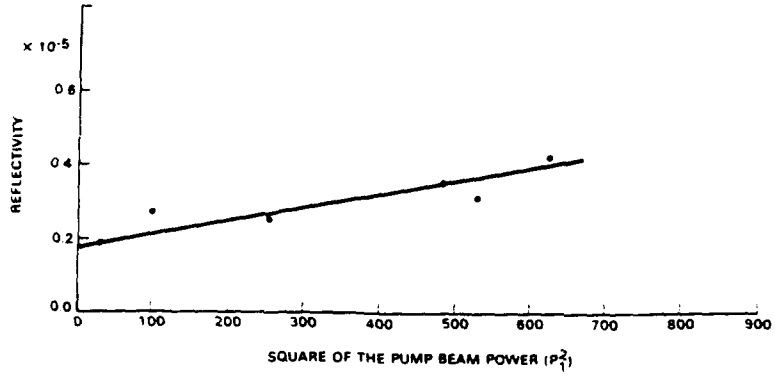

Fig. 2. Phase conjugate reflectivity as a function of laser power. Laser intensities are much less than the saturation intensity.

dard retroreflection configuration which does not require any explanation. In these experiments some of the retroreflected light gets diffracted collinearly in opposite direction of the probe beam and is referred to as PC signal. PC signals were detected even for total laser powers of the order of 10 mW and for more than 90° angular separation of the writing beams. PC signal growth and decay were measured. The PC decay was quite complex and the expression used in curve fitting always required more than one exponential function for all angular separations of the writing beams. PC signal grew in magnitude with time and attained maximum value in about 30 min at 10 mW of total input power but the time reduced to 12 min at 40 mW of input power. In the absence of photochemical effects (at lower concentrations of the dye) PC reflectivities are of the order of 10^{-5} but increased to about 10% in about half an hour for those samples in which photochemical effects are significant which in turn depended on the position of the laser wavelength with respect to the absorption spectrum. PC reflectivities varied quadratically with the pump beam power (fig. 2) at low laser powers and is in accordance with the theory developed for saturable absorbers [13]. At higher laser powers the reflectivity decreased again (not shown). For constant pump power the PC signal was found to vary linearly with the probe beam power and finally saturated. Spatial frequency dependence of the PC signal strength peaked at intermediate grating period (fig. 3) and the peak position depended on the concentration of the dye also. This suggests that there is some type of interaction or coupling in the medium.

Other supportive evidence for this coupling is found as follows. After the PC signal reached a steady maximum value the retroreflected beam was blocked for a minute and opened again. Then it was found that the PC signal increased slightly above the earlier maximum value and then decreased again slowly to reach the previous steady value, which could be due to self erasing and/or beam-coupling effects. This coupling is such that the PC signal is weaker at small as well as large angular separation of the writing beams. The signal is less at higher angles because of less overlap and small grating periods. PC reflectivities were measured as a function of laser wavelength

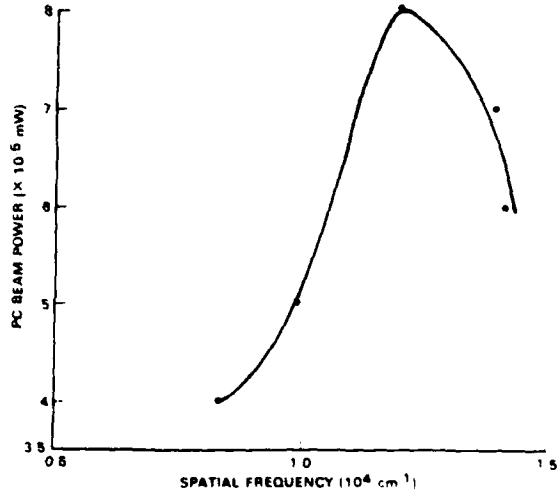

Fig. 3. Spatial frequency dependence of PC signal

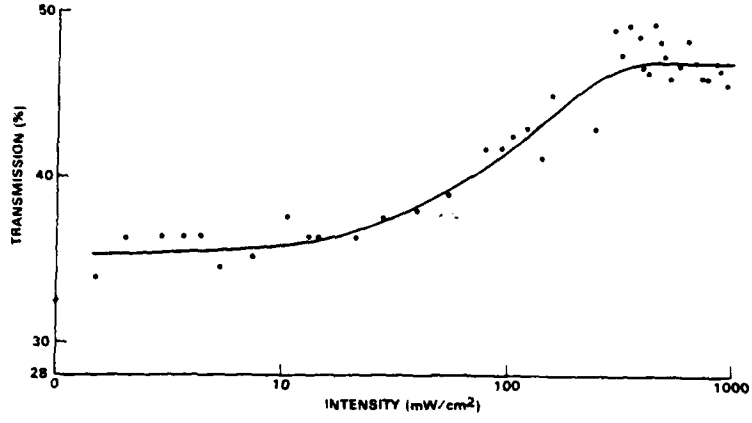

Fig. 4. Transmission data of a styryl 7 sample. Dye concentration is $\approx 10^{18}$ molecule/cm^3.

also. At 514.5 nm the absorption is very weak and hence the PC signals were also very weak. At 458 and 466 nm most of the laser power was absorbed and hence there was no PC beam to get diffracted. The absorption at 488 nm was such that the conditions were optimum for DFWM and photochemical effects and hence the PC signals were strong.

We also investigated the image processing capabilities of this sample. When an air force resolution target was inserted in either direction of the writing beam paths its clearly resolved image appeared in the PC signal as well as in the transmitted direction of the probe beam. The image stored using 488 nm could be read back by shining the sample with any other laser wavelengths (e.g., 632.8 nm) during the absence of writing beams. This suggests that the sample can be used to store information using the wavelengths which fall within the absorption spectrum and later on read back the same using inexpensive HeNe lasers.

An estimate of the magnitude of nonlinearity was made for a sample containing 10^{18} molecule/cm^3 using the saturation data. For this sample a plot of transmission versus incident intensity is shown in fig. 4, that exhibits saturation behaviour. The absorption coefficient of this sample was estimated to be 108 cm^{-1} at 488 nm and the gratings formed lasted for less than half an hour. For this sample the standard pump–probe technique did not reveal any evidence for the occurrence of excited state absorption and hence the measured value for the absorption coefficient was assumed to be that from the ground state only. The third-order susceptibility was estimated using [1]

$$\chi^{(3)} = (n^2c^2\alpha/24\pi^2\omega I_s)(\delta + i)\,, \qquad (1)$$

where n is the unsaturated refractive index, c is the speed of light, $I_s = 86$ mW/cm^2 and ω is the laser frequency. For $n = 1$ the magnitude of nonlinearity, $|\chi^{(3)}|$ was found to be 1.7×10^{-9} esu when δ was set to 1. This value is a factor of 100 less when compared to that measured for fluorescein and is mainly due to the low value for the absorption coefficient and large saturation intensity.

Our results suggest that optical materials doped with styryl dye will have potential applications in several areas (e.g., information processing, optical memories, laser shows etc.).

Acknowledgement

This work has been supported by a grant from the Department of the Air Force grant no. AFOSR-90-0160.

References

[1] M.A. Kramer, W.R. Tompkin and R.W. Boyd, Phys. Rev. A 34 (1986) 2026.
[2] W.R. Tompkin, R.W. Boyd, D.W. Hall and P.A. Tick, J. Opt. Soc. Am. B 4 (1987) 1030.

[3] H. Fujiwara and K. Nakagawa, Optics Comm. 55 (1985) 386.
[4] Y. Silberberg and I. Bar-Joseph, Optics Comm. 39 (1981) 265.
[5] T.A. Shankoff, Appl. Optics 8 (1969) 2282.
[6] G.R. Kumar, B.P. Singh, K.D. Rao and K.K. Sharma, Optics Lett. 15 (1990) 245.
[7] T.G. Alley, M.A. Kramer, D.R. Martinez and L.P. Schelonka, Optics Lett. 15 (1990) 81.
[8] B.R. Reddy, P. Venkateswarlu and M.C. George, Technical Digest 1990 Annual meeting (OSA), Boston, MA, November 4–9 (1990).
[9] P. Horan, W. Blau, H. Byrne and P. Berglund, Appl. Optics 29 (1990) 31.
[10] H.J. Eichler, P. Gunter and D.W. Pohl, Laser-induced dynamic gratings, Springer series in Optical Sciences, Vol. 50 (Springer, Berlin, 1986).
[11] D.M. Burland, G.C. Bjorklund and D.E. Alvarez, J. Am. Chem. Soc. 102 (1980) 7117.
[12] S.L. Clapham, R.W. Eason and N.A. Vainos, Optics comm. 74 (1990) 290.
[13] R.G. Caro and M.C. Gower, IEEE J. Quantum Electron. QE-18 (1982) 1376.

Optical phase-conjugate studies of organic dyes doped in a boric acid host

B. R. Reddy and P. Venkateswarlu

Department of Physics, Alabama A & M University, Normal, Alabama 35762

Received November 26, 1991; revised manuscript received July 13, 1992

Nonlinear optical studies of Dichlorofluorescein, Arcridine Yellow, 4-(*Dicyanomethylene*)-2-methyl-6-(*p*-dimethylaminostyryl)-4H-pyran, Rhodamine 110, and Pyridine-1 dyes doped in a boric acid host have been studied at Ar^+ laser wavelengths. Excited-state absorption was demonstrated directly by use of the pump–probe technique. Ground- and excited-state absorption cross sections and saturation intensities, phase-conjugate reflectivities, grating formation, and decay times were measured for all dyes. Phase-conjugate signals of Pyridine-1 exhibited oscillatory behavior in time, which was found to be due to heat produced during the nonradiative relaxation of the excited molecules. Third-order susceptibilities were also estimated for the dye-doped samples from the saturation measurements. The parameters derived from the saturation data are used to predict phase-conjugate reflectivities and are compared with the measurements.

INTRODUCTION

To identify new nonlinear materials, we investigated different substances. Saturable absorbers were known to exhibit large third-order susceptibilities.[1] Dyes doped in condensed media are one category of samples that generate optical phase-conjugate (PC) signals.[1–9] For device applications, only those substances are useful that are chemically stable for a long time, possess large nonlinearities, have fast response times, are efficient in diffraction, can be studied with the available lasers at low powers, and can be prepared easily. Some organic molecules undergo photochemical changes in the excited state and alter the optical properties of the system. Such systems may be useful for long-term information storage. The efficiency and response time of these systems depend not only on the structure of the dye molecules but also on the other optical phenomena that occur when these materials are exposed to radiation. For example, excited-state absorption (ESA) limits dye laser efficiency and alters the strength of the nonlinearity. Therefore the basic phenomena exhibited by these molecules must be thoroughly understood if they are to be improved. Only a few substances were studied previously, and not every aspect of the phenomena exhibited by the molecules was covered. Hence other dye-doped samples need to be studied so that ones that meet the device requirements mentioned above can be found.

Therefore we studied a few new dyes that exhibit PC signals at low laser powers and measured their nonlinearities. We suggested an easy method for sample preparation. We detected oscillations in PC signals of organic systems and explained the phenomenon. Here we will experimentally demonstrate that ESA modifies the transmission characteristics of saturable absorbers, and we will use easy methods to measure ESA cross sections that are useful in laser and waveguide research.

EXPERIMENT

Organic dyes have low melting points and decompose at high temperatures. Hence the host materials used should have low melting points. Boric acid melts at a temperature of 171°C. The dyes that we selected have melting points in the same range.

The sample preparation method that we adopted is different from that used previously.[1] Appropriate quantities of boric acid and dye were measured and mixed thoroughly before heating. A microscopic glass slide was preheated on a hot plate until it reached the melting temperature of the sample, which is lower than the dye decomposition temperature. Then a small amount of the dye–boric acid mixture was spread uniformly over the glass plate and melted. Another microscope slide was used to make a sandwich of the sample, and we pressed down hard, simultaneously rubbing the slides against each other. The dye was also spread uniformly in the sample. The samples obtained were of good quality, and the dye molecules were not decomposed. These samples lasted for several months.

Sample thickness was measured with a micrometer and was typically in the range ~30–100 μm, and the concentration of the dye molecules ranged from $\sim 10^{18}$ to 10^{20} cm^{-3}. At thicknesses above 100 μm, the samples cracked.

Pyridine-1-doped samples needed special preparation because some Pyridine-1 decomposed when melted. When the boric acid was about to melt, a measured quantity of dye was spread over it and then was immediately covered with another glass slide. For this sample, the dye concentration may not have been uniform throughout the sample. Such samples were yellow in color and exhibited interesting nonlinear phenomena, which are discussed below. If the dye decomposed during the heating process, the resulting sample was colorless and did not show any PC signal. Remember, if boric acid loses all its water content during the heating process, then the resulting product is boron trioxide and melts at approximately 450°C, and dye doping is impossible because most dyes decompose at that temperature. If the host loses all the water content, the remaining sample is distributed randomly on the glass slide and is hard to spread uniformly. When such materials are sandwiched, cracks developed in them. Such cracks can appear because B_2O_3 tends to grow as

0740-3224/93/030438-08$05.00

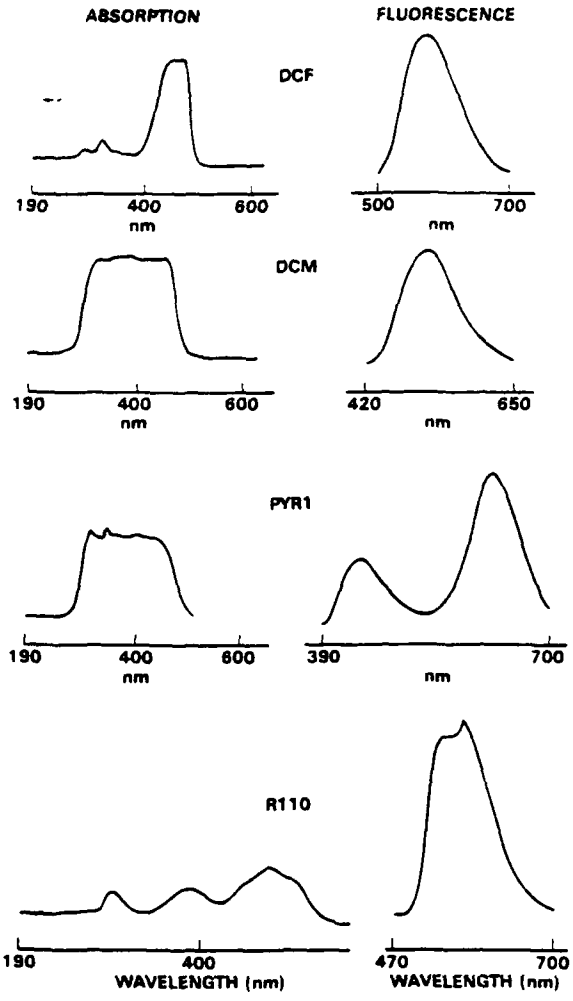

Fig. 1. Absorption and fluorescence spectra of DCF-, DCM-, Pyridine-1-, and R110-doped boric acid glasses. Fluorescence was obtained by irradiation with a 308-nm excimer laser.

microcrystallites.[10] Boric acid glass is complex and contains[10] B_2O_3 and H_2O. The dyes studied are 2', 7'-Dichlorofluorescein (DCF) ($C_{20}H_{10}Cl_2O_5$; molecular weight, 401.2), Acridine yellow (AY) ($C_{15}H_{16}ClN_3$; molecular weight, 273.77), Rhodamine 110 (R110) ($C_{20}H_{15}ClN_2O_3$; molecular weight, 366.8), Pyridine-1 ($C_{19}H_{23}BF_4N_2$; molecular weight, 366.21) and 4-(Dicyanomethylene)-2-methyl-6-(*p*-dimethylaminostyryl)-4H-pyran (DCM) ($C_{19}H_{17}N_3O$; molecular weight 303.37). Pyridine-1 and R110 were obtained from Lambda Physik; the others, from Kodak.

The absorption and fluorescence spectra shown in Fig. 1 have strong bands in their expected regions, indicating that these dyes were not decomposed. In the case of Pyridine-1, some decomposition products may appear, and if so they are unknown. The decomposed sample is colorless and did not show any PC signal. All the dyes exhibited additional absorption peaks on the short-wavelength side at higher dye concentrations. For example, the absorption and fluorescence spectras of AY taken at different concentrations of the dye are shown in Fig. 2. The short-wavelength peak in absorption grows in strength at higher concentrations and indicates the formation of dimers.[11] The absorption spectra of the other dyes also increased on the high-energy side at higher dye concentrations (indicating the formation of dimers), creating a flat region in the absorption spectrum. Samples containing DCF, AY, and R110 showed phosphorescence in the visible region when exposed to argon-ion laser beams of 476.5–488 nm. The phosphorescence decay times have been estimated by fitting the experimental decay curves. The values thus obtained are 63, 65, and 218 ms for DCF, AY, and R110, respectively. In case of DCM and Pyridine-1, the signal decayed in ~1 ms, which is the response time of the electronic shutter, and no phosphorescence effect was detected.

EXCITED-STATE ABSORPTION MEASUREMENTS

Transmission data were measured as a function of laser power. In DCF the transmitted intensity of 488 nm decreased at high input powers (Fig. 3), which is contradictory to the normal behavior expected of saturable absorbers. But DCF exhibited strong delayed emission (a phosphorescence effect), suggesting that it has a long triplet lifetime. So it should be possible to demonstrate ESA,

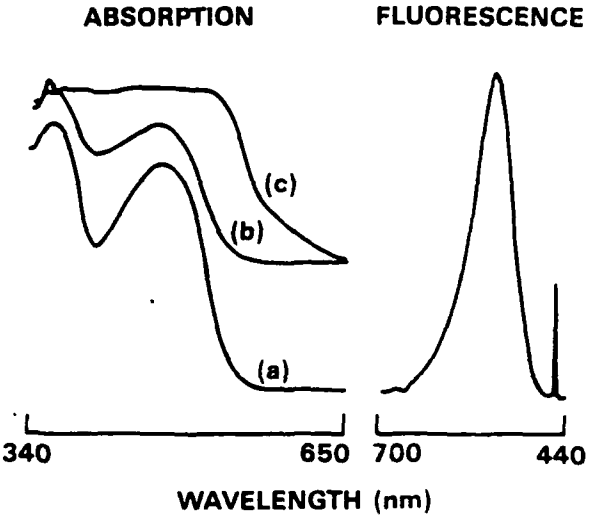

Fig. 2. Absorption and fluorescence spectra of AY in boric acid host. The concentrations of the dye are (a) $5 \times 10^{19}/cm^3$, (b) $7 \times 10^{19}/cm^3$, and (c) $2.4 \times 10^{20}/cm^3$. Fluorescence is induced by irradiation with 458-nm Ar^+ laser.

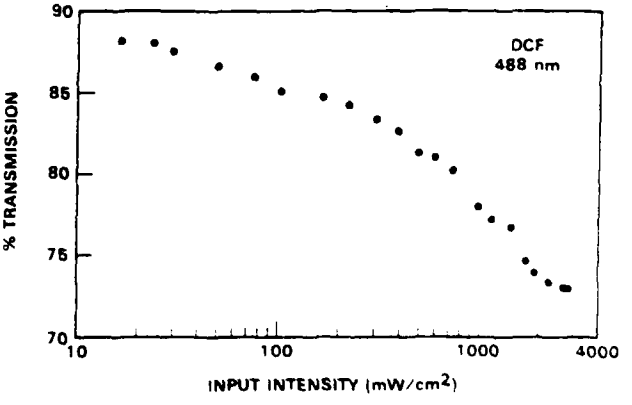

Fig. 3. Transmission of DCF at 488 nm as a function of input intensity.

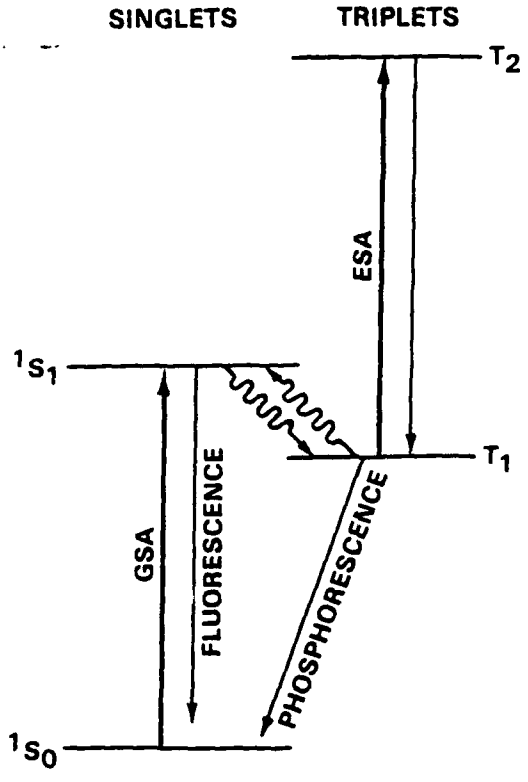

Fig. 4. Typical energy-level diagram showing the GSA and ESA absorption transitions. The wavy arrows indicate intersystem crossing.

that is, transition from a lower triplet state to a higher triplet state, in these samples, as shown in Fig. 4. Hence we carried out ESA measurements by using the standard pump–probe technique.[12] In our experiments the pump and probe beams are incoherent but are of the same wavelength unless specified. In these experiments a weaker proble beam and a strong pump beam irradiate the same location of the sample. The transmitted probe beam intensity is measured during the absence (I_u) and the presence (I_p) of the strong pump beam and is given by

$$I_u = I_0 \exp(-\sigma_0 N l), \tag{1}$$

$$I_p = I_0 \exp(-\sigma_1 N_1 l - \sigma_0 N_0 l), \tag{2}$$

$$N = N_0 + N_1, \tag{3}$$

$$N_1 = NI/(I + I_s), \tag{4}$$

where I_0 is the incident probe beam intensity, N is the number density of the dye molecules, l is the thickness of the sample, σ_0 and σ_1 are the ground-state absorption (GSA) and ESA cross sections, and N_0 and N_1 are the number densities of the dye molecules in the ground and excited states in the presence of the strong pump beam. At the saturation intensity (I_s), $N_1 = N/2$. If ESA occurs in the medium, then the transmitted probe beam intensity and, consequently, the absorption will vary. The change in absorption coefficient $\Delta\alpha$ is obtained from Eqs. (1)–(4) as

$$\Delta\alpha = \alpha_1 - \alpha_0 = n_1(\sigma_1 - \sigma_0) = \ln(I_u/I_p)/l, \tag{5}$$

where α_0 and α_1 are the absorption coefficients of the ground and excited states, respectively. If $\sigma_0 = \sigma_1$, these measurements do not reveal any evidence for ESA. If $\sigma_1 > \sigma_0$, then $\Delta\alpha$ is positive, and Eq. (4) predicts a decrease in the transmitted probe beam power when the pump beam is turned on, as in DCF at 488, 496.5, and 514.5 nm (Fig. 5). Thus we did not see any evidence of saturation behavior in the transmitted data of DCF (Fig. 3). However, if $\sigma_1 < \sigma_0$, then $\Delta\alpha$ is negative, and, accordingly, the transmitted probe beam power increases when the pump beam is turned on, as for R110, AY, and DCM at most of the ion laser wavelengths. Using this technique, we could obtain information on the ESA difference spectrum; our data are plotted in Fig. 5 for all the dyes except Pyridine-1, which did not reveal any evidence of ESA. All these samples do not have any absorption from the ground state at the 632.8-nm wavelength of the He–Ne laser. But when the pump beam was at 488 nm and the probe beam was at 632.8 nm, all the samples showed ESA, and in all, the transmitted probe beam power decreased when the pump beam was turned on. Because $\alpha_0 = 0$ at 632.8 nm, the measurement yields the ESA coefficient directly. Figure 5 indicates that the ESA coefficients are less than the GSA coefficients at all the ion laser wavelengths for DCM, R110, and AY. For DCF, the ESA coefficient is less than the GSA coefficient at 476.5 nm but is larger at the other wavelengths of the ion laser. By curve fitting the transmission data for fluorescein and AY[1,2] at 476.5 nm, they also saw that $\sigma_1 < \sigma_0$, and our experiment demonstrates that inequality. Our results demonstrate that dyes doped in solids do not exhibit the expected transmission characteristics of true saturable absorbers because of ESA and dimer formation.

OPTICAL PHASE-CONJUGATE STUDIES

From Fig. 1 we see that all these dyes demonstrate absorption at argon-ion laser wavelengths, which facilitates PC studies. Degenerate four-wave mixing experiments have been performed in the standard experimental configura-

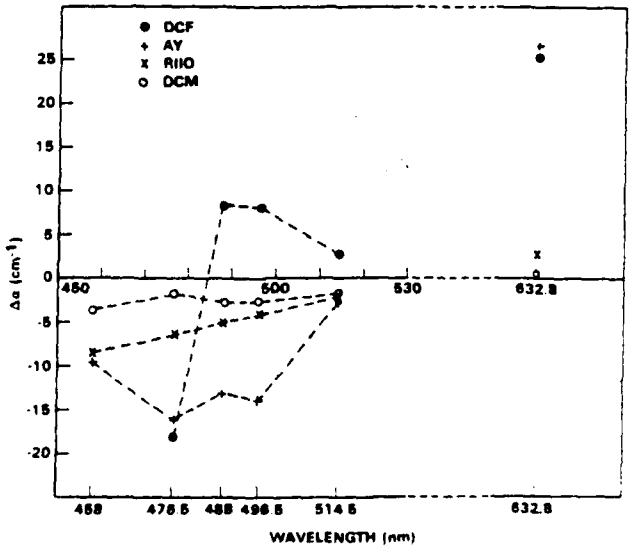

Fig. 5. ESA difference spectra of DCF (●), AY (+), R110 (×), and DCM (○).

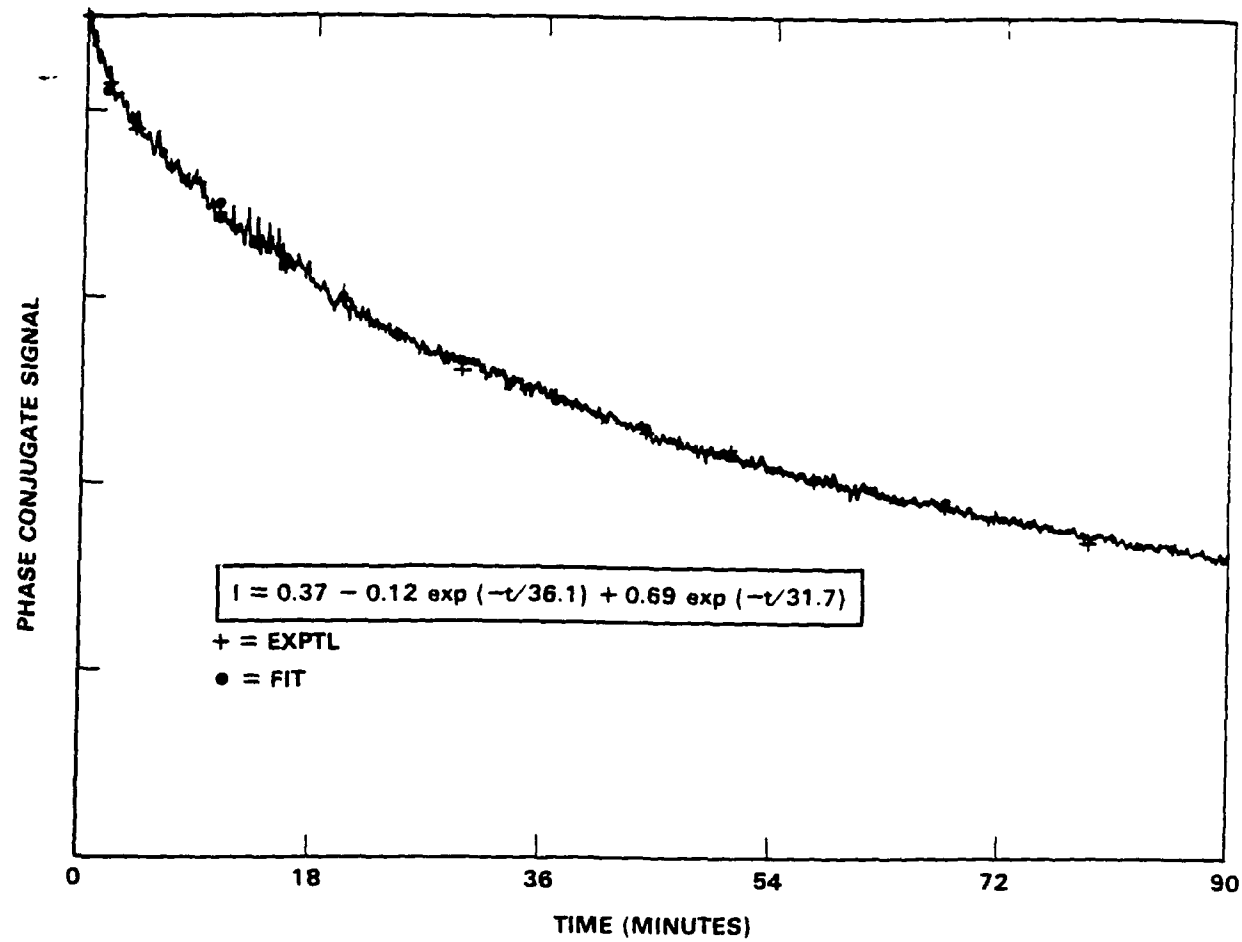

Fig. 6. Temporal variation of PC signal in Pyridine-1. The inset shows the expression used to fit the normalized experimental curve.

tion,[6] and these experiments do not require any detailed explanation. PC signals were observed even for large angular separations (~90°) and exhibited vector phase conjugation,[13] and the reflectivities were $\sim 10^{-5}$.

PC reflectivities were also measured as a function of laser wavelength. Large signals were observed for moderate absorption of the input beam, and no signal was seen for strong absorption or for no absorption at all. However, it was possible to detect the same signals at low concentrations of the dye. In DCF, PC reflectivities were measured at 488 nm as a function of laser power and spatial frequency. PC reflectivities were found to be inversely proportional to the pump beam power and agree with the model of Caro and Gower,[14] who predicted the same type of variation whenever the input pump intensity exceeded the saturation intensity. The PC signal peaked slightly at a spatial frequency of approximately 10^4 cm^{-1}.

Grating growth and decay times are measured for all samples. The grating decay curves were fitted by using a single exponential function, and the decay times were found to be less than 12 ms. The gratings lasted much longer than the fluorescence lifetimes, as expected, but less than the phosphorescence times, suggesting that the gratings are population gratings only. Samples that do not exhibit phosphorescence (for example, DCM) have fast growth and decay times. The PC signals of samples that exhibited phosphorescence have fast growth followed by slower growth, and the slower growth may be due to a slower buildup of the triplet state (for example, the PC signal saturated in approximately 30 ms for DCM and 156 ms for R110). The decay time of the PC signal in DCF did not show any systematic variation with the grating period.

For Pyridine-1 the decay time was much longer and depended on the writing time. A typical decay signal is shown in Fig. 6; the inset shows the equation used to fit the decay, and the expression contains more than one exponential term. In some cases the grating lasted even for a couple of days if the sample had been irradiated for an optimum length of time at optimum power levels. This relatively long life could be due to photochemical effects that occurred in the material at a slow rate. When the transmission was monitored as a function of time it increased for a couple of minutes in the beginning, suggesting that some type of photodissociation was taking place. However, when the transmission was monitored for longer periods of time no measurable change was detected in transmission, implying that only a small fraction of the dye molecules may be undergoing photochemical change or optical damage. A typical PC signal obtained as a function of writing time is shown in Fig. 7, which shows oscillatory behavior and suggests that the number of oscillations depended on the laser intensity. We observed such oscillations even when the read beam was replaced by a He–Ne laser, thus ruling out the possibility of beam feedback into the laser cavity. We also observed

that the number of oscillations increased with writing beam power. Hence the oscillations could arise only from the heating effect. At low input powers the amplitudes of successive oscillations are decreased, whereas at high input powers the oscillations are closer to sinusoidal behavior. We could not detect any transfer of energy from one beam to the other along the transmitted beam directions because the magnitude of oscillation is $\sim 10^{-5}$ that of the input beam strength. Similarly we did not see any self-diffraction effects. Decomposition products of the dye, if any, did not play any role here because the decomposed sample did not generate any PC signal. For thick holograms, as in our case, the diffraction efficiency is given by[15-17]

$$\eta = A[\sinh^2(\pi\Delta kl/\lambda \cos\Theta) + \sin^2(\pi\Delta nl/\lambda \cos\Theta)], \quad (6)$$

where A is a proportionality constant. The first and second terms on the right-hand side of Eq. (6) describe the diffraction efficiency that is due to amplitude/absorption and phase/refractive index gratings, respectively. The angle of the second term describes the strength of the phase grating and is represented by

$$\nu = \pi\Delta nl/\lambda \cos\Theta, \quad (7)$$

where Θ is the angle between the writing beams and Δn is the change in refractive index (peak to valley). Analysis of the absorption spectrum reveals that $\delta = 1.1$ (where δ is the normalized detuning parameter), and hence the contribution of the phase grating to the nonlinearity dominates the contribution that is due to amplitude grating. The contribution of the phase grating arises from the nonradiative relaxation of the excited molecules. Pyridine-1 absorbs in the blue region and emits in the red–infrared region (large Stokes shift of ~ 6000 cm^{-1}). This characteristic implies that excited molecules are undergoing nonradiative relaxation, and the energy equivalent converts into heat, thus modulating the refractive index of he medium. As ν varies, the second term in Eq. (6) and hence the diffraction efficiency η exhibits oscillatory behavior. ν varies if the thickness of the sample l varies, which in turn changes when the material is subjected to heating. Thermal expansion resulting from a rise in temperature of 1°C was known to produce oscillations in the diffracted signal, and in the steady state the period of oscillation was found by Cornish and Young to be several minutes.[18] They also observed that the period of oscillation is longer for thinner gratings and vice versa. Our findings are similar to those of Cornish and Young. At low input powers the rate of rise in temperature is low, and hence the period of oscillation is longer. At high input powers the rate of change in temperature is high, and so the period of oscillation decreased. Hence we conclude that the oscillatory behavior observed in the diffracted signal of Pyridine-1 is due to heating effects only.

THIRD-ORDER SUSCEPTIBILITY MEASUREMENTS

To find the third-order susceptibility, one needs reliable estimates of saturation intensity and absorption coefficients. For saturable absorbers the absorption coefficient is a function of input laser intensity and is expressed by[19]

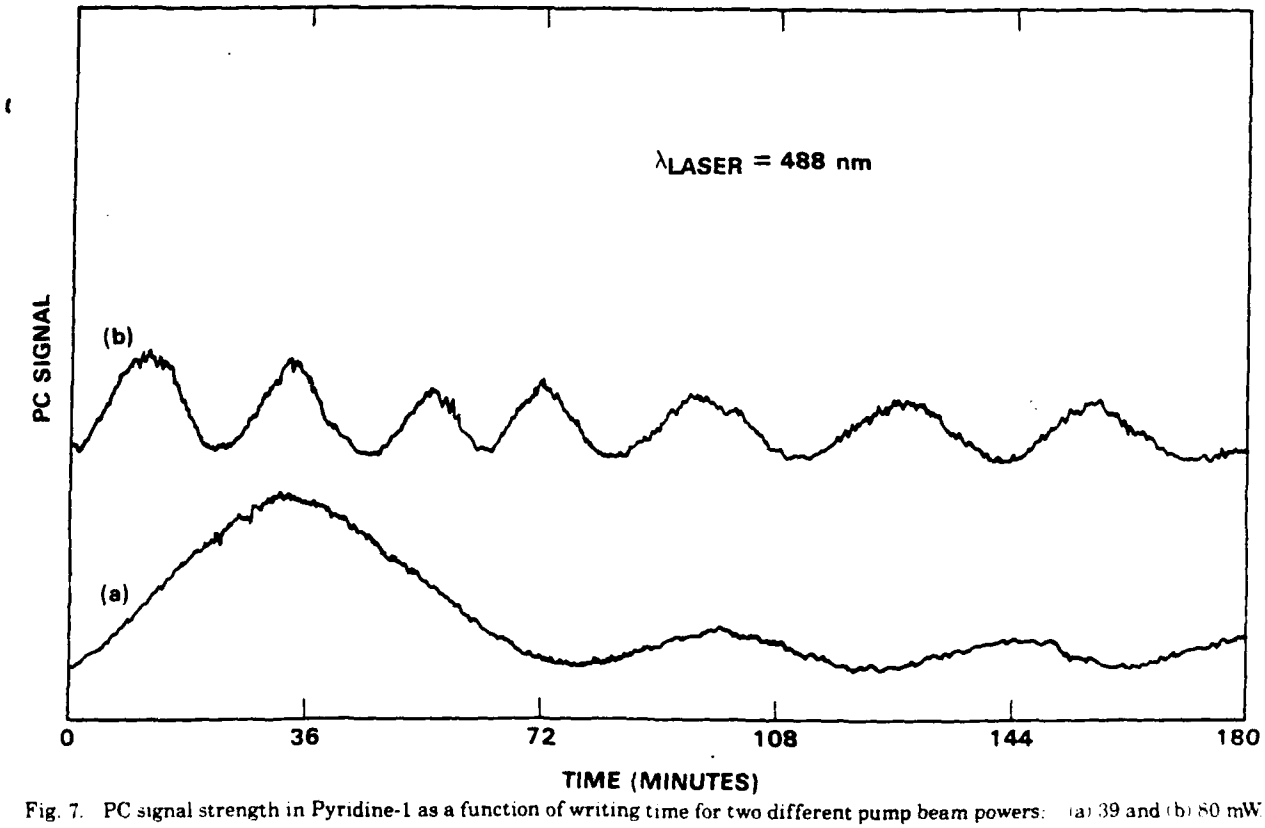

Fig. 7. PC signal strength in Pyridine-1 as a function of writing time for two different pump beam powers: (a) 39 and (b) 80 mW.

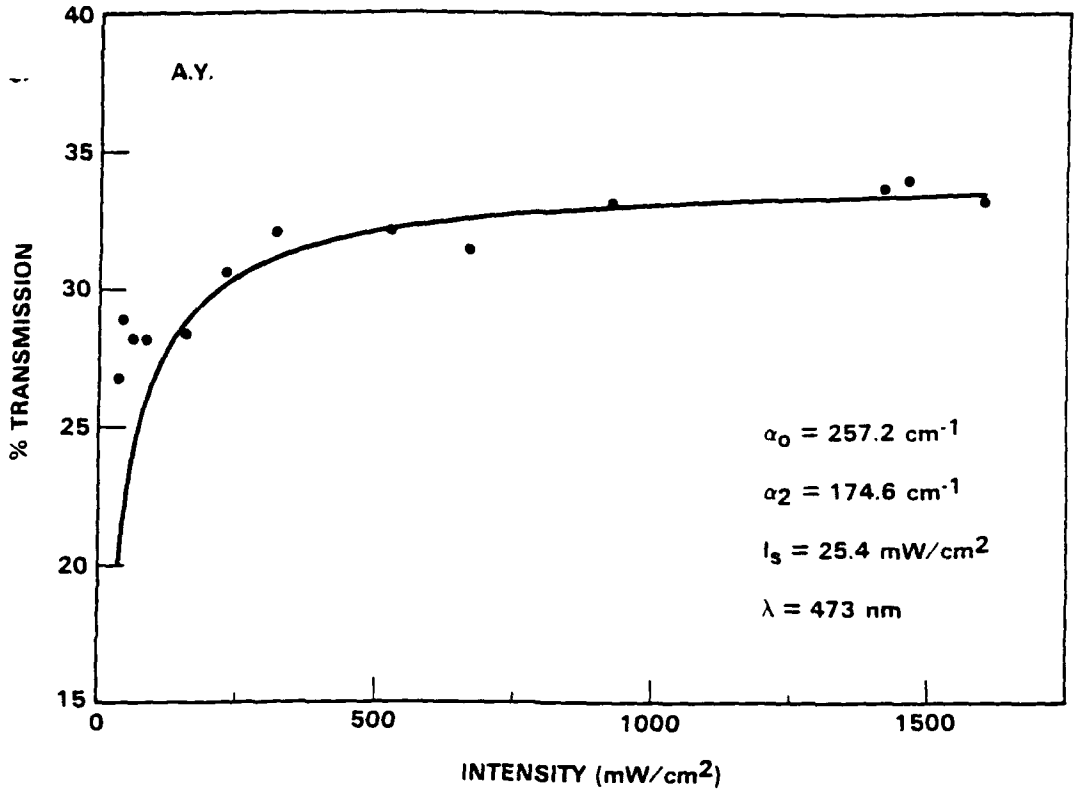

Fig. 8. Transmission of AY as a function of input intensity at 473 nm. The solid curve is the theoretical curve obtained with $\alpha_0 = 257.2\ \text{cm}^{-1}$, $\alpha_2 = 174.6\ \text{cm}^{-1}$, $I_s = 25.4\ \text{mW/cm}^2$, $l = 61\ \mu\text{m}$, and the sample concentration is $5.5 \times 10^{19}\ \text{cm}^{-3}$.

$$\alpha(I) = \frac{\alpha_0}{1 + I/I_s}, \tag{8}$$

where α_0 is the small-signal absorption coefficient and I_s is the saturation intensity at which the absorption coefficient is reduced by a factor of 2. However, dye-doped samples do not obey such ideal characteristics because of ESA (Fig. 3) and the formation of dimers (Fig. 2), as discussed above. In condensed media the GSA coefficient of the dyes is given by[1]

$$\alpha_1 = \frac{\alpha_0}{S}\left[1 - \frac{\tan^{-1}(3S)^{1/2}}{(3S)^{1/2}}\right], \tag{9}$$

where S is the saturation parameter, given by $S = I/I_s$. As expected from Eq. (8), the absorption coefficient decreased or the transmission increased at high input powers for DCM, R110, and AY. A typical transmission plot of an AY sample measured at 473 nm is shown in Fig. 8. The sample thickness and concentration of the dye are 61 μm and $5.5 \times 10^{19}\ \text{cm}^{-3}$, respectively. The solid curve is the theoretical curve obtained by integrating

$$\frac{dI}{dz} = -(\alpha_1 + \alpha_2)I \tag{10}$$

and fitting with the experimental data. In Eq. (10) α_2 is the ESA coefficient. The data in Fig. 8 were fitted with $\alpha_0 = 257.2\ \text{cm}^{-1}$, $\alpha_2 = 174.6\ \text{cm}^{-1}$, and $I_s = 25.4\ \text{mW/cm}^2$. The α_0 value obtained from the fit closely agrees with the measurement of $216.5\ \text{cm}^{-1}$. Some discrepancy exists because the measurement does not account for ESA. At 473 nm the nonlinearity of AY is due to absorption/amplitude grating only, whereas at other wavelengths it is due to a mixture of amplitude and phase grating contributions. We obtain the GSA cross section σ by using $\alpha_0 = N\sigma$, as $4.7 \times 10^{-18}\ \text{cm}^2$. We estimate its ESA cross section at 473 nm as $4.0 \times 10^{-18}\ \text{cm}^2$ by using Eqs. (4) and (5) and from the measured $\Delta\alpha$ value of $-19.3\ \text{cm}^{-1}$ when the pump beam is set at I_s.

The transmission data of the DCM sample (concentration = $3 \times 10^{19}\ \text{cm}^{-3}$ and thickness = 46 μm) is shown in Fig. 9. The best fit was obtained with $\alpha_0 = 53.6\ \text{cm}^{-1}$,

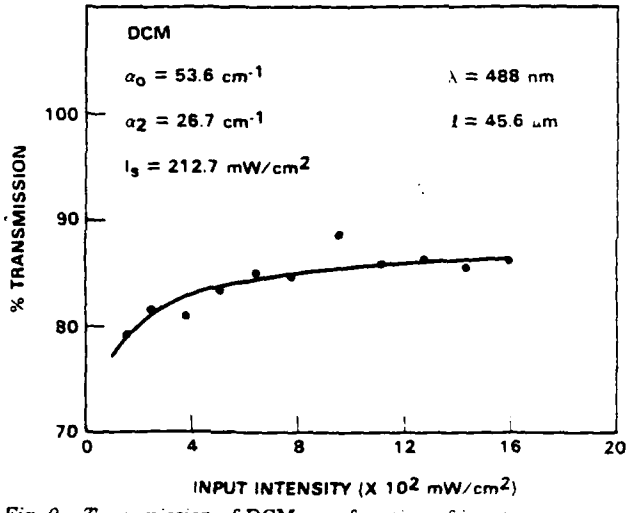

Fig. 9. Transmission of DCM as a function of input intensity at 488 nm. The solid curve is the theoretical curve obtained with $\alpha_0 = 53.6\ \text{cm}^{-1}$, $\alpha_2 = 26.7\ \text{cm}^{-1}$, $I_s = 212.7\ \text{mW/cm}^2$. Sample thickness is 46 μm, and concentration is $\sim 3 \times 10^{19}$ cm

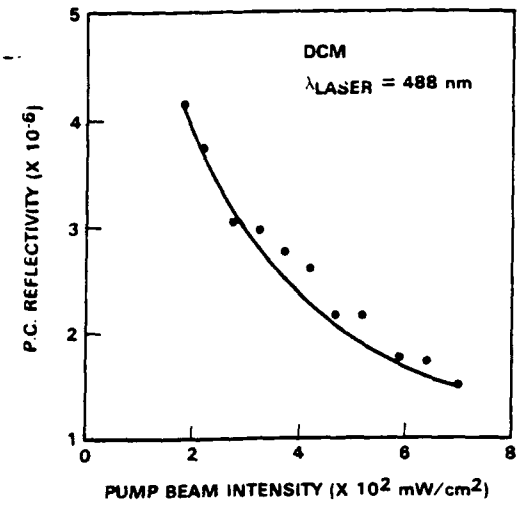

Fig. 10. PC reflectivity of DCM as a function of input power at 488 nm. The solid curve is the theoretical curve obtained with $\delta = 0.91$, $Q = 0.3$, $\alpha_0 = 53.6\ cm^{-1}$, $\alpha_2 = 26.7\ cm^{-1}$, and $l = 46\ \mu m$.

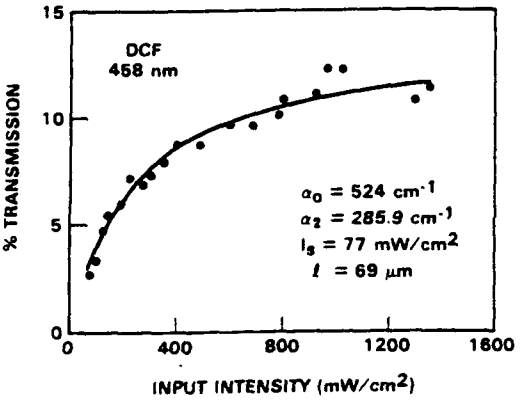

Fig. 11. Transmission of DCF as a function of input intensity at 458 nm. The solid curve is the theoretical curve obtained with $\alpha_0 = 524\ cm^{-1}$, $\alpha_2 = 285.9\ cm^{-1}$, $I_s = 77\ mW/cm^2$. The sample thickness is 69 μm, and concentration is $\sim 6.6 \times 10^{18}\ cm^{-3}$.

$\alpha_2 = 26.7\ cm^{-1}$, and $I_s = 212.7\ mW/cm^2$. Its GSA cross section at 488 nm is $1.8 \times 10^{-18}\ cm^2$. These estimates of α_1 and α_2 obtained from the transmission data are used to predict the PC reflectivity and are then compared with the measurements. A plot of PC reflectivity as a function of input power is shown in Fig. 10 for DCM at 488-nm irradiation. The solid curve is the theoretical fit obtained by using[1,20]

$$R = \frac{Q|k \sin(\omega l)|^2}{|\omega \cos(\omega l) + (\alpha_u + \gamma)\sin(\omega l)|^2}, \tag{11}$$

where

$$\omega = [|k|^2 - (\alpha_u + \gamma)^2]^{1/2}, \tag{12}$$

$$\gamma = N(\sigma_0 - \sigma_e)\frac{1 + 2S_0}{(1 + \delta^2)(1 + 4S_0)^{3/2}}, \tag{13}$$

$$k^* = \frac{iN(\sigma_0 - \sigma_e)(1 - i\delta)S_0}{(1 + \delta^2)(1 + 4S_0)^{3/2}}, \tag{14}$$

where S_0 is the saturation parameter at the resonance[1] and Q is a numerical factor lying in the range 0–1, which accounts for grating washout. This figure shows that the estimates for I_s and α_0 are correct. $\Delta\alpha$ was found to be -3.68 at 488 nm. The corresponding ESA cross section is $1.6 \times 10^{-18}\ cm^2$ when the pump intensity is equal to the saturation intensity. We also fitted the transmission data of R110 (concentration $2.6 \times 10^{19}\ cm^{-3}$ and thickness 31 μm) at 501.7 nm with $\alpha_0 = 418.7\ cm^{-1}$, $\alpha_2 = 264.3\ cm^{-1}$, and $I_s = 107.5\ mW/cm^2$. The GSA cross section at 501.7 nm is $15.9 \times 10^{-18}\ cm^2$. $\Delta\alpha$ was measured to be $-35.2\ cm^{-1}$, and the corresponding ESA cross section was estimated to be $13.2 \times 10^{-18}\ cm^2$. The transmission-versus-intensity plot of DCF is shown in Fig. 11 for 458-nm irradiation. The dye concentration is $\sim 6.6 \times 10^{18}\ cm^{-3}$, and the sample thickness is 69 μm. The solid curve is the theoretical curve obtained for $\alpha_0 = 524\ cm^{-1}$, $\alpha_2 = 285.9\ cm^{-1}$, and $I_s = 77\ mW/cm^2$. Its GSA cross section is $8 \times 10^{-17}\ cm^2$. $\Delta\alpha$ was measured to be $-147.8\ cm^{-1}$ for a pump intensity of 377 mW/cm^2 of 458 nm. The corresponding ESA cross section becomes $5.3 \times 10^{-17}\ cm^2$. The third-order nonlinear susceptibility was estimated by using[1,20]

$$\chi^{(3)} = \frac{n_0^2 c^2 \alpha_0(\delta + i)}{24\pi^2 \omega I_s}, \tag{15}$$

with

$$\delta = (\omega - \omega_0)\tau_2, \tag{16}$$

where ω is the laser frequency, ω_0 is the resonance frequency, α_0 is the low-power absorption coefficient, c is the speed of light, n_0 is the refractive index (set to 1), and δ is the normalized detuning parameter.[1] τ_2^{-1} equals the half-width at half-maximum of a homogeneously broadened absorption transition. The δ values are 0.91 for DCM at 488 nm, 0.03 for AY at 473 nm, 0.57 for R110 at 501.7 nm, and 0.2 for DCF at 458 nm. The third-order susceptibilities estimated are $0.02 + 0.03i$ esu at 488 nm for DCM, $0.03 + 0.96i$ esu at 473 nm for AY, $0.22 + 0.39i$ esu at 501.7 nm for R110, and $0.13 + 0.63i$ esu for DCF at 458 nm.

CONCLUSIONS

We measured GSA and ESA cross sections as well as nonlinear susceptibilities in organic dyes. Our experience shows that the fit of Eq. (10) to the transmission data converges even for different sets of values of the same parameters. However, we chose only that set of values that could predict PC reflectivities and that agreed with the ESA measurements made by the pump–probe technique. This study confirms the presence of ESA. Thus, when the transmission data and the ESA data are used, ESA coefficients can be unambiguously measured. Our data from the pump–probe technique also confirmed that the values derived for σ_0 and σ_1 from the saturation data[1,2] were correct. DCM- and R110-doped samples are found to be chemically stable and lasted for more than two years, whereas the other samples decomposed after six months. We experimentally demonstrated that ESA and dimer formation were responsible for the deviation of transmission data from the ideal saturation behavior. The $\chi^{(3)}$ value

that we measured in DCF is of the same order of magnitude reported by Kramer *et al.*[1] in Fluorescein. The third-order susceptibility of AY is larger than the value reported by Tompkin *et al.*[2] in lead–tin fluorophosphate glass because the dye concentration and the laser wavelength that we used are different from those used in Ref. 2. It also appears that host material has no influence on the magnitude of nonlinearity. However, when the dyes were doped in polymers such as PMMA, PVA, and gelatin, several photoinduced phenomena (photoreduction, photoisomerization, photoinduced birefringence, etc.) were noticed.[21-24] Our measurements also suggest that excited Pyridine-1 molecules are undergoing a type of photochemical effect or optical damage. The observed oscillations in the PC reflectivity of Pyridine-1 were due to large Stokes shift, nonradiative relaxation of the excited molecules. Such oscillations were not seen in other dye molecules, possibly because of the absence of such a large Stokes shift. We believe that our findings have led to a better understanding of dye-doped systems.

ACKNOWLEDGMENT

This research was supported by U.S. Air Force grant AFOSR-90-0160.

REFERENCES

1. M. A Kramer, W. R. Tompkin, and R. W. Boyd, "Nonlinear optical interactions in fluorescein doped boric acid glass," Phys. Rev. A **34**, 2026–2031 (1986).
2. W. R. Tompkin, R. W. Boyd, D. W. Hall, and P. A. Tick, "Nonlinear optical properties of lead–tin fluorophosphate glass containing acridine dyes," J. Opt. Soc. Am. B **4**, 1030–1034 (1987).
3. W. R. Tompkin, M. S. Malcuit, and R. W. Boyd, "Enhancement of the nonlinear optical properties of fluorescein-doped boric-acid glass through cooling," Appl. Opt. **29**, 3921–3926 (1990).
4. T. A. Shankoff, "Recording holograms in luminescent materials," Appl. Opt. **8**, 2282–2284 (1969).
5. Y. Silberberg and I. Bar-Joseph, "Low power phase conjugation in thin films of saturable absorbers," Opt. Commun. **39**, 265–268 (1981).
6. B. R. Reddy, P. Venkateswarlu, and M. C. George, "Laser induced gratings in a styryl dye, " Opt. Commun. **84**, 334–338 (1991); **86**, 555 (1991).
7. H. Fujiwara, K. Shio, and S. Miyanaga, "Power transfer by nearly degenerate two-wave mixing in a saturable dye-doped film," J. Opt. Soc. Am. B **8**, 1740–1746 (1991).
8. G. R. Kumar, B P. Singh, and K. K. Sharma, "Continuous-wave self-diffraction in dye-doped glasses," J. Opt. Soc. Am. B **8**, 2119–2127 (1991).
9. S. A. Boothroyd, J. Chrowstowski, and M. S. O'Sullivan, "Determination of phase of the complex nonlinear refractive index by transient two-wave mixing in saturable absorbers," Opt. Lett. **14**, 946–948 (1989).
10. F. C. Kracek, G. W. Morey, and H. E. Merwin, "The system, water-boron oxide," Am. J. Sci. **35A**, 143–171 (1938).
11. S. Speiser, V. H. Houlding, and J. T. Yardley, "Nonlinear optical properties of organic dye dimer-monomer systems," Appl. Phys. B **45**, 237–243 (1988).
12. R. Moncorge and T. Benyattou, "Excited state absorption of Ni^{2+} in MgF_2 and MgO," Phys. Rev. B **37**, 9186–9196 (1988).
13. W. R. Tompkin, M. S. Malcuit, R. W. Boyd, and J. E. Sipe, "Polarization properties of phase conjugation by degenerate four-wave mixing in a medium of rigidly held dye molecules," J. Opt. Soc. Am. B **6**, 757–760 (1989).
14. R. C. Caro and M. C. Gower, "Phase conjugation by degenerate four wave mixing in absorbing media," IEEE J. Quantum Electron. **QE-18**, 1376–1380 (1982).
15. H. Kogelnik, "Coupled wave theory for thick hologram gratings," Bell Syst. Tech. J. **48**, 2909–2947 (1969).
16. W. J. Tomilson and E. A. Chandross, "Organic photochemical refractive index image recording systems," in *Advances in Photochemistry*, J N. Pitts, G. S. Hammond, K. Gollnick, and D. Grosjean, eds. (Wiley, New York, 1980), Vol. 12, pp. 201–281.
17. K. A. Nelson, R. Casalegno, R. W. D. Miller, and M. D. Fayer, "Laser-induced excited state and ultrasonic wave gratings: amplitude and phase grating contributions to diffraction," J. Chem. Phys. **77**, 1144–1152 (1982).
18. W. D. Cornish and L. Young, "Influence of multiple internal reflections and thermal expansion on the effective diffraction efficiency of holograms stored in lithium niobate," J. Appl. Phys. **46**, 1252–1255 (1975).
19. M. Hercher, "An analysis of saturable absorbers," Appl. Opt. **6**, 947–954 (1967).
20. R. L. Abrams and R. C. Lind, "Degenerate four wave mixing in absorbing media," Opt. Lett. **2**, 94–96 (1978); **3**, 205 (1978).
21. T. Todrov, L. Nikolova, N. Tomova, and V. Dragostinova, "Photoinduced anisotropy in rigid dye solutions for transient polarization holography," IEEE J. Quantum Electron. **QE-22**, 1262–1267 (1986).
22. Y. Shi, W. H. Steier, L. Yu, M. Chen, and L. R. Dalton, "Large photoinduced birefringence in an optically nonlinear polyester polymer," Appl. Phys. Lett. **59**, 2935–2937 (1991).
23. N. Capolla, R. A. Lessard, C. Cane, and D. J. Lougnot, "Study of the photoreduction of methylene blue in gelatin solution and films with a view to improving the holographic recording process at 633 nm," Appl. Phys. B **52**, 326–330 (1991).
24. S. Caron, J. J. A. Couture, and R. A. Lessard, "Real time hologram reinforcement demonstrated by thionine/PVA photoreducible thin layers," Appl. Opt. **29**, 599–603 (1990).

TECHNICAL NOTE

Optical phase conjugation in polycarbonate resin doped with Coumarin 314 dye

B. R. Reddy and Putcha Venkateswarlu

Optical phase conjugate wave generation in Coumarin 314–doped polycarbonate resin is investigated by using 488-nm light for writing the grating and 632.8-nm light for reading it. The observed oscillatory behavior of grating growth as a function of writing time is attributed to heating effects.

Key words: Phase conjugation, nonlinear optics, polycarbonate doped with Coumarin dye.

Dyes doped in condensed media are considered useful in the development of phase conjugate (PC) optics.[1–12] LEXAN polycarbonate resin is known to be one of the toughest and most durable thermoplastics, and it is transparent in the visible region (90% transmission) with a refractive index of 1.586. It is highly viscous in molten form and is found to be nonhygroscopic at room temperature. After prolonged heating at 350 °C, however, even an undoped resin showed some absorption at 297 nm. In light of its desirable stable properties we thought that it may be a good host for the development of dye-doped PC optics. Therefore we explored Coumarin 314–doped LEXAN polycarbonate resin for PC wave generation, and we did observe it. The purpose of this note is to report our findings.

A measured quantity of the resin was placed on a microscope slide and was then heated at 350 °C for ~10 min. Upon melting, the resin became clear and viscous and at that time a measured quantity of the dye was spread uniformly over it. Then another glass slide was placed on top of the first slide and the two were rubbed against each other lightly so as to get samples of uniform thickness (0.1 to 0.5 mm thick, depending on the amount of material used).

The dye-doped sample showed broad absorption in the 250–490-nm wavelength region and a peak in fluorescence at 490 nm (not shown). For a typical dye concentration of $5 \times 10^{19}/\text{cm}^3$ and a sample thickness of 0.21 mm, the low-power absorption coefficient and cross section were found to be 29.5 cm^{-1} and 5.9×10^{-19} cm^2, respectively, at 488 nm. Under Ar^+ laser irradiation the sample showed delayed emission (phosphorescence effect) in the visible region with a decay constant of ~115 ± 20 ms. Its transmission data at 488 nm did not reveal any saturation behavior. So the saturation intensity was estimated by using the relation $I_s = h\nu/\sigma\tau$, where ν is the laser frequency, σ is the ground-state absorption cross section, and τ is the lifetime. On substituting for these values, $I_s = 6$ W/cm². On the other hand, these samples did show excited-state absorption (ESA) in the standard pump-probe configuration.[13] Transmitted probe beam power decreased when the pump beam was turned on. But the change in absorption $l\Delta\alpha$ that was due to ESA[13] was very small ($l\Delta\alpha \approx 0.06$), where sample thickness l = 0.21 mm. The third-order nonlinear susceptibility was estimated by using the relation[11]

$$\chi^{(3)} = \frac{n_0^2 c^2 \alpha_0 (\delta + i)}{24\pi^2 \omega I_s}, \qquad (1)$$

where n_0 is the refractive index of the medium, c is the speed of light, α_0 is the low-power absorption coefficient, ω is the laser frequency, and δ is the normalized detuning parameter obtained from the absorption spectrum. The value of $\chi^{(3)} \sim 10^{-3}$ esu at 488 nm with $\alpha_0 = 29.5$ cm^{-1}, $n_0 = 1.586$, and $I_s = 6$ W/cm².

Degenerate four-wave mixing (DFWM) experiments were performed to detect an optical PC wave by using the experimental procedure described elsewhere.[11] The PC signal was found to have a long decay time constant (~hours) that is dependent on the grating writing time. Whenever the sample was irradiated for ~10 min with the writing beams, it generated diffracted signals even after two days.

The authors are with the Department of Physics, Alabama Agricultural and Mechanical University, P.O. Box 1268, Normal, Alabama 35762.

Received 26 October 1992.
0003-6935/93/000001-02$05.00/0.

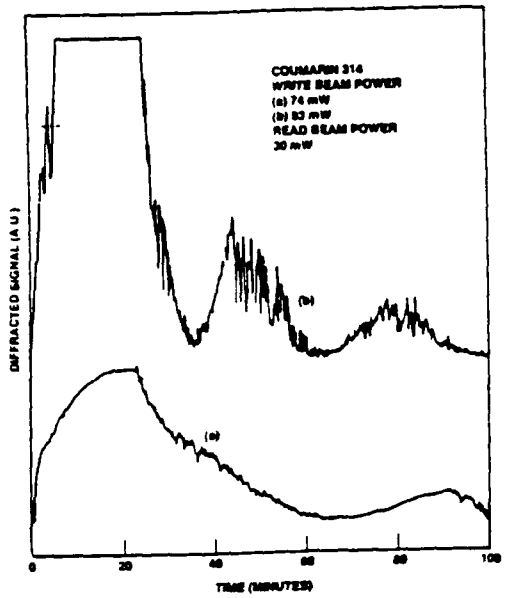

Fig. 1. Time dependence of grating growth in Coumarin 314–doped polycarbonate sample for two different writing beam powers. Grating was written and read by 488- and 632.8-nm laser beams, respectively.

Such things can happen only if there is a permanent grating developed in the material that is due to photochemical effects. When the transmission of a single input beam was monitored as a function of time it kept on increasing (with a significant change at 458 nm), suggesting that some of the dye molecules had undergone photochemical effects or optical damage. The time dependence of grating growth exhibited oscillatory behavior (Fig. 1.). The number of oscillations increased with the laser power. Such oscillations were observed even when the read beam was replaced by a 30-mW He–Ne laser (nondegenerate four-wave mixing). The diffraction efficiency η of such a system is given by the relation[14]

$$\eta = \text{const}(\sinh^2 \theta_1 + \sin^2 \theta_2) \qquad (2)$$

where the first and second terms are due to absorption (amplitude) and refractive-index (phase) gratings, respectively, and the angular factors describe the strength of the respective gratings. The phase grating arises because of the nonradiative relaxation of the excited dye molecules. The energy equivalent of the nonradiative relaxation gets converted to heat and that, in turn, modulates the refractive index of the medium. The strength of the phase grating is given by[14]

$$\theta_2 = \pi \Delta n l / \lambda \cos \theta, \qquad (3)$$

where $\theta = 18°$ is the angle between the writing beams and Δn is the modulation in the refractive index. The thickness of the sample and hence θ_2 vary with temperature (which is induced by laser power). The phase grating efficiency varies sinusoidally with θ_2, and hence the measured diffraction efficiency exhibits oscillatory behavior. A temperature variation of 1 °C was known to cause oscillations[15] in inorganic materials. At higher laser powers the sample temperature and hence θ_2 varies much faster, resulting in a larger number of oscillations, as shown in Fig. 1. This suggests that these oscillations are due to temperature effects only. These samples were not damaged even for input laser intensities of 14 W/cm^2.

Experiments were also performed with boric acid and sucrose as hosts. We found that polycarbonate samples are easy to make, nontoxic, nonhygroscopic, and possess a higher damage threshold and therefore they may prove to be better material for making PC devices. In addition to Coumarines we succcessfully doped polycarbonate with several other dyes like Rhodamines. Some polymers were known to encourage the guest molecules to undergo photochemical effects[5,7,16,17] but not all. Our experience showed that the nonlinearities of the dyes depend on the structure of the dye molecules, and the role played by the host material is to hold the dye molecules rigidly. Of all the materials we tried, polycarbonate was found to be the best host for dyes.

This research was supported by the U.S. Air Force Office of Scientific Research grant AFOSR-90-0160.

References

1. A. T. Raghunath, C. K. Subramanian, P. S. Narayanan, and M. R. Sajan, "Optical phase conjugation in methylene blue films," Appl. Opt. **31**, 4905–4906 (1992).
2. G. M. Naik and S. V. Pappu, "Generation of phase conjugate waves in dichromated gelatin and related materials," Appl. Opt. **30**, 1890–1892 (1991).
3. K. P. B. Moosad, T. M. Abdul Rasheed, V. P. N. Nampoori, and K. Sathianandan, "Low power optical phase conjugation in dyes embedded in polyvinyl alcohol films," Appl. Opt. **29**, 449–450 (1990).
4. M. H. Jeong, J. B. Song, and I. W. Lee, "Simplified processing method of dichromated gelatin holographic recording material," Appl. Opt. **30**, 4172–4173 (1991).
5. Y. Shi, W. H. Steier, L. Yu, M. Chen, and L. R. Dalton, "Large photoinduced birefringence in an optically nonlinear polyester polymer," Appl. Phys. Lett. **59**, 2935–2937 (1991).
6. Y. Silberberg and I. Bar-Joseph, "Low power phase conjugation in thin films of saturable absorbers," Opt. Commun. **39**, 265–268 (1981).
7. T. Todorov, L. Nikolova, N. Tomova, and V. Dragostinova, "Photoinduced anisotropy in rigid dye solutions for transient polarization holography," IEEE J. Quantum Electron. **QE-22**, 1262–1267 (1986).
8. W. E. Torruellas, K. B. Rochford, R. Zanoni, S. Aramaki, and G. I. Stegeman, "The cubic susceptibility dispersion of poly (4-BCMU) thin films: third harmonic generation and two photon absorption measurements," Opt. Commun. **82**, 94–100 (1991).
9. I. V. Tomov, B. VanWonterghem, A. S. Dvornikov, T. E. Dutton, and P. M. Rentzpis, "Degenerate four-wave mixing in azo-dye-doped polymer films," J. Opt. Soc. Am. B **8**, 1477–1483 (1991).
10. H. Fujiwara and K. Nakagawa, "Phase conjugation in fluorescein film by degenerate four-wave mixing," Opt. Commun. **55**, 386–390 (1985).
11. B. R. Reddy, P. Venkateswarlu, and M. C. George, "Laser induced gratings in a styryl dye," Opt. Commun. **84**, 334–338 (1991); **86**, 555 (1991).

12. W. R. Topkin, R. W. Boyd, D. W. Hall, and P. A. Tick, "Nonlinear-optical properties of lead-tin fluorophosphate glass containing acridine dyes," J. Opt. Soc. Am. B **4**, 1030–1034 (1987).
13. R. Moncorge and T. Benyattou, "Excited state absorption of Ni^{2+} in MgF_2 and MgO," Phys. Rev. B **37**, 9186–9196 (1988).
14. W. J. Tomlinson and E. A. Chandross, "Organic photochemical refractive-index image recording systems," in *Advances in Photochemistry*, J. N. Pitts, G. S. Hamond, K. Gollnick and D. Grosjean, eds. (Wiley, New York, 1980), Vol. 12, pp. 201–281.
15. W. D. Cornish and L. Young, "Influence of multiple internal reflections and thermal expansion on the effective diffraction efficiency of holograms stored in lithium niobate," J. Appl. Phys. **46**, 1252–1256 (1975).
16. S. Caron, J. J. A. Couture, and R. A. Lessard, "Real time hologram reinforcement demonstrated by thionine/PVA photoreducible thin layers," Appl. Opt. **29**, 599–603 (1990).
17. N. Capolla, R. A. Lessard, C. Carre, and D. J. Lougnot, "Studies of the photoreduction of methylene blue in gelatin solutions and films with a view to improving the holographic recording process at 633 nm," Appl. Phys B **52**, 326–330 (1991).

Applied Physics Letters (submitted).

Infrared to visible energy upconversion in Er^{3+} doped oxide glass

B.R. Reddy and P. Venkateswarlu

Department of Physics, P.O. Box 1268, Alabama A&M University

Normal, Alabama 35762

Abstract

Intense green emission was observed at room temperature from the $^4S_{3/2}$ level of Er^{3+} doped in a multicomponent oxide glass when its $^4I_{9/2}$ level was resonantly excited with a near infrared laser beam of 797 nm. Our studies indicate that energy transfer and excited state absorption are responsible for the upconverted emission from the sample.

There has been an intense search for upconversion laser materials because of their possible applications in several areas. Upconversion laser action in rare earth ions was detected in different crystals[1] at cryogenic temperatures and in fibers[2] at room temperature. The reasons for the low upconversion efficiency in crystals[1] are due to (1) the nonradiative relaxation (quenching and multiphonon decay) of the energy levels involved in the energy upconversion process and to some extent (2) the Boltzmann distribution of the electronic population. The adverse effect of the latter can be minimized only by cooling the material. If we can select a system in which the effect of nonradiative relaxation is minimized then it is possible to detect efficient energy upconversion. Er^{3+} doped in different solid media was investigated in the past for energy upconversion and laser action purposes.[3-12] Here we report the results of efficient energy upconversion in Er^{3+} doped multicomponent oxide glass observed at room temperature.

We made a multicomponent oxide glass with the following composition: La_2O_3 (2.3 mol%), PbO (13.7 mol%), TeO_2 (28.7 mol%), $MgTiO_3$ (6.4 mol%), SiO_2(25.4 mol%), B_2O_3 (21.9 mol%), $Ba_3Y_3WO_9$ (1.6 mol%). For this composition the resulting glass has the desirable optical properties, has lower cutoff phonon frequency than pure silicate glasses, is nonhygroscopic, stable and could withstand high irradiation powers. The rare earth ion concentration is ~$2.4 \times 10^{20}/cm^3$. The polished glasses are transparent from 405 nm and above. The absorption spectrum of Er^{3+} doped glass had shown peaks in their expected positions and the levels derived from it are shown in Fig. 1. When the material was irradiated with a tunable Ti:Sapphire infrared laser of 797 nm (typical power~200 mW), it showed bright green fluorescence (F,E--->Z) at room

temperature visible to the naked eye (Fig.2). Of course, green emission was visible even for 50mW of focused laser beam.

A logarithmic plot of upconverted fluorescence intensity versus laser power is shown in Fig.3 which has a gradient of 1.5. This suggests that more than one photon is responsible for the population of the E levels. A direct step wise two-photon excitation of the type $Z\xrightarrow{h\nu}B\xrightarrow{h\nu}K$ is not occurring because no emission was detected from the K ($^2H_{9/2}$) or other states located above the F state. But, the ion in the B state can relax to the Y level and then get upconverted to the F state. To confirm this process, Er^{3+} fluorescence was recorded for two different concentrations of the rare earth ion. For low Er^{3+} concentration (~$2.4\times10^{20}/cm^3$), the upconverted emission in the region 520-555 (F,E---->Z) is about 1% of the resonant emission at 803 nm (B---->Z). On the other hand, for high Er^{3+} concentration (~$1.9\times10^{21}/cm^3$) the upconverted emission is equally intense, while the resonant emission at 803 nm disappeared completely (not shown). This suggests that the only mechanism responsible for quenching the B level population is the phonon-assisted ion-pair relaxation of the type,

$$^4I_{9/2}(B) + {}^4I_{15/2}(Z) \longrightarrow {}^4I_{13/2}(Y) + {}^4I_{13/2}(Y). \qquad (1)$$

So, for each excited ion in the B state, two ions are formed in the Y state. An observation of the energy level structure reveals that the pump photon matches with Z-->B as well as Y--->F transitions with a slight mismatch in energy which can be attributed to the phonons. Because the Y multiplet is about 6800 cm^{-1} above the ground state, it is expected to have long lifetime, for example, the measured value is ~13 msec in LaF_3 host.[13] So, Y state

population can be further excited to the F state by another laser photon or by energy transfer interaction between two excited ions in the B and Y states respectively. These two mechanisms can be summarized by the equations,

$$^4I_{13/2}(Y) \xrightarrow{h\nu} {}^2H_{11/2}(F), \qquad (2)$$

and

$$^4I_{9/2}(B)+{}^4I_{13/2}(Y)\text{------}>{}^2H_{11/2}(F) + {}^4I_{15/2}(Z). \qquad (3)$$

The ion in the F state undergoes multiphonon relaxation to its lower E state causing the latter to emit. The transition probability for the Y-F transition was found to be more than that for the B-Z transition[14] in $LaF_3:Er^{3+}$. Hence efficient upconversion is possible. Under steady state excitation conditions the population in the upconverted levels F(E), derived from a simple rate equation model is expressed by

$$N_3 = I^2 N_0 A_{02} A_{13} (\sigma_t N_0 + A_{21}) / \tau_3^{-1} (\tau_1^{-1} + A_{13} I)(\tau_2^{-1} + \sigma_t N_0), \qquad (4)$$

where N_0, N_1, N_2 and N_3 represent populations in the Z, Y, B and F(E) levels, A_{ij} is the transition probability from level i to level j, σ_t is the energy transfer rate from level B to Y and τ_i is the lifetime of level i.

Since the upconverted emission is proportional to the population in N_3, eq.(4) indicates that it should be quadratic in laser power and our measurements support this. However, the slope in Fig.3 is less than 2 because of (1) the consequence of the quenching mechanism represented by eq.(1), where one photon is responsible for the production of two ions in the Y level, and to some extent (2) the saturation of Y state population due to its long

lifetime. We also tried to measure the temporal evolution of the upconverted signal by switching on the laser light with a fast electronic shutter. The resonant signal at 803 nm grew to its maximum value in about 3 msec while the 548 nm signal showed a fast rise (~3 msec) followed by a slow rise (for another 2 msec) which indicates that energy transfer is present. The emission at 526 nm arises because of the Boltzmann distribution/thermalization of the F levels from the E levels. Hence, we conclude that energy transfer upconversion as well as excited state absorption are responsible for the green emission. We have seen such efficient emission because of the expected lower cut-off phonon frequency of the host material and the very weak multiphonon decay of the E state to its lower D state ($^4F_{9/2}$) because no significant emission was detected from the latter. The $^4I_{9/2}$ is not relaxing to its lower $^4I_{11/2}$ because, no emission was seen from the latter. The oscillator strengths of these two states from the ground state were found to be comparable[15] in Y_2O_3. Hence, $^4I_{11/2}$ state was not considered to explain the upconversion phenomenon.

Our studies indicate that this material may be useful for the development of diode pumped visible lasers.

This research was supported by the U.S. Air Force grant# AFOSR-90-0160.

References:

[1]W. Length and R.M. Macfarlane, Opt. & phot. News, 3(3), 8 (1992); and the references there in.

[2]S.G. Grubb, K.W. Bennett, R.S. Cannon and W.F. Humer, Opt. & Phot. News 3(12), 40 (1992).

[3]A. Gharavi and G.L. Mcpherson, Appl.Phys.Lett. **61**, 2635 (1992).

[4]J. Thogersen, N. Bjerre and J. Mark, Opt.Lett. **18**, 197 (1993).

[5]P. Xie and S.C. Rand, Opt. Lett. **17**, 1198 (1992).

[6]Y.M. Hua, Q. Li, Y.L. Chen and Y.X. Chen, Opt. Commun. **88**, 441 (1992).

[7]S.B. Pollack, D.B. Chang and Birnbaum, Appl.Phys.Lett. **54**, 869 (1989).

[8]D.S. Knowles and H.P. Jenssen, IEEE J. Quant. Electron. **28**, 1197 (1992).

[9]A. J. Silversmith, W. Lenth and R.M. Macfarlane, Appl. Phys. Lett. **25**, 1389 (1989).

[10]T. Hebert, R. Wannemacher, W. Lenth and R.M. Macfarlane, Appl.Phys.Lett. **57**, 1727 (1990).

[11]L.F. Johnson and H.J. Guggenheim, Appl.Phys.Lett. **19**, 44 (1971).

[12]J.L. Jackel, A. Yi-Yan, E.M. Vogel and A. Von Lehmen, J.J. Johnson and E. Snitzer, Appl. Opt. **31**, 3390 (1992).

[13]M.J. Weber, Phys. Rev. **156**, 231 (1967).

[14]W.T. Carnall, H. Crosswhite and H.M. Crosswhite, "Enerfy level structure and transition probabilities of the trivalent lanthanides in LaF_3" Argonne National Laboratory report ANL-78-XX-95 (1978).

[15]W.F. Krupke, Phys. Rev. **145**, 325 (1966).

Figure captions:

Fig. 1 Partial energy level diagram of Er^{3+} in oxide glass derived from the absorption spectrum. The A level was not covered by our experiment and the Y level was derived from the fluorescence spectrum. ===>, ⟶ and ---> indicate laser excitation, fluorescence and ion-pair relaxation transitions respectively.

Fig. 2 Resonance fluorescence and energy upconversion spectra of Er^{3+} doped oxide glass. The material was excited with a 797 nm laser beam.

Fig. 3 Power dependence of the upconverted emission intensity at 548 nm.

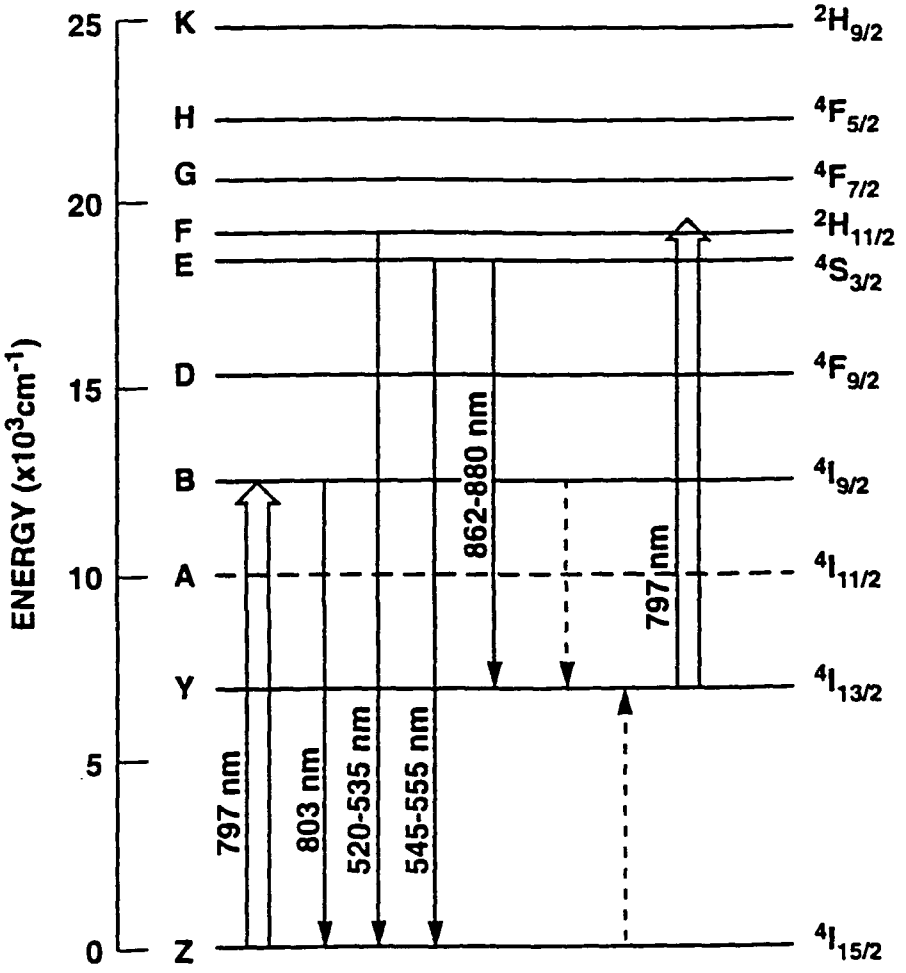
ENERGY (x10^{3}cm^{-1})
25
20
15
10
5
0
K
H
G
F
E
D
B
A
Y
Z
$^2H_{9/2}$
$^4F_{5/2}$
$^4F_{7/2}$
$^2H_{11/2}$
$^4S_{3/2}$
$^4F_{9/2}$
$^4I_{9/2}$
$^4I_{11/2}$
$^4I_{13/2}$
$^4I_{15/2}$
797 nm
803 nm
520-535 nm
545-555 nm
862-880 nm
797 nm

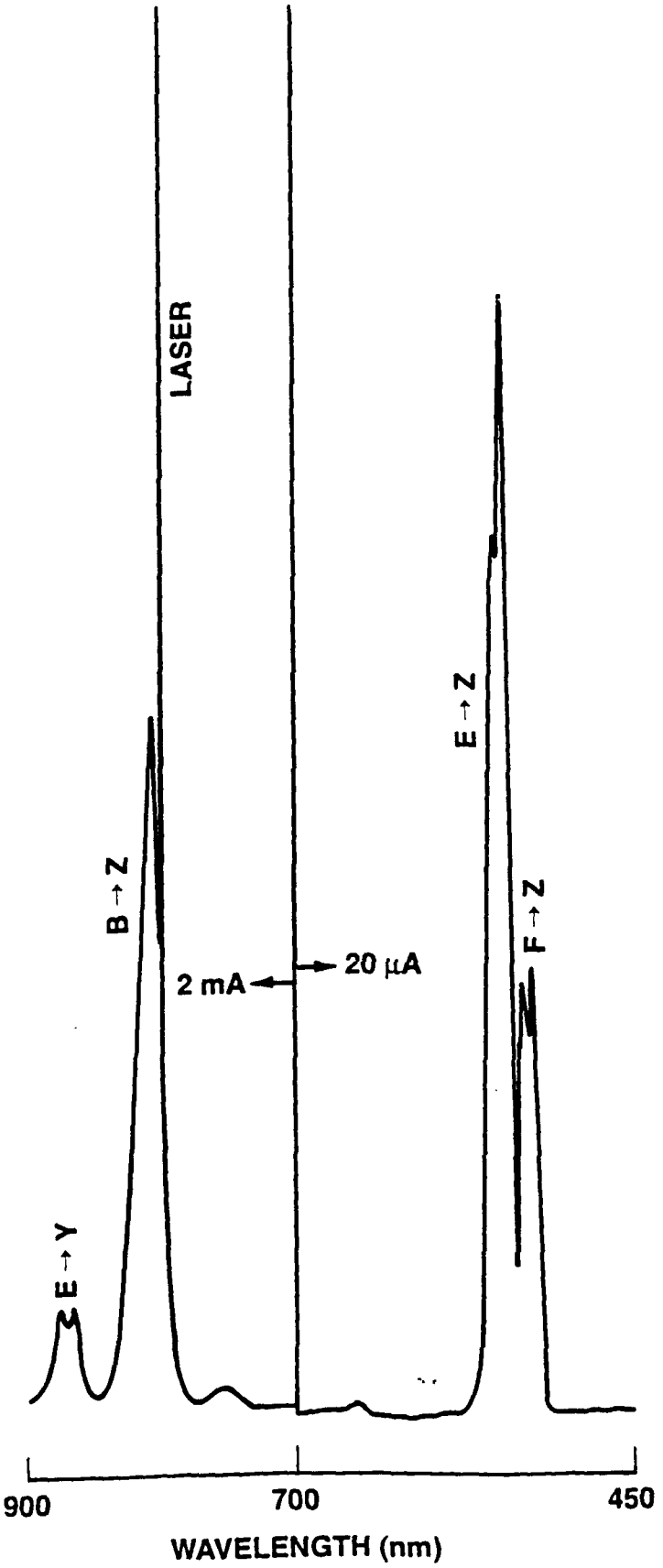
LASER
B → Z
E → Z
F → Z
E → Y
2 mA
20 μA
900
700
450
WAVELENGTH (nm)

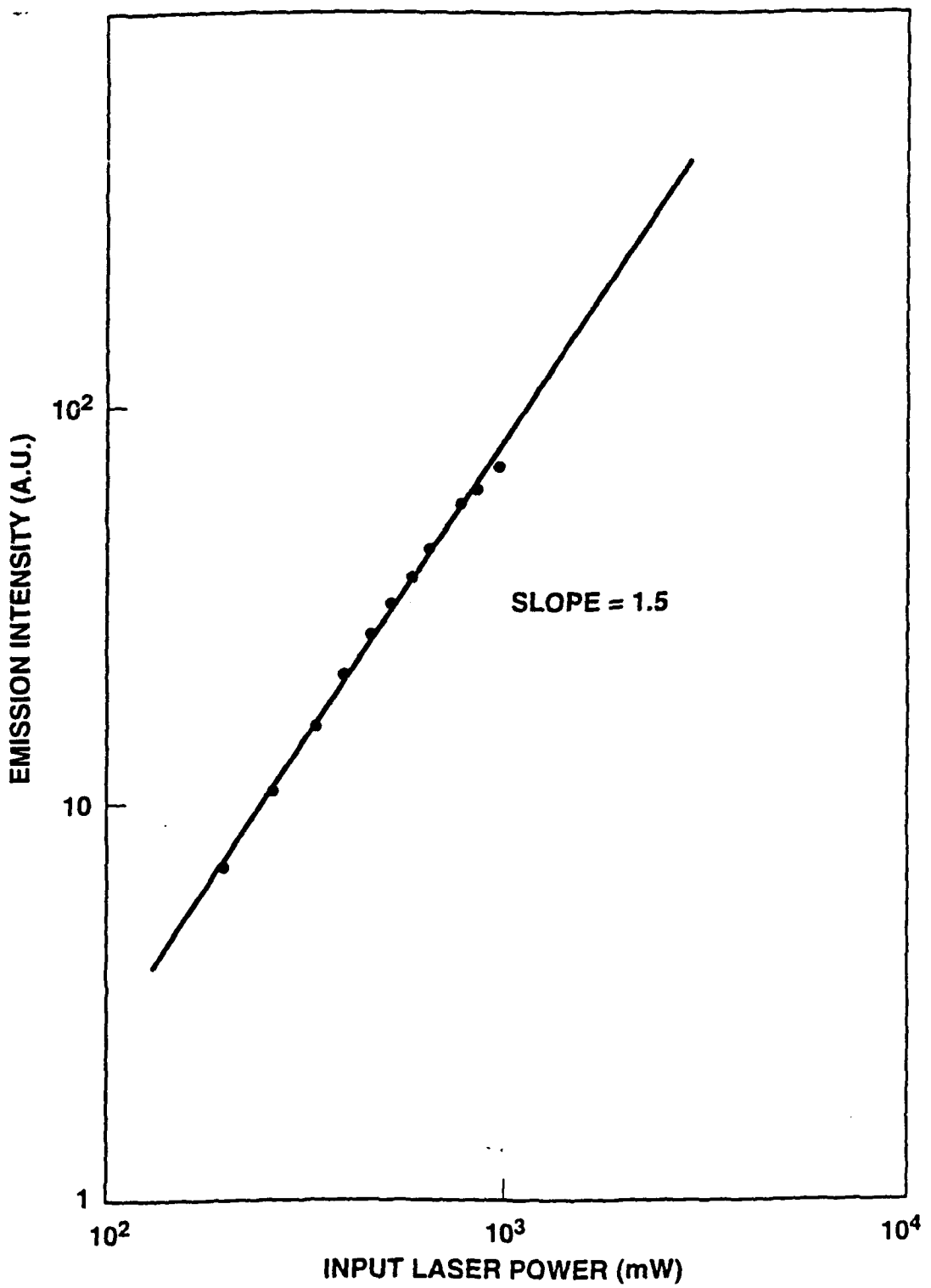
EMISSION INTENSITY (A.U.)
10^2
10
1
SLOPE = 1.5
10^2
10^3
10^4
INPUT LASER POWER (mW)

Interdisciplinary Laser Science Conference IX, Toronto, Canada (October 3-8,1993).

Title: Energy Upconversion in $LaF_3:Ho^{3+}$

Authors: B.R. Reddy, Shelia Nash-Stevenson* and Putcha Venkateswarlu, Alabama A&M University, Department of Physics, P.O. Box 1268, Normal, AL 35762

Address: *NASA Marshall Space Flight Center, EB22, Huntsville, AL 35812

Abstract: Blue and green emissions were detected from $LaF_3:Ho^{3+}$ when the material was irradiated with a red or near infrared laser.

Summary: Energy upconversion studies are performed in $LaF_3:Ho^{3+}$ at room temperature. When the $^5I_4$ of Ho^{3+} was resonantly excited with a near infrared laser beam of 800 nm, we have detected upconverted emission from the higher $^5F_5$, $^5S_2$ and $^5G_4$ states to the lower multiplets at 646, 548 and 486 nm respectively. When the $^5F_5$ level was resonantly excited with a rhodamine 6G dye laser we have detected resonant emission as well as upconverted emission from $^5S_2$, $^5G_4$ and $^5G_5$ states to lower levels. Growth and decay of the upconverted signals as well as their power dependence were recorded. All these results will be discussed in detail.

This research was supported by the U.S. Air Force grant No. AFOSR-90-0160 and NASA, CDDF, P10.

SUMMARY (200 word maximum)

Type entire manuscript, including any references, **double spaced** in a **single paragraph.** Capitalize only the first letter of the first word of the title. Address should be as brief as possible, but sufficient for postal service. do not use abbreviations.

Annual Meeting of the Optical Society Of America (1991)San Jose, California (accepted)

TITLE *Energy upconversion in neodymium doped sodium borosilicate glass*

AUTHOR B. R. Reddy, Anthony Ololo and Putcha Venkateswarlu

ADDRESS Alabama A&M University, Department of Physics, Normal, AL 35762

Summary

Energy upconversion was known to occur in rare earths by ion-ion interactions and sequential two photon excitation processes.[1] Recently there has been a renewed interest in these studies after the development of upconverted lasers.[2] The phonon spectrum of the host lattice influences not only the resonant fluorescence quantum efficiency but also that of upconverted fluorescence and hence the laser efficiency. So far upconverted laser action was seen only in single crystals. To extend these studies to other materials we prepared sodium borosilicate glasses doped with neodymium. All the prominent absorption peaks of Nd^{3+} are identified in this host. When the D and E levels are resonantly excited upconverted violet fluorescence is detected from the L levels of Nd^{3+} in the glass host. These results will be discussed in detail.

This work is supported by the Department of Air Force (grant # AFOSR-90-0160).

1.B.R.Reddy and P.Venkateswarlu, J.Chem.Phys.79,5845(1983).

2.R.M.Macfarlane, F.Tong, A.J.Silversmith and W.Lenth, Appl.Phys.Letts. 52,1300(1988).

SPECTROSCOPIC INVESTIGATION OF SILICATE GLASSES DOPED WITH CERTAIN RARE EARTH IONS

by
ANTHONY OLOLO

A THESIS

Submitted in partial fulfillment of the requirements
for the degree of Master of Science
in the Department of Physics
in the School of Graduate Studies

Alabama Agricultural and Mechanical University
Normal, Alabama 35762

December 1991

ABSTRACT

SPECTROSCOPIC INVESTIGATION OF SILICATE GLASSES DOPED WITH CERTAIN RARE EARTH IONS

Anthony Ololo, M.S. Alabama A&M University, 1991. 80pp.

Thesis Advisors: B.R. Reddy and P. Venkateswarlu

The aim of the work is to prepare Sodium borosilicate glasses doped with Pr^{3+}, Nd^{3+}, and Er^{3+} ions and to study their absorption and fluorescence spectra. The samples have been made by mixing and melting appropriate quantities of the chemicals Na_2CO_3, H_3BO_3, SiO_2 and $R_2(SO_4)_3$, where R = Pr, Nd, or Er. The resulting melt was cooled to obtain the glass, which was then polished to reduce scattering from the surfaces. Absorption spectra of the samples were recorded using Beckman DB-GT and Perkin Elmer Spectrophotometers. All the energy levels in the visible region were mapped. Fluorescence spectra of these samples were recorded using SPEX and ARC monochromators by resonantly exciting the samples with Ar^+ laser, Excimer pumped dye lasers, Second and Third harmonics of YAG laser. Pink color fluorescence was detected from Pr^{3+} due to $^3P_0$ - $^3H_{4,5,6}$, $^3F_{2,3,4}$ and $^1D_2$ - $^3H_{4,5,6}$. $^3P_{1,2}$ levels were found to relax nonradiatively. Nd^{3+} fluorescence is predominately in the near infrared region and is mainly due to R - Z. and very weak emission was also seen from D, C, B, and S levels. At liquid nitrogen

temperature some weak emission was also detected in the violet/blue wavelength region when the sample was excited with 488/514.5 nm lasers. No fluorescence was detected from Er^{3+} on excitation with R6G dye laser. But on excitation with Ar^{+} laser, strong fluorescence was seen due to E - Z and weaker emission at 527 nm due to F - Z was seen. The F - Z emission at room temperature was due to thermalization. However, even at liquid nitrogen temperature a weak fluorescence was seen at 527 nm which could be due to weak upconversion phenomena taking place in the material simultaneously and requires more work to fully confirm..

KEY WORDS: rare earth spectra, energy upconversion, glass.

Excited state absorption cross section measurement in rhodamine 6G tetrafluoroborate

B.R.Reddy and P. Venkateswarlu

Alabama A&M University, Department of Physics, P.O.Box 1268, Normal, Alabama 35762 USA

Abstract

Excited state absorption and optical phase conjugation have been demonstrated in rhodamine 6G tetrafluoroborate doped in sucrose at 514.5 nm. Excited absorption cross section has been estimated to be $(2\sim0.3)\times10^{-17}$ cm^2 using the data of pump-probe technique and saturation measurements. The magnitude of it's third order nonlinear susceptibility is estimated as $(3\sim0.2)\times10^{-2}$esu.

Organic dyes are useful as laser media [1] and nonlinear substances [2-7]. In future dye doped condensed media may be useful in waveguide applications also. Excited dye molecules always undergo intersystem crossing from the singlet states to the triplet states. In condensed media triplet states possess long lifetimes due to the absence of their quenching mechanisms. Hence a laser that is resonant with the singlet states is also resonant with the triplet states due to their comparable energy spacing and causes excited state absorption. This sets a serious limitation on the lasing efficiency and as well alters the magnitude of its third order nonlinearity. Hence for any quantitative analysis a meaningful estimate of ground and excited state absorption (ESA) cross sections of the transitions is needed. There is not enough information on ESA cross sections in the literature [1]. Here we present an unambiguous way for demonstrating and measuring the excited state absorption cross section of organic dyes. We also measured the magnitude of its third order susceptibility in this sample for the first time.

Sample preparation is quite easy. Appropriate quantities of sucrose and dye are measured so that their molecules are in the ratio of 10^4:1. Sucrose is heated at 200^0C for about ten minutes and then the dye is added, mixed well and then sandwiched between two glass slides. The thickness of samples used in this study is ~1.3 mm and the concentration of the dye is ~$6.9 \times 10^{17} cm^{-3}$. The samples lasted for several days in air conditioned rooms. In hot (above 30^0C) and humid rooms the sample makes a slow transition from rigidity to the syrup state after couple of weeks time because sucrose is hygroscopic. An absorption spectrum showed two peaks at ~300 and 534 nm (fig.1). The sample exhibited fluorescence in the region

520-700 nm when irradiated with an excimer laser operating at 308 nm. When the laser was suddenly turned off the sample exhibited much weaker delayed emission which lasted for about 2.8 sec. This indicates that the triplet state is getting populated and the intersystem crossing rate/triplet yield is much less.

Measurement of transmission data as a function of laser intensity exhibited saturation behavior and the absorption coefficient was estimated at all these input powers. For ideal saturable absorbers the absorption coefficient varies as [8]

$$a(I) = a_0/(1+I/I_s), \qquad (1)$$

where I_s is the saturation intensity at which the absorption coefficient is reduced by a factor of two from the small signal value (a_0). However the transmission data of dyes doped in condensed media deviate from such ideal behavior due to the formation of dimers [2] and excited state absorption [6]. The kink on the high energy side in the absorption spectrum is due to formation of dimers. A typical energy level diagram shown in fig.2 depicts these transitions. Hence the absorption coefficients and the saturation intensity were estimated by numerically integrating the equation

$$\frac{dI}{dz} = -(a_1 + a_2)I , \qquad (2)$$

and fitting with the experimental data. In the above a_1 and a_2 are the ground and excited state absorption coefficients. For a linearly polarized laser beam the ground state absorption coefficient is given by [6]

$$a_1 = \frac{a_0}{s}\left[1 - \frac{\tan^{-1}\sqrt{s}}{\sqrt{s}}\right], \qquad (3)$$

where s is the saturation parameter given by $s=I/I_s$. The percentage

transmission of the sample is plotted as a function of input laser intensity in fig.3. The solid curve is the theoretical fit obtained for a_0 = 9.4 cm^{-1}, a_2 = 7.5 cm^{-1} and I_s=109 mW/cm^2. We fitted such theoretical curves to different sets of transmission data of the same sample. The mean values of these parameters are a_0 = 10~0.6 cm^{-1}, a_2 = 6.5~1 cm^{-1} and I_s=107~2 mW/cm^2 and the uncertainties are the standard deviations. Our estimates are reliable because the low power absorption coefficient (a_0) estimated from the fit agrees with the mean value of the measurements. Since the concentration of the dye molecules, N is known the ground state absorption cross section, r_1 is estimated using a=Nr, as $(1.45\sim0.08)\times10^{-17}$ cm^2. Under steady state the population in the excited state, n_2 is given by [2]

$$n_2 = NI/(I+I_s). \qquad (4)$$

For an input intensity of 90.5 mW/cm^2, $n_2=3.16\times10^{17}$ cm^{-3} When a_2=6.5 cm^{-1} the corresponding excited state absorption cross section r_2 becomes $(2\sim0.3)\times10^{-17}$ cm^2.

Since the metastable triplet state is populated in intersystem crossing it should be possible to experimentally demonstrate excited state absorption (ESA) using the standard pump-probe configuration [9] In this experiment incoherent pump and probe beams at 514.5 nm irradiate the same location of the sample. The transmitted probe beam power is measured during the absence and presence of a strong pump beam.

$$I_u = I_0 \exp(-r_1 N l) \qquad (5)$$

$$I_p = I_0 \exp(-r_1 n_1 l - r_2 n_2 l) \qquad (6)$$

where l is the thickness of the sample, I_0 is the incident probe beam power, I_u and I_p are the transmitted probe beam intensities during the absence and presence of the strong pump beam, n_1 and n_2 are the populations in the

ground and excited states and r_1 and r_2 are the ground and excited state absorption cross sections. The transmitted probe beam power increased when the pump beam was turned on. The change in absorption coefficient is given by

$$Da = a_2 - a_1 = n_2(r_2 - r_1) = \ln(I_u/I_p)/l \ , \qquad (7)$$

Da was estimated for different input powers and was found to be negative. This indicates that $r_2 < r_1$. Da=-0.34 when the pump beam intensity is of 90.5 mW/cm^2. By substituting for n_2, r_1 and Da into eq.(5) r_2 is estimated as $1.34 \times 10^{-17} cm^2$. Da was measured at several pump beam intensities. The mean estimate for $r_2 = (1.2 \sim 0.14) \times 10^{-17} cm^2$. This value is comparable to that obtained from curvefitting of the transmission data (fig.3).

Degenerate four wave mixing (DFWM) experiments were performed with an Ar^+ laser in the standard retroreflected configuration to detect phase conjugate (PC) signals [7]. PC signals were generated with 514.5 nm laser wavelength only because the other argon ion laser wavelengths are not falling in the absorption spectrum of the sample. PC reflectivities are $\sim 10^{-5}$ but the required input powers are about 50 mW in this configuration which is due to less triplet yield. PC signals were found to be exponential and decayed with a time constant of 137 msec (fig.4). This clearly suggests that PC signals lasted only so long as there exists population in the excited state. The expression used to fit the signal is shown in the inset. The first term represents the background due to scattered light and its magnitude was found to be correct.

The third order nonlinear susceptibility $v^{(3)}$ is estimated by using [6]

$$v^{(3)} = n^2 c^2 a_0 (d+i)/24p^2 x I_s , \qquad (8)$$

where n is the refractive index, c is the speed of light, x is the laser

frequency and d is the normalized detuning parameter given by

$$d = (x - x_0)s_2 , \qquad (9)$$

where x_0 is the the resonance frequency and s_2^{-1} equals half-width at half maximum of a homogeneously broadened absorption transition. The absorption transition was assumed to be homogeneous in this case. d was estimated to be 0.7. The refractive index at 514.5 nm is estimated using the relation

$$n^2 = A + \frac{B k^2}{k^2 - C} - D k^2 , \qquad (10)$$

where A, B, C and D are the sellmeier's constants [10] and k is the laser wavelength. Since the sucrose sample is amorphous, an average value for $n=(n_x + n_y + n_z)/3$ was obtained as 1.56. By substituting the values for n, a_0, I_s and d into Eq.(6), $v^{(3)}$ is estimated as $2.4(0.7+i)\times10^{-2}$ esu whose magnitude is $\sim(3\sim0.2)\times10^{-2}$ esu. This value is much smaller when compared to that of *fluorescein* [6] because of the small absorption coefficient and large saturation intensity. The absorption coefficient is smaller because the laser wavelength falls in the wing of the absorption spectrum. The saturation intensity is much higher because the intersystem crossing rate/triplet yield is much less.

We have demonstrated optical phase conjugation in sucrose doped with R6G tetrafluoroborate that was not studied in the past and measured its nonlinearity. The PC reflectivities ($\sim10^{-5}$) of this sample are a factor of 10 more than those measured in boric acid host [11]. Thicker samples of sucrose can be prepared easily while that is not possible with boric acid glass [6]. The performance of this host material is as good as any other host except for its long term stability. Our measurements indicate that sucrose sample is certainly useful as a host to characterize organic dyes for nonlinear optical phenomena. Excited state absorption measurements are

useful in characterizing the efficiency of laser dyes and of dye doped waveguides because ESA limits their efficiency. We have discussed two different approaches to estimate ESA cross sections. There is not much information about ESA cross sections in the literature. Hence sucrose material is particularly suitable to measure the much needed excited state absorption cross sections of laser dyes.

Acknowledgement

This work has been supported by a grant from the Department of Air Force grant# AFOSR-90-0160.

References

[1] F.P. Schafer, Dye lasers, 3rd edition; Topics in Appl. Phys. Vol.1 (Springer-Verlag, Berlin 1990).

[2] Y. Silberberg and I. Bar-Joseph, Optics Commun. 39 (1981) 265.

[3] H. Fujiwara and K. Nakagawa, Optics Common. 55 (1985) 386.

[4] T.Todorov, L. Nikolova, N.Timova and V. Dragostinova, IEEE J.Quan. Elect. QE-23 (1986) 1262.

[5] I.V. Tomov, B. VanWonterghem, A.S. Dornikov, T.E. Dutton and P.M. Rentzepis, J.Opt.Soc.A me.B8 (1991) 1477.

[6] M.A. Kramer, W.R. Tompkin and R.W. Boyd, Phys.Rev.A 34 (1986) 2026.

[7] B.R.Reddy, P.Venkateswarlu and M.C.George, Optics Common. 84 (1991) 334; 86 (1991) 555.

[8] M. Hercher, Appl.Optics 6 (1967) 947.

[9] R. Moncorge and T. Benyattou, Phys.Rev. B27 (1988) 9186.

[10] J.M. Halbout and C.L. Tang, IEEE J. Quant. Electron. QE-18 (1982) 410.

[11] G.R. Kumar, B.P. Singh and K.K. Sharma, Optics Commun. 73 (1989) 81.

FIGURE CAPTIONS

Fig.1 Absorption and fluorescence spectra of sucrose doped with R6G tetrafluoroborate.

Fig.2 Partial energy level diagram of a typical dye molecule showing the ground and excited state absorption transitions.

Fig.3 Transmission of the dye doped sample as a function of the incident intensity.

Fig.4 Phase conjugate signal decay in the dye doped sucrose sample.

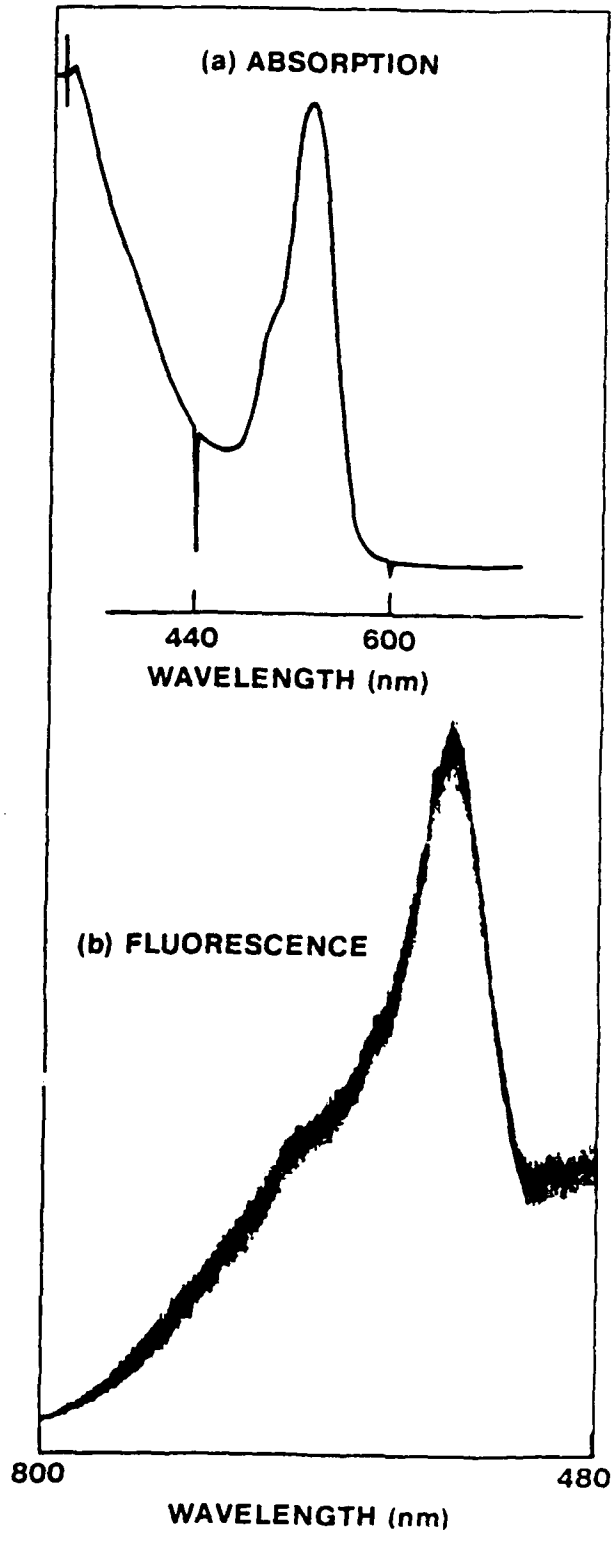
(a) ABSORPTION
440
600
WAVELENGTH (nm)
(b) FLUORESCENCE
800
480
WAVELENGTH (nm)

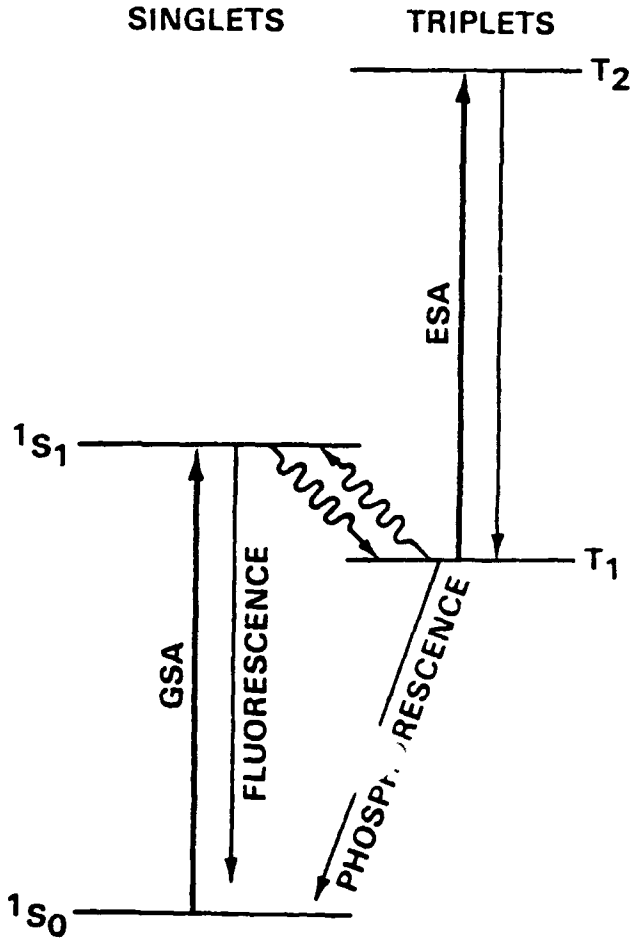
SINGLETS
TRIPLETS
T2
ESA
1S1
T1
GSA
FLUORESCENCE
PHOSPHORESCENCE
1S0

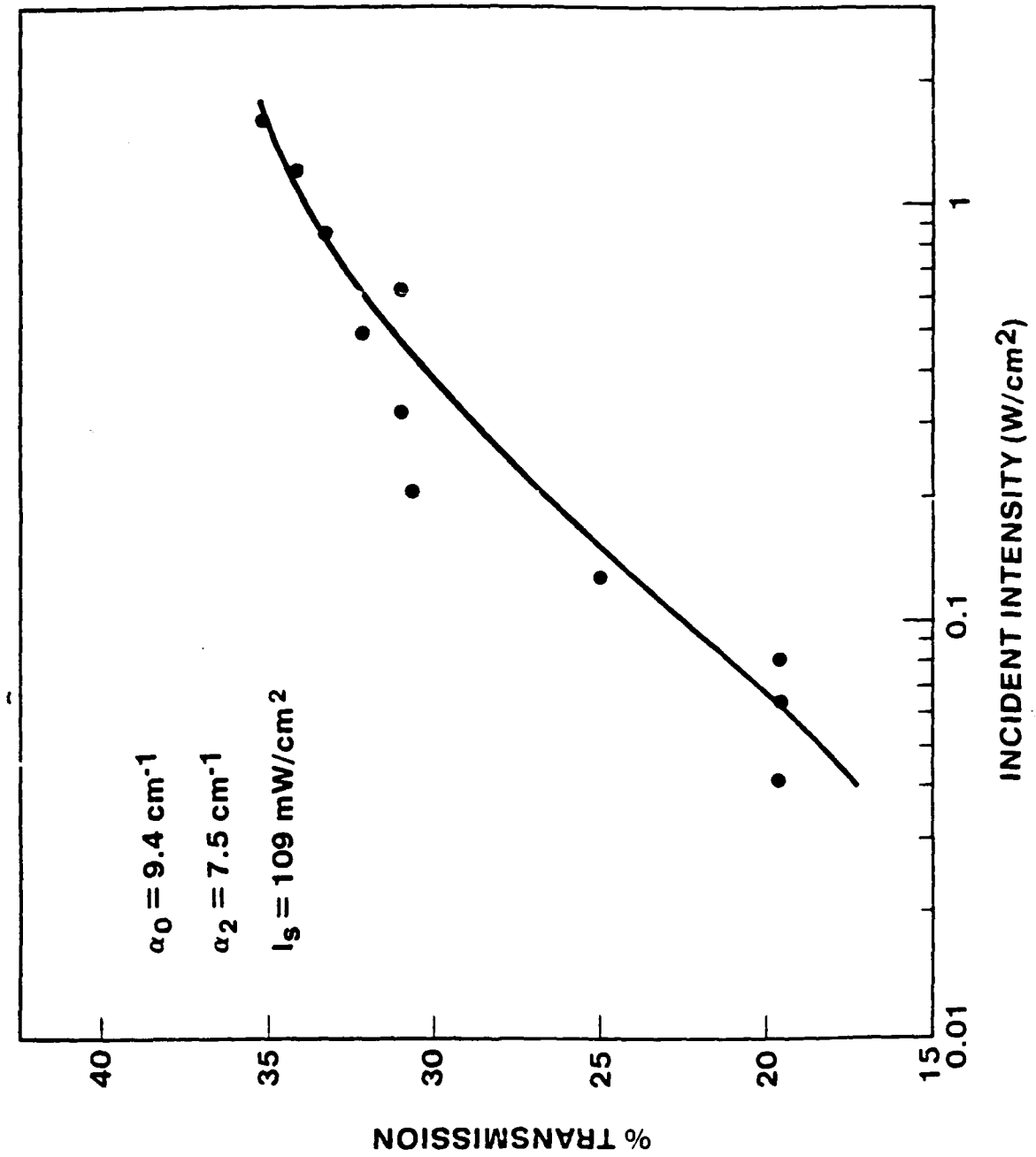
% TRANSMISSION
40
35
30
25
20
15
0.01
0.1
1
INCIDENT INTENSITY (W/cm²)
$\alpha_0 = 9.4\ cm^{-1}$
$\alpha_2 = 7.5\ cm^{-1}$
$I_S = 109\ mW/cm^2$

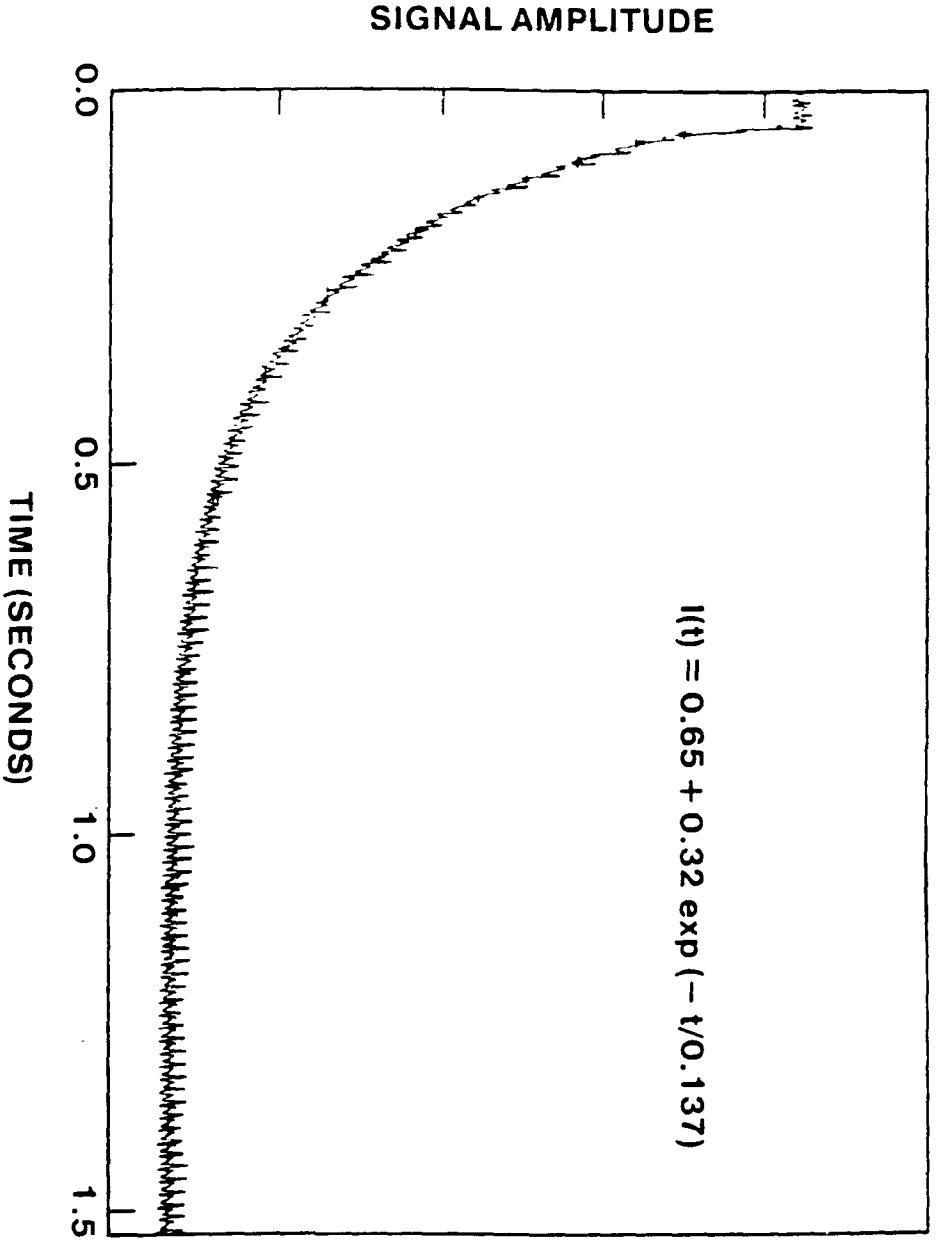
SIGNAL AMPLITUDE
0.0
0.5
1.0
1.5
TIME (SECONDS)
I(t) = 0.65 + 0.32 exp (− t/0.137)

Physics and Chemistry of Glasses (to be submitted)

Spectroscopic Studies of Silicate Glasses doped with Rare Earth Ions

B.R. Reddy, Anthony Ololo and P. Venkateswarlu

Department of Physics, P.O. Box 1268, Alabama A&M University, Normal, Alabama 35762 USA

Abstract

Sodium borosilicate glasses were prepared with Pr^{3+}, Nd^{3+} and Er^{3+}as dopants. Refractive index of the pure glass was found to be 1.49±0.01. The absorption and laser excited fluorescence spectra of the rare earth ion doped materials were recorded to understand their relaxation mechanisms. Energy upconversion efficiency is found be very weak due to nonradiative relaxation of the excited levels.

Introduction

Rare earth ion doped solids have been studied extensively[1] because of their suitability in the development of lasers. Rare earth ions also generate upconverted emission[2] due to sequential multiphoton excitation (single ion process) or energy transfer interaction (multi-ion process). Recently upconverted lasers were developed in different crystals and fibers doped with rare earth ions[3]. So there has been a renewed interest to look for different materials which can upconvert energy. In an effort to identify new upconversion materials we prepared sodium borosilicate glasses doped with rare earth ions and performed optical studies of these materials.

Sample Preparation and Characterization

The starting materials used were Na_2CO_3, H_3BO_3, SiO_2 and $R_2(SO_4)_3$, where R is a rare earth element. At higher temperatures these chemicals were known to oxidize/pyrolize to the corresponding oxides. Boric acid was added to reduce the viscosity of the melt. These chemicals were ground, mixed thoroughly and heated in a box furnace using an aluminum crucible in ambient atmosphere at 800^0C for two hours, and at 1350^0C for another two hours, and then the melt was allowed to cool naturally in aluminum molds. The resulting glass is highly transparent, hard and nonhygroscopic. They are polished using silicon carbide (grit 600), aluminum oxide (9.5 micron) and iron oxide (3 micron) powders for 15 minutes with each powder on each face in that order. When the glass was viewed under polariscope it exhibited a fringe pattern characteristic of strain. Nonetheless, these glasses were not annealed because it did not affect our measurements. Based on the the selected quantities, the glass is expected to have the following composition: Na_2O(13.6 mol%), SiO_2(24 mol%), B_2O_3(62.4 mol%). When the sample surface was observed for elemental analysis using a scanning electron microscope and energy dispersive X-ray analysis technique, it revealed a peak corresponding to aluminum in addition to those of other elements. Aluminum must have come from the crucible because the starting chemicals did not contain it. However, Al_2O_3 was known to strengthen the glass.[4] Refractive index of an undoped glass prism was measured using the angle of minimum deviation technique[5] with a prism spectrometer. Refractive index η is computed using the relation

$$\eta = \frac{\mathrm{Sin}(\alpha+\delta_0)/2}{\mathrm{Sin}\ \alpha/2} \qquad (1)$$

where α (60^0) is the refracting angle of the prism and δ_0 is the angle of minimum deviation. The mean refractive index is found to be 1.49±0.01 and remained the same in the whole visible region (measured at Ar^+ and He-Ne laser wavelengths). Pure glass also exhibited very weak emission when excited with a R6G dye laser which may be due to impurities present in the host glass material or the host glass itself. The concentrations of these elements are very low and hence were not detected in the X-ray analysis. However the signals due to the rare earth impurities are several orders of magnitude larger than those due to the other impurities.

Absorption Spectra

Absorption spectra of the rare earth doped samples were measured using Perkin-Elmer and Beckman spectrophotometers. A pure glass was used as reference. The absorption spectra of Pr^{3+}, Nd^{3+} and Er^{3+} are shown in figs. 1-3. All the characteristic peaks of these elements are present in their expected positions. Absorption due to host glass is below 340 nm. The spectra of rare earths is due to transitions within the f^n electronic energy levels. The crystal field splitting is less than the strength of the spin-orbit coupling. Hence the centers of gravity of these multiplets approximately remain the same. The identification of the transitions is done by comparing the spectra with those observed in the other host materials.[1,6] The transitions are identified in tables 1-3.

Fluorescence Spectra

Excited ions relax radiatively and nonradiatively.[7] The nonradiative relaxation is of two types (1) phonon/multi-phonon decay and (2) ion-ion interactions. The former depends on the energy gap between the energy levels and the cut-off phonon frequency of the host lattice and exhibits temperature dependence.[7] Multiphonon decay was observed even when the energy gap was matched with six phonons. The energy transfer efficiency depends on the energy gap matching of the ion-pair transitions, nature of the coupling between the interacting ions and on inter-ion separation.[8]

We have used Ar^{+}, second and third harmonics of YAG:Nd^{3+} and dye lasers to induce fluorescence in the glasses. The sample fluorescence was processed by an Acton Research Corporation triple grating monochromator equipped with R928 photomultiplier tube (PMT) or a SPEX double monochromator fitted with R943-02 PMT. The PMT output was amplified and then plotted on a strip chart recorder. To measure the time dependence of the signals the samples were irradiated with an excimer pumped dye laser. The PMT output was given to an oscilloscope to observe the transient signals and then 1/e decay time was directly measured from the scope display. Fluorescence was recorded when the sample was at room temperature (RT) as well as at liquid nitrogen temperature (LNT).

Pr^{3+} Fluorescence

With 580 nm excitation we have seen three bands at 601.7 ($^1D_2$-- $^3H_4$), 698.4 ($^1D_2$-- $^3H_5$) and 805.3 nm ($^1D_2$--$^3H_6$). On excitation with 476.5 nm we have seen fluorescence from $^3P_0$ to $^3H_{4,5,6}$; $^3F_{2,3,4}$ and $^1D_2$ to $^3H_6$. In

summary, fluorescence is seen only from $^1D_2$ and $^3P_0$ and $^3P_{1,2}$ levels are relaxing nonradiatively to $^3P_0$. In this material, $^3P_0$ state is undergoing some nonradiative relaxation to $^1D_2$ which was absent in LaF_3 due to lower cut-off phonon frequency in the latter.[7]

Nd^{3+} Fluorescence

In general fluorescence is detected from the R and S levels only whenever the energy levels higher to them were excited (fig.4). The energy gap between the R and S levels, $\Delta E \cong 900\ cm^{-1}$. The population ratio of the levels $S/R \sim \exp(-\Delta E/kT) = 0.012$, where k is the Boltzmann constant. The oscillator strengths of S-->Z and R-->Z in LaF_3 are[9] 3.49 and 1.09 respectively. If we assume the same oscillator strengths to be valid for this glass host then the intensity ratio of S-->Z to R-->Z transitions is ~1:25 and the measurement is in agreement with the predicted ratio. In such a case, the S level population exists so long as there is population in the R level. Accordingly, the lifetimes of the S and R levels were found to be equal and was ~265 μsec. When the material was cooled, the S-->Z emission intensity decreased. Hence, at RT the emission of S levels is due to Boltzmann distribution/thermalization only. However, at high incident laser powers we did find fluorescence from B, D and E levels also. When the sample was irradiated with 355 nm (TH of YAG) we did observe violet/blue emission from Nd^{3+} in the 380 - 453 nm region. Hence, it may be possible to upconvert energy in this material.

Er^{3+} Fluorescence

No fluorescence was seen when the material was excited with R6G dye laser. Emission was always seen from the E and B levels at 870 nm (E--->Y) and 820 (B--->Z) whenever any level above E was excited. On excitation with 488 nm, we have observed fluorescence from G--Z (very weak), F--Z (medium intensity) and E--Z (strong) at 500, 527 and 546.6 nm respectively (fig.5). The energy gap between the E and F levels is 743 cm^{-1}. For small energy gaps the upper level was not known to radiate but relaxes nonradiatively. At RT the Boltzmann distribution predicts a population ratio of the levels, F/E ~ 0.026. The oscillator strengths of Z--F and Z--E are found[9] to be 11.03 and 0.34 respectively in $LaF_3:Er^{3+}$. If we assume the same values of oscillator strengths to be valid for this material also, then, the expected ratio of their fluorescence transitions is ~0.8. In our measurements the intensities of the peaks are in the ratio of 0.4. Such a deviation is expected, because, (1) in our estimation we assumed a constant energy gap of ~743 cm^{-1} between the levels E and F, while the electrons are distributed among all the Stark components; (2) the oscillator strengths are only approximate for this material and not accurate and (3) the detector (R928) sensitivity decreased by 3% at 546 nm. A plot of peak intensity of 527 nm versus laser power revealed linearity suggesting taht a single photon is involved in the generation of 527 nm. At LNT the emission from the F level was not absent but was very weak possibly because, the material might not be exactly at LNT due to improper contact with the cold finger of the cryostat. Hence, the F and G levels are populated by thermalization only. On excitation of the

material with 355 nm, we did observe emission in the region 350-450 nm.

Energy Upconversion

Energy upconversion occurs by excited state absorption, sequential multiphoton excitation (single ion process) and/or energy transfer interaction.[2,10] Rare earth ion doped materials are favorable for such interactions because of their complex energy level structure and a photon that is resonant from the ground state may also be resonant from an excited state. We have detected weak upconverted emission from the L levels of Nd^{3+} in sodium borosilicate glass (fig.6) when its E levels were resonantly excited with 514.5 nm (the sample was at cryogenic temperature). The excited ion relaxes to the longlived R levels which is then picked up by another photon to L levels. The energy gap between the L and K multiplets ~2000 cm^{-1}, hence the former tends to relax nonradiatively and hence no upconverted emission was detected at RT. The intensity of the upconverted signals depended on the spatial location of the exciting beam in the material. We also observed energy upconverted emission from the E levels of Er^{3+} in sodium borosilicate glass (fig.7), when its B levels were resonantly excited with a near IR laser of 800 nm at room temperature. The excited ion in the B level relaxes to the Y level which is then picked up by another photon to a higher level, F. The energy gap between the E and D levels is ~3000 cm^{-1} (larger than in Nd^{3+}) hence the multiphonon decay rate is lower than for the case of Nd^{3+}. So, upconverted emission was detected in Er^{3+} at RT while it was absent in Nd^{3+} at RT. In general, the upconverted emission is too weak because of the high nonradiative relaxation rate of the excited

levels[7] due to large cut-off phonon frequency expected for this host, due to the presence of lighter elements like boron, silicon, sodium, oxygen and hydrogen in the starting chemicals. To improve the upconversion efficiency one has to select a glass composition of heavy metallic elements, so that the cut-off phonon frequency is lower. Our results indicate that for energy upconversion purposes, only those materials posessing low cut-off phonon frequency are suitable.[11] In a glass there is no long range order. So, the number of lighter elements in the vicinity of rare earth ion site will vary depending on the spatial location. An excited ion surrounded by heavy elements tends to relax radiatively rather than nonradiatively. That is the reason why, the upconverted emission intensity depended on the spatial location of the laser beam.

This research was supported by U.S Air Force, grant # AFOSR-90-0160.

References

(1) G.H. Dieke, Spectra and energy levels of rare earth ions in crystals (Wiley, New York, 1968).

(2) F. Auzel, Proc. IEEE, 61, 758 (1973).

(3) R. M. MacFarlane, Upconversion lasers, Optics & Photonics News, March 1992, page 8.

(4) R.H. Doremus, Glass Science, Wiley, NY 1973.

(5) Central Scientific Instruments, Catalog

(6) J.G. Edward, Glass Lasers, CRC Press, Cleveland, Ohio 1970.

(7) M.J. Weber, phys.rev. 157, 262 (1967).

(8) B.R. Reddy and P. Venkateswarlu, J. Chem. Phys. 77, (1982).

(9) W.F.Krupke, Phys.Rev 145, 325 (1968).

(10) B.R.Reddy and P. Venkateswarlu, J. Chem. Phys.79, 5845 (1983).

(11) B.R. Reddy and P. Venkateswarlu, Appl. Phys. Lett. (submitted).

Figure Captions

(1) Absorption Spectrum of Pr^{3+} in Sodium borosilicate glass.

(2) Absorption Spectrum of Nd^{3+} in Sodium borosilicate glass.

(3) Absorption Spectrum of Er^{3+} in Sodium borosilicate glass.

(4) Fluorescence Spectrum of Nd^{3+} in Sodium borosilicate glass.

(5) Fluorescence Spectrum of Er^{3+} in Sodium borosilicate glass.

(6) Energy upconverted spectrum of Nd^{3+} in Sodium borosilicate glass.

(7) Energy upconverted spectrum of Er^{3+} in Sodium borosilicate glass.

Table 1 Absorption Spectrum of Pr^{3+} in Sodium Borosilicate Glass

Wavelength (nm)	Energy (cm^{-1})	Transition Initial Level	Transition Final Level	Relative Intensity
444	22,516.2	$^3H_4$	$^3P_2$	Medium
470	21,270.7	"	$^3P_1$	Medium
482	20,741.1	"	$^3P_0$	Medium
590	16,944.5	"	$^1D_2$	weak
939	10,646.7	"		
964	10,370.6	"	$^1G_4$	Medium

Table 2 Absorption Spectrum of Nd^{3+} in Sodium Borosilicate Glass

Wavelength (nm)	Energy (cm^{-1})	Transition Initial Level	Transition Final Level	Dieke's Notation	Relative Intensity
351	28,481.9	$^4I_{9/2}$	$^4D_{1/2}$	L	Shoulder
357	28,003.2	"	$^4D_{3/2}$	L	Strong
429	23,303.5	"	$^2P_{1/2}$	I	Weak
460	21,733.1	"	$^4G_{11/2}$	G	Weak
471	21,225.5	"	$^2D_{3/2}$	G	Weak
474	21,091.2	"	$^4G_{9/2}$	G	Weak
511	19,564	"	$^2G_{9/2}$	F	Medium
524	19,078.4	"	$^4G_{7/2}$	E	Strong
581	17,207	"	$^4G_{5/2}$	D	Strong
626	15,970	"	$^2H_{11/2}$	C	Very weak
679	14,723.5	"	$^4F_{9/2}$	B	Medium
738	13,546.4	"	$^2S_{3/2}$	A	Strong
745	13,419	"	$^4F_{7/2}$	A	Strong
794	12,591	"	$^4F_{5/2}$	S	Strong
800	12,496.6	"	$^4F_{5/2}$	S	Strong
862	11,597.8	"	$^4F_{3/2}$	R	Weak
872	11,451.6	"	$^4F_{3/2}$	R	Weak
950	10,523.4	"			

Table 3 Absorption Spectrum of Er^{3+} in Sodium Borosilicate Glass

Wavelength (nm)	Energy (cm^{-1})	Transition Initial Level	Transition Final Level	Dieke's Notation	Relative Intensity
341	29,343				Shoulder
357	28,003.2	$^4I_{15/2}$	$^2G_{7/2}$	O	Weak
365	27,389.5	"	$^2K_{15/2}$		
			$^2G_{9/2}$	N	Medium
377	26,517.7	"	$^4G_{11/2}$	L	Strong
408	24,502.9	"	$^2H_{9/2}$	K	Weak
450	22,216	"	$^4F_{3/2}$, $^4F_{5/2}$	I,H	Weak
487	20,528.2	"	$^4F_{7/2}$	G	Medium
521	19,188.5	"	$^2H_{11/2}$	F	Strong
542	18,445.1	"	$^4S_{3/2}$	E	Very weak
574	17,416.78				Nd^{3+}
581	17,207				Nd^{3+}
650	15,380.4	"	$^4F_{9/2}$	D	Medium
742	13,473.4	"		B	Weak
801	12,481	"	$^4I_{9/2}$	A	Weak
976	10,241.1	"	$^4I_{11/2}$		Weak

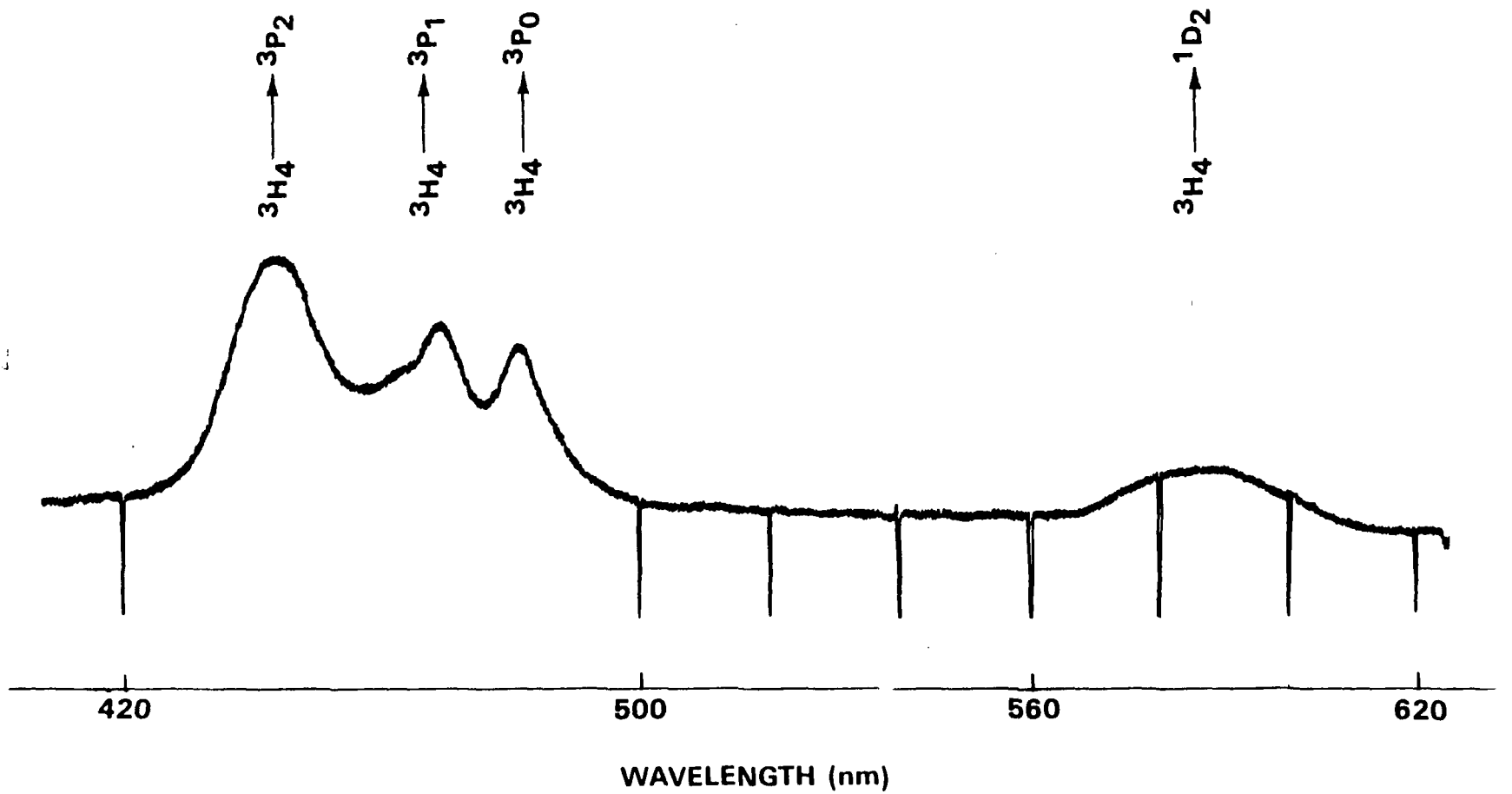
$^3H_4 \rightarrow {}^3P_2$
$^3H_4 \rightarrow {}^3P_1$
$^3H_4 \rightarrow {}^3P_0$
$^3H_4 \rightarrow {}^1D_2$
420
500
560
620
WAVELENGTH (nm)

960
600
400
320
Z → R
Z → S
Z → A
Z → B
Z → C
Z → D
Z →
Z → F
Z → G
Z → G
Z → I
Z → L
Z → L

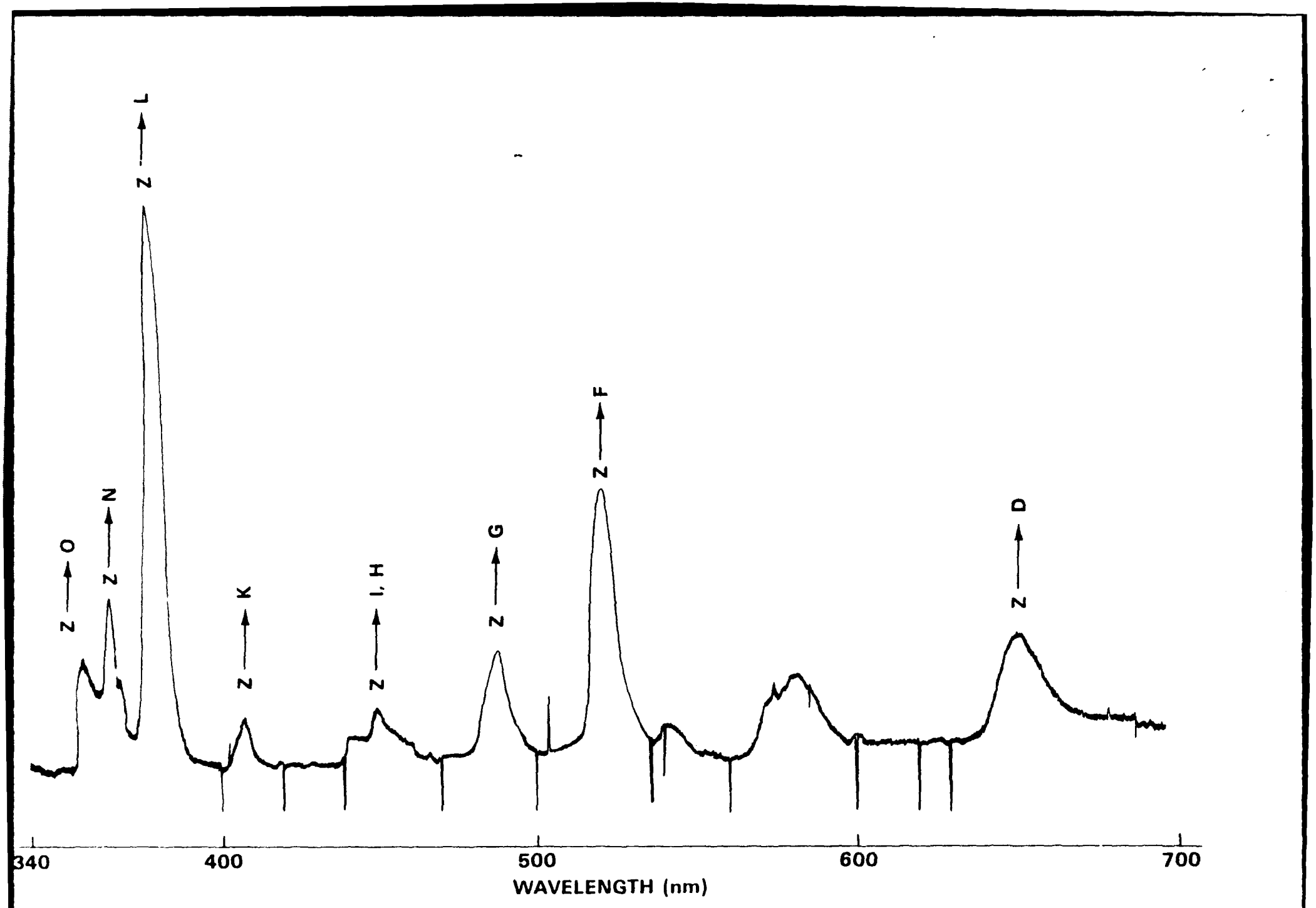
Z → O
Z → N
Z → L
Z → K
Z → I, H
Z → G
Z → F
Z → D
340
400
500
600
700
WAVELENGTH (nm)

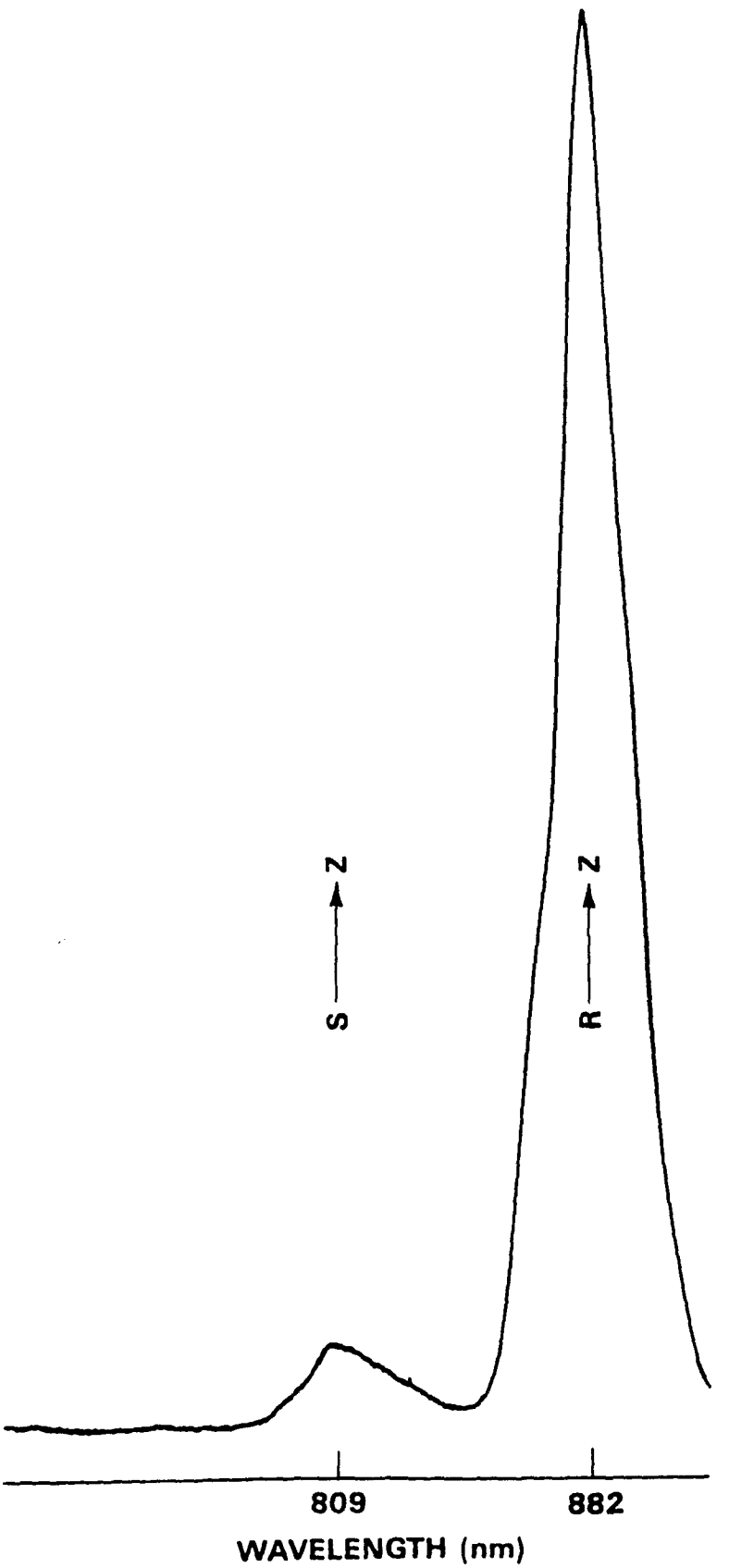
S
Z
R
Z
809
882
WAVELENGTH (nm)

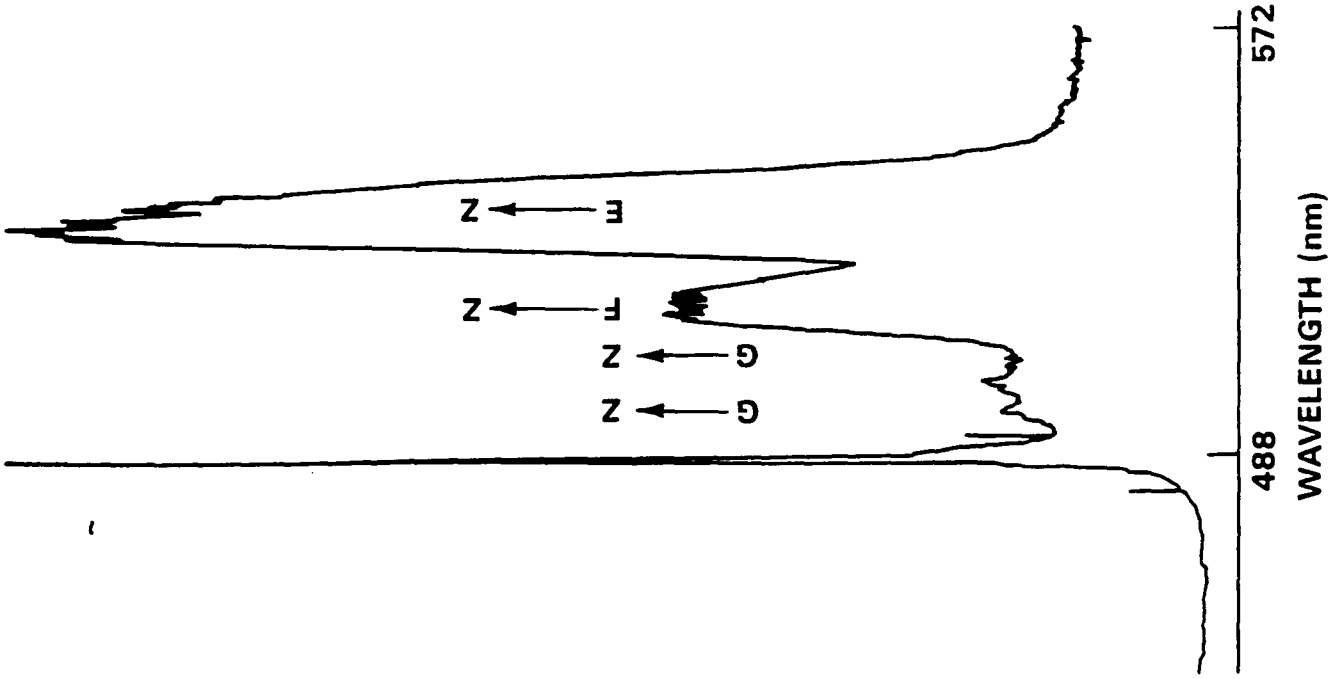
572
488
WAVELENGTH (nm)
E → Z
F → Z
G → Z
G → Z

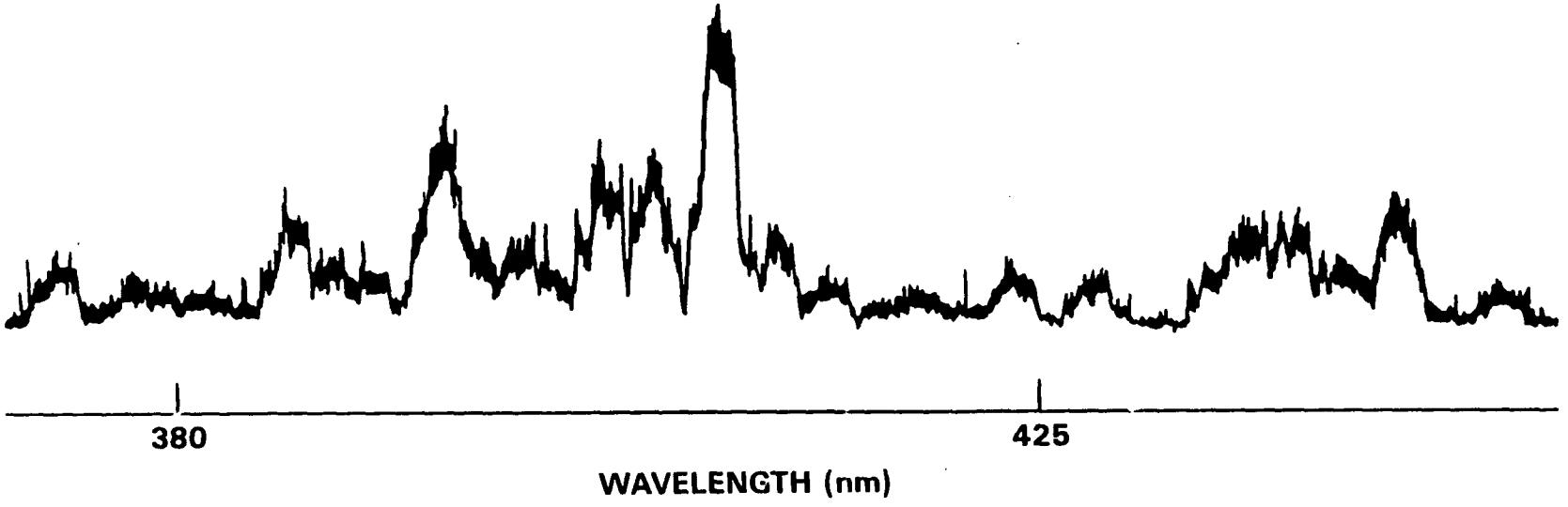
380
425
WAVELENGTH (nm)

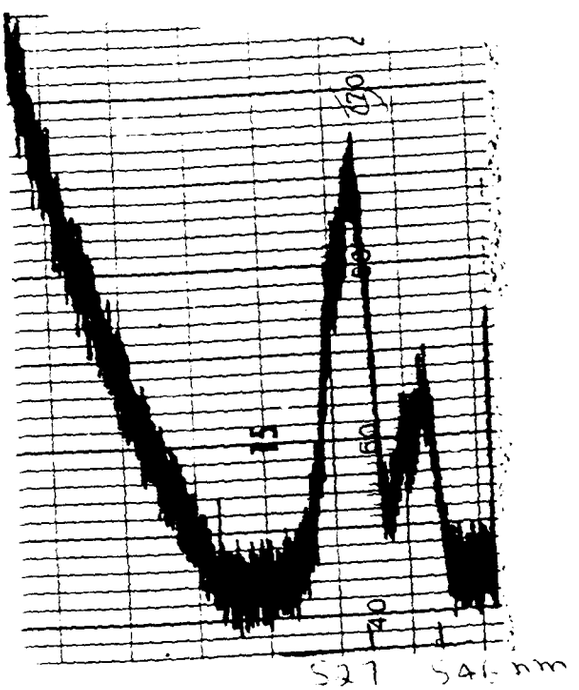
120
80
40
527
541 nm

NEAR-INFRARED TO BLUE ENERGY UPCONVERSION IN $LaF_3:Ho^{3+}$

B.R. Reddy, S.N. Stevenson and P. Venkateswarlu
Department of Physics, P.O. Box 1268
Alabama A&M University, Normal, AL 35762

Abstract

When the D levels of Ho^{3+} in LaF_3 were resonantly excited with a red dye laser beam of 640 nm blue and green emission was detected from the J, F and E levels at 416, 485 and 546 nm respectively. Excited ion in the D state is undergoing nonradiative relaxation to the A state and then is getting upconverted by another photon to the J state. The upconversion efficiency into the F state was estimated as $\sim 5.7 \times 10^{-4}$. We also observed energy upconverted emission from the F and E levels when the phonon coupled levels of of the B state were excited with 800 nm near infrared laser. The absorption of a second laser photon from the A state was found to be responsible for the upconverted green emission.

Introduction

Sequential two-photon/multi-photon excitation, energy transfer interaction, and excited state absorption/avalanche absorption were found to be responsible for the production of energy upconverted emission in rare earth ion doped crystals.[1] Rare earth ion doped materials were investigated extensively because of their use in the generation of laser sources, luminescent materials, detection of infrared radiation and recently for the production of upconversion lasers.[2] However, the efficiency of upconverted lasers was limited by nonradiative relaxation[3] of the excited and upconverted energy levels and Boltzmann distribution of electronic population. Boltzmann distribution can be minimized by cooling the material. Upconverted emission intensity will be significant if the host material has low cut-off phonon frequency and wide energy gap between the upconverted energy level and its next lower level. There is an energy gap of ~3000 cm^{-1} between the E and D levels of Ho^{3+} and the cut-off phonon frequency[3] of LaF_3 is about 350 cm^{-1}. Also, Z-D energy gap is comparable with that of A-J. Hence LaF_3:Ho^{3+} is an ideal system to pursue energy upconversion studies.

Energy upconversion in Ho^{3+} was studied earlier in doubly doped crystals,[4-6] glasses,[7,8] fibers[9] and other crystals.[10,11] Ours is the first observation in LaF_3:Ho^{3+} and is the most efficient system for energy upconversion.

The crystals used in the study were obtained fron Optovac. An Ar^+ pumped CW dye laser and a Ti:Sapphire laser were used to excite the material. A medium resolution monochromator was used to process the signals and was

detected by a R928 photomultiplier tube. The PMT output was amplified and then given to a picoammeter and a chart recorder. In all these measurements the sample was at room temperature.

Near infrared to blue energy upconversion

A typical energy level diagram[12] of Ho^{3+} in LaF_3 is shown in Fig.1. The dye laser excited fluorescence is identified with solid lines and the infrared laser excited fluorescence is identified with dashed lines. When the crystal is exposed to the 800 nm radiation, we detected bright green emission from the material and is visible to the naked eye even for 40 mW of the laser beam. The resulting fluorescence was analyzed and found to arise from the E and F levels. The 800 nm laser excites the phonon coupled levels of the B state but is also in resonance from the excited state A to the F state. A plot of the fluorescence versus laser power exhibited a gradient of 1.5. Hence, at least two photons are responsible for the production of green emission. A direct two photon excitation is not possible because of the restriction $\Delta J \leq 2$. A step-wise excitation of the type Z-->B-->J is not happening because, no emission was seen from the J state with near infrared laser pumping. The last alternative left out is for the excited ion to relax to the A state and then get excited to the G state. In this case, the 800 nm photon is resonant with the A-->G transition also. The transition probability for the A-->G is about three times more than that from Z-->B. The G state relaxes to the F and E sates in cascade which emit the blue, 485 nm (F-->Z) and green 546 nm (E-->Z) radiation. The population in the A state saturates at high laser intensities because of its long lifetime ~5 msec

(estimated using the radiative[13] rate of 106 sec^{-1} and nonradiative[3] rate of 80 sec^{-1}). Hence the the upconverted emission exhibits a gradient of 1.5 in the power dependence. With 800 nm excitation, growth and decay were monitored at different emission wavelengths by turning the laser on and off with a fast light shutter. The resonant signals have grown and decayed within the response time of the electronic shutter ~3 msec. The signals at 488 and 540 nm grown to the maximum value in about 22 msec. This is the time required for the population in the A state to reach the steady state value.

Red to blue energy upconversion

When the D levels were resonantly excited with a dye laser we detected upconverted emission from the E, F and J levels at 548 (E-->Z), 485 (F-->Z) and 416 nm (J-->Z) respectively. The sample exhibited bright green fluorescence visible to the naked eye even for 30 mW of input laser power. A plot of signal intensity versus laser power exhibited a gradient of 1.5 when the laser beam was focused in a narrow region in the material and a value of 1.8 for a broad focus. This is a clear indication that excitation is getting saturated. A step-wise excitation of the type Z-->D-->P,Q or a direct two-photon excitation is not possible because no emission was observed from energy levels higher to the J state. In fact the levels M, N, P and Q were known to emit in LaF_3 host.[13] For the same region a step-wise excitation from either the B or the C levels was also ruled out. However, the 640 nm laser photon is resonant with Z-->D and A-->J transitions. F and E levels were populated in cascade by phonon emission from the J state and emit blue and green light. This suggests that sequential two-photon excitation is the

dominant mechanism in upconverting the excitation energy. We estimated the energy upconversion efficiency, η into the F state using

η = upconverted signal intensity/absorbed light intensity (1)

The upconverted signal intensity is estimated by comparing it with the directly excited emission intensity from the F state. For direct excitation its quantum efficiency, η_q is given by

η_q = emitted light intensity/absorbed light intensity = τ_{exp}/τ_{rad} (2)

where τ_{rad} and τ_{exp} are the radiative and experimentally measured lifetimes of the F state. The quantum efficiency of the F state is 0.85 and was obtained from the estimates of its radiative[13] and nonradiative rates.[3] Absorbed light intensity was determined from the measured incident light intensity, absorption coefficient and absorption pathlength in the sample. On substituting for these values, the upconverted efficiency is found to be $\sim 5.7 \times 10^{-4}$. This efficiency is much higher than the values obtained in other systems.[7]

Rate equations

Let N_0, N_1, N_2 and N_3 represent populations in the ground (Z), intermediate (A), resonantly excited (D), and upconverted (F) states respectively. These states are also represented by |0>, |1>, |2> and |3> respectively. Under steady state excitation conditions

$$\dot{N}_2 = 0 = N_0 A_{02} I_0 - N_2 \tau_2^{-1} \quad (3)$$

$$\dot{N}_1 = 0 = N_2 \sigma_{21} - N_1 \tau_1^{-1} - N_1 A_{13} I_0 \quad (4)$$

$$N_3 = 0 = N_1 A_{13} I_0 - N_3 \tau_3^{-1} \qquad (5)$$

where τ_1^{-1}, τ_2^{-1}, and τ_3^{-1} are the relaxation rates of the states |1>, |2> and |3> respectively and A_{ij} is the transition rate from level i to j. σ_{ij} is the nonradiative relaxation rate from level i to j. A solution of the rate equations yields

$$N_3 = N_0 A_{02} A_{13} I_0^2 \tau_2 \sigma_{21} \; / \; (A_{13} I_0 + \tau_1^{-1}) \; \tau_3^{-1} \qquad (6)$$

Since the upconverted emission intensity is proportional to the population in the F state, N_3, equation (6) predicts that the upconverted signal should vary linearly with ground state population/ ionic concentration and quadratically with the incident laser power. Our measurements of upconverted signal intensity as a function of concentration and laser power supports this model. However, the gradient in the signal versus laser power is less than two because of the saturation of excitation due to long lifetime of the intermediate level |1> (~5 msec) and high pump rate from the the ground state. The oscillator strength of Z-->B is about twice that of A-->J. Then the rate limiting process in the excitation mechanism is the absorption of the second photon. Hence the measured power dependence deviates from quadratic dependence. Since the D and A states possess long lifetimes[13] and there exists energy gap overlaps, an energy transfer upconversion interaction described by the following equation is also possible.

ion (D) + ion (A) ----> ion (J) + ion (Z) (7)

Two ions in the excited D and A states undergo energy transfer interaction

causing one ion to excite to the J state and simultaneously relaxing the other ion to the ground state, Z.

Conclusions

Our studies on $LaF_3:Ho^{3+}$ indicate that sequential two-photon excitation is the dominant mechanism in upconverting energy. The upconversion efficiency is found to be ~0.06%. We believe that this material will be useful to develop an efficient upconversion laser to operate at room temperature.

This research was supported by U.S. Air Force grant # AFOSR-90-0160 and NASA.

Figure Caption

Fig. 1: Partial energy level diagram of Ho^{3+} in LaF_3. ===> and ---> indicate 640 nm laser excitation and the resulting emission. ===> and ---> indicate 800 nm laser excitation and the resulting emission.

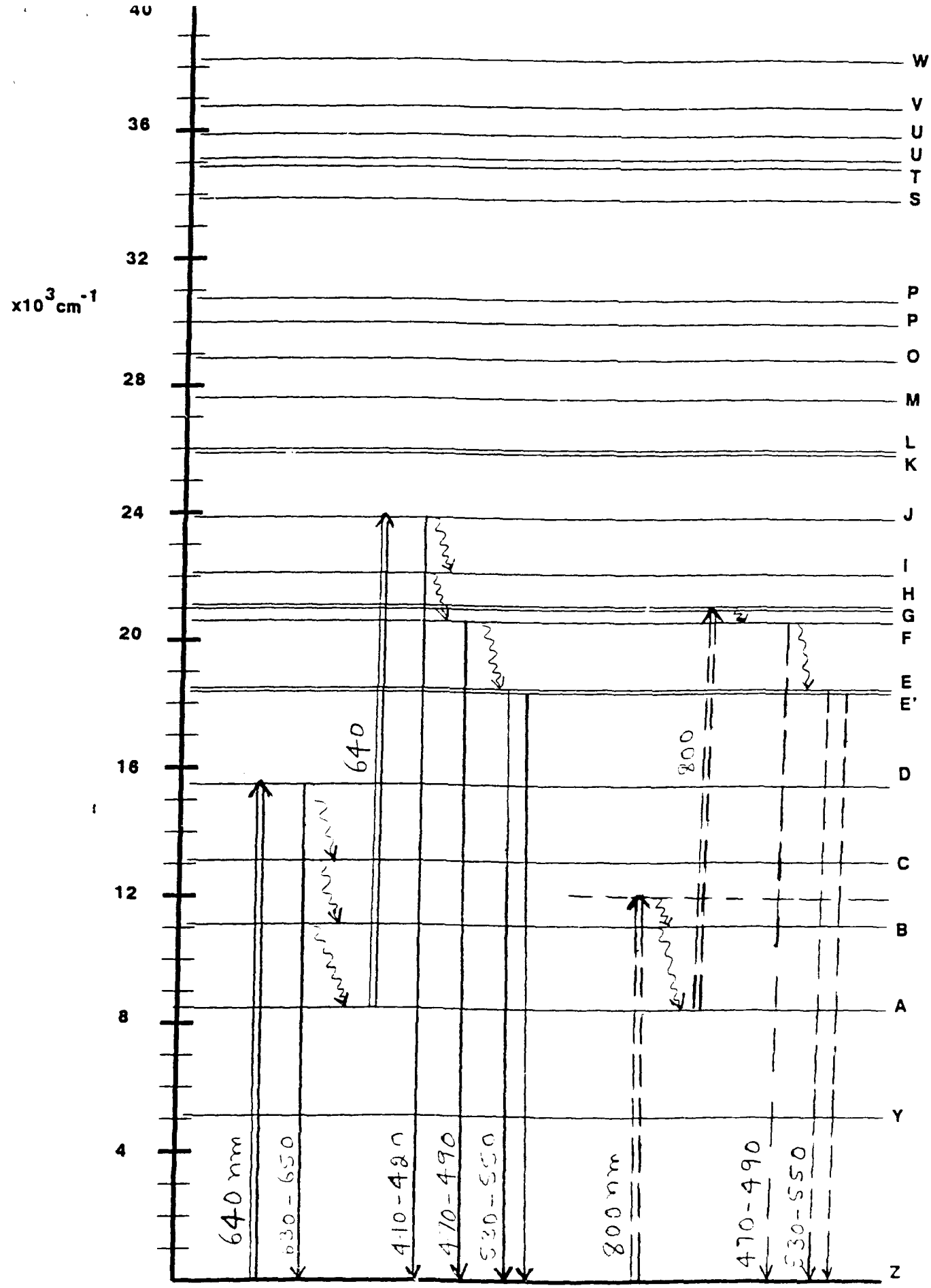
40
36
32
28
24
20
16
12
8
4
x10³cm⁻¹
W
V
U
U
T
S
P
P
O
M
L
K
J
I
H
G
F
E
E'
D
C
B
A
Y
Z
640
800
640 nm
630-650
410-490
410-490
530-550
800 nm
470-490
530-550

References

(1) F. Auzel, Proceedings IEEE 61, 758 (1973).

(2) W. Lenth and R.M. Macfarlane, Optics and Photonics News March 1992, pp8.

(3) M.J. Weber, Phys. Rev. 157, 262 (1967).

(4) R.K. Watts, J. Chem. Phys. 53, 3552 (1970).

(5) R.A. Hewes, J. Luminescence 1-2, 778 (1970).

(6) L.F. Johnsson and H.J. Guggenheim, Appl. Phys. Letts. 19, 44 (1971).

(7) M.A. Chamarro and R. Cases, J. Luminescence 42, 267 (1988).

(8) K. Hirao, S. Kishimoto, K. tanaka, S. Tanabe and N. Soga, J. Non-crystalline Solids 139, 151 (1992).

(9) G.R. Atkins, M.G. Sceats and S.B. Poole, J. Non-crystalline Solids 140, 123 (1992).

(10) S.H. Tang, H.Y. Zhang, M.H. Kuok and S.C. Kee, Physica Status Solidi (b) 168, 351 (1991).

(11) D.N. Rao, J. Prasad, and P.N. Prasad, Phys.Rev.B.28, 20 (1983).

(12) H.H. Caspers, H.E. Rast and J.L. Fry, J. Chem. Phys. 53, 3208 (1970).

(13) M.J. Weber, B.H. Matsinger, V.L. Donlan and G.T. Surratt, J. Chem. Phys. 57, 562 (1972).

Optics Communications 85 (1991) 491–499
North-Holland

OPTICS
COMMUNICATIONS

Full length article

Optogalvanic effect in neon hollow cathode discharge

B.R. Reddy and P. Venkateswarlu
Department of Physics, Alabama A&M University, Normal, AL 35762, USA

Received 22 May 1991

About 300 transitions have been recorded in the optogalvanic spectrum of neon in the visible wavelength region 410–670 nm by axially irradiating a hollow cathode discharge with an excimer pumped dye laser. Several weak lines have been recorded including the 632.8 nm neon laser wavelength. Temporal evolution of the optogalvanic signals was studied at several wavelengths. An explanation is given for the occasional absence of correlation in intensities observed in optogalvanic effect with those measured in emission. An explanation is also given for the voltage dependent polarity changes of optogalvanic signals. Energy transfer collisions were also detected in iron–neon discharge.

1. Introduction

In tunable laser spectroscopy dye laser wavelengths should be measured very accurately. Optogalvanic (OG) effect is a convenient technique in which the accuracy in the estimation of wavelengths is limited by laser linewidths [1–4]. The optogalvanic spectrum is similar to the excitation spectrum and probes the population in the excited levels. The neon atom has dense energy level structure and in a discharge electrons exist in several higher levels, up to an energy ~20 eV [5] and as a result the $1s_n$ levels and to some extent $2p_n$ levels are populated. Hence the OG spectrum resembles the emission spectrum more than the absorption spectrum. Commercial hollow cathode lamps are filled with a buffer gas like neon and hence they are easily available. To calibrate any dye laser wavelength it is useful to have a standard spectrum in the whole visible region. Though the neon spectrum covers the whole visible region it is not clear whether all of it can be excited in OG effect because most of the published work was limited to the wavelength region 565–740 nm [6] and there was no report of the spectrum in the region less than 560 nm except for two photon absorption [7]. There are numerous investigations on the neon OG spectrum but most of them were to understand the effect itself and were limited to the region covered by the Rh6G dye laser. Also there has been some confusion in the assignment of optogalvanic signal polarity/activity [8,9] and it also changed from positive to negative in some cases when the discharge voltage was varied. No signals of the group $2p_n$–$3s_n$ were detected in the past [9]. Some of the strong emission spectral lines were found to be either too weak or absent in OG effect [10]. So we reinvestigated the OG effect in neon to address these problems and recorded about 300 transitions in the region 410–670 nm. A discussion is also presented on the voltage dependent polarity changes of optogalvanic signals and a technique to record a large number of spectral transitions in OG effect is described.

2. Experimental details

Four commercial hollow cathode lamps having B, Fe, Hg or U for cathode element and filled with neon buffer gas were used in this study. An excimer pumped dye laser was used to excite the discharge and a boxcar integrator was used to process the signals. A full description of the experimental details and the wavelength estimation procedures were given elsewhere [4,11].

3. Identification

The ground state configuration of neon atom $1s^2 2s^2 2p^6$ gives the term $^1S_0$. The excited states follow neither *LS* coupling nor *jj* coupling but obey the intermediate coupling suggested by Racah [12]. Under the *jl* coupling scheme the excited configuration $1s^2 2s^2 2p^5 3s$ gives the terms 3s[3/2]2, 3s[3/2]1, 3s'[1/2]1 and 3s'[1/2]0 where the number inside the brackets is one of the vector sum values of the ionic J and l value of the excited electron. A prime is used to identify the terms generated from the ionic J value of 1/2. The spin of the excited electron is coupled with this J value of the ionic core to generate the total J value and is given outside the brackets. In Paschen notation these levels are designated $1s_n$ (where $n=2$–5). Similarly the excited configuration $1s^2 2s^2 2p^5 3p$ generates the terms 3p[5/2]3, 3p[5/2]2, 3p[3/2]2, 3p[3/2]1, 3p[1/2]1, 3p[1/2]0, 3p'[3/2]2, 3p'[3/2]1, 3p'[1/2]1 and 3p'[1/2]0. These levels are termed $2p_n$ (where $n=1$–10) in Paschen notation, and the n value decreases for higher energy levels.

4. Results and discussion

In the absence of laser pulse there exists equilibrium in electron distribution of various levels and a steady discharge current flows. During the laser pulse some of the electrons are transferred to higher levels thus the electronic population deviates temporarily from the steady state equilibrium value. In between laser pulses the electronic population redistributes to reach the steady state value. This affects the ionization rate and hence the discharge current varies. The $1s_2$ and $1s_4$ levels of neon radiate with lifetimes [13] of 2 and 32 ns and $1s_3$ and $1s_5$ are metastable with lifetimes of several seconds [14]. The lifetimes of $2p_n$ levels are $\approx$ 10–25 ns. Normally electrons in the metastable levels tend to get ionized and contribute to the discharge current. When such electrons are excited to higher levels (say $2p_n$) the latter may be strongly radiating. In such a case the electrons which otherwise were contributing to the discharge current are no longer available and hence the discharge current decreases or the discharge impedance/voltage increases. When laser excites electrons from the radiating levels to much higher levels the ionization rate increases because less energy is required to ionize and a large number of electrons have sufficient energy. In such cases the voltage drop across the discharge tube decreases. The maximum voltage change detected by us in OG experiment was < 1 V for a discharge voltage of < 500 V and current of < 10 mA. The electron redistribution process during the absence of laser pulse reflects on the temporal evolution of the OG signal and it has been successfully explained by a rate equation model given by [15]

$$\Delta V(t) = -\text{const.}\,[a_2 \exp(-t/\tau_2) - a_1 \exp(-t/\tau_1)] \qquad (1)$$

where $\Delta V(t)$ is the amplitude of the signal, τ_1 and τ_2 are collisional relaxation times of the levels 1 and 2 coupled by the laser and a_1 and a_2 are their respective ionization rates ($a_2 > a_1$). For $\tau_1 \approx \tau_2$, eq. (1) predicts a negative signal whenever excitation takes place from radiating levels such as $2p_n$ (e.g. 576.5 nm), and the signals lasted for less than 6 μs. For excitation from $1s_n$ ($n=3$, 5), $\tau_1 > \tau_2$, eq. (1) predicts a signal that decreases first and later on increases above the steady state value and finally reaches the equilibrium value in about 100 μs and the length of time depended on the probability of the transition coupled by the laser. The reverse type of situation occurs for excitation from $1s_2$ to $2p_n$ levels (e.g., 585.2 nm connects $1s_2$ to $2p_1$ and is strongly allowed) $\tau_1 < \tau_2$ and population inversion exists between the levels coupled by the laser [11,16]. For a typical pressure of 1 Torr the neon atom concentration is $3.23 \times 10^{16}/\text{cm}^3$. Assuming a discharge temperature of 400 K the collisional interval is about 8.8 ns among neon atoms. The excited electron can also relax among the excited group of levels without radiation, which involves rearrangement of electronic distribution. Only a fraction of them are in the desired excited level and more over every collision need not be effective in energy transfer. Hence there is no surprise in finding the collisional effects after a few microseconds though the laser pulse is in nanoseconds. The concentration of sputtered atoms is several orders less than that of neon and the former also influences the discharge characteristics. Such effects are revealed at longer times in the temporal evolution of OG signals at specific wavelengths. The sig-

nal processing electronics will also introduce distortion in some cases.

About 300 transitions have been recorded in the region 410–670 nm and a majority of them have been identified (see table 1) and all agree within the experimental errors with those listed by Striganov and Sventitskii [17]. In some cases the errors are more than the laser linewidth because of the uncertainties involved in the measurement of spectral positions. The spectrum is mainly due to the following groups $3s \rightarrow 3p$, 4p and $3p \rightarrow ns$, nd where $n > 4$ and ns and np are the excited states of the atomic neon (Racah's notation). Several weak transitions are not included in the table. Ionization potentials of neutral and ionized neon are respectively 21.6 and 41.07 eV. Hence in OG effect ionic transitions are not expected because discharge electrons do not have enough energy to produce doubly ionized neon. But some of the wavelengths are close to the ionic transitions and are identified with an "*". Transitions identified with "**" were observed in two photon measurements in OG effect [7]. Transitions identified with "+" were reported in MIT wavelength tables [18] but not identified. The remainder of the transitions could arise from impurities present in the cathode material and as we are not interested in analyzing them they are not identified.

In wavelength spectral recordings the boxcar gate duration and delay are preset and the laser frequency is tuned to cover the desired region. A typical spectrum is shown in fig. 1 of the region 600–640 nm. The spectrum recorded by Nestor is shown in fig. 1c and in that some peaks point upward and the others downward. Accordingly the wavelengths were characterized to have either positive or negative polarity. In our recordings of the OG spectrum for the same wavelength region all the peaks appeared upward when the gate was delayed to 2.2 μs (fig. 1a). So our measurements contradict the earlier work [8]. To understand this behaviour temporal evolution has been studied for all these transitions. The signal at 630.5 nm is predominantly negative and reached the steady state value in about 10 μs. The signals at 607.5, 609.6, 614.3, 616.5, 621.8, 626.7 and 633.4 nm are initially negative peaking at ~ 2.5 μs, followed by a broad positive signal peaking at ≈ 20 μs and finally reached the steady state value in about 100 μs. Hence when a gate of 0.5 μs in duration was delayed to 3 μs to sample from the negative portion of the OG signal all the peaks appeared downwards (fig. 1b). When the gate was delayed to 22 μs to sample from the positive portion of the signals all of the peaks appeared upwards (fig. 1a). But the signal at 630.5 nm decayed in about 10 μs and hence is absent in fig. 1a. If the gate is delayed to an intermediate value of, say ≈ 5 μs some of the peaks would appear upward and some downward similar to the observation made in argon [4] and neon [19]. The spectra recorded by Nestor [8] (see fig. 1c), Bridges [9] and several others are of this kind. Also if the gate is such it samples equal portions of the negative and positive signals then the peak is absent at its expected location though its emission probability is high. When the discharge voltage is increased the negative and positive signals grow unequally and the signals change polarity with the discharge current. A detailed explanation of this effect was given elsewhere [20]. Transition probabilities for 630.5 and 612.8 nm ($1s_4$ to $2p_{5,6}$) are too weak when compared to those of other wavelengths [18]. As a result very few electrons are excited and hence the amplitude of OG signal is small and dies down much faster. The signals having large transition probability lasted for longer time duration. The signals which reach equilibrium much faster than 22 μs (e.g., 630.5 nm) did not appear when the gate was delayed to 22 μs. This clearly shows that OG activity has to be made based on the oscilloscope observation but not on the wavelength spectrum. With one preset value for the gate position it is not possible to record all the spectral lines. To record the missing lines one has to vary the gate delay and repeat the spectral recording. When this approach was used we observed several of the weakest transitions including 632.8 nm laser wavelength in OG effect for the first time (not shown). In our OG spectral recordings the observed signal strengths are proportional to the emission probabilities when the sample gate duration and delay are optimized (and the spectra are corrected for dye laser output power variation) with respect to each transition and of course this procedure is time consuming. This procedure is useful to record the OG spectra of other atoms and molecules.

Table 1
Optogalvanic spectra of neon [a)]

Wavelength (nm)	Spectral transition		Wavelength (nm)	Spectral transition	
	JI coupling	*J–J*		*JI* coupling	*J–J*
413.11	3p[1/2]–7d'[5/2]°	1–2	439.40	3p[5/2]–9d[5/2]°	2–2
416.48	3p[1/2]–8s'[1/2]°	1–1		3p[3/2]–10d'[5/2]°	2–3,2
416.60	3p[1/2]–8s'[1/2]°	1–0	440.28	3p[3/2]–11d[5/2]°	2–3
416.97			441.23	3p[5/2]–10s[3/2]°	2–1
417.14			441.65	3p[5/2]–7d[5/2]°	2–3
417.28	+		442.25	3p[1/2]–6d[3/2]°	1–2
417.44	3p[1/2]–8d[3/2]°	1–2	442.47	3p[1/2]–6d[1/2]°	1–1
417.54	3p[1/2]–8d[1/2]°	1–0	442.77	3p'[3/2]–9d[3/2]°	1–1
	3p[1/2]–8d[1/2]°	1–1	442.91	3p'[1/2]–10d'[5/2]°	1–2
417.94			443.25	3p[5/2]–8d[5/2]°	3–3
418.53			443.38	3p[5/2]–8d[7/2]°	3–4
418.90			444.02	3p[3/2]–10d[5/2]°	2–3
419.20			444.49	3p'[3/2]–9d'[5/2]°	2–2
419.43			445.33	3p[3/2]–9d[5/2]°	1–2
419.78	3p[1/2]–9s[3/2]°	1–2	446.10	3p[5/2]–9s[3/2]°	3–2
419.97	+		446.57	3p[5/2]–8d[5/2]°	2–2
420.25	3p[5/2]–10d'[5/2]°	2–3	446.70	3p[5/2]–8d[7/2]°	2–3
420.57	*		447.52	3p[3/2]–7d[3/2]°	1–1
420.92			447.58	3p[3/2]–7d'[3/2]°	1–2
421.70	*		448.08	3p'[1/2]–9d'[5/2]°	1–2
421.98	*		448.33	3p[1/2]–7s[3/2]°	1–1
422.54	*		448.82	3p[1/2]–7s[3/2]°	1–2
422.80			449.19	3p[5/2]–9s[3/2]°	2–1
423.45				3p[3/2]–5d[5/2]°	2–2,3
423.85			450.02	3p'[3/2]–8d'[3/2]°	1–2
423.97	*		451.15	3p[3/2]–10s[3/2]°	2–2
424.75			451.49	3p[3/2]–7d'[5/2]°	2–3
425.07	*		451.79	3p'[3/2]–8d'[5/2]°	2–3
425.16	3p[5/2]–12d[5/2]°	3–3	452.59	3p[3/2]–8d[5/2]°	1–2
425.74	3p[3/2]–10d'[5/2]°	1–2	452.94	3p[1/2]–8d'[3/2]°	0–1
426.05	3p[5/2]–13s[3/2]°	3–2	453.24	3p'[3/2]–10d[3/2]°	1–1
426.31	3p[5/2]–13d[7/2]°	2–3	453.67	3p[1/2]–5d'[3/2]°	1–1
426.67	3p[1/2]–7d[5/2]°	1–2	453.79	3p[1/2]–5d'[3/2]°	1–2
426.76	3p[1/2]–7d[3/2]°	1–1	453.84	3p[1/2]–5d'[5/2]°	1–2
426.85	3p[1/2]–7d[3/2]°	1–2		3p[5/2]–7d[5/2]°	3–3
427.04	3p[1/2]–7d[1/2]°	1–1	454.05	3p[5/2]–7d[7/2]°	3–4
427.095	3p[1/2]–7d[1/2]°	1–0	455.44	3p'[1/2]–8d'[3/2]°	1–1
427.48	3p[1/2]–6d'[3/2]°	1–1		3p[3/2]–9s[3/2]°	1–2
427.58	3p[1/2]–6d'[3/2]°	1–2	455.53	3p[3/2]–8s'[1/2]°	2–1
427.93	3p[5/2]–11d[7/2]°	3–4,3	456.59	3p[3/2]–8d[5/2]°	2–3
428.31	3p[5/2]–12d[7/2]°	2–3	456.695	3p[3/2]–8d[3/2]°	2–2
428.69			456.79	3p[3/2]–8d[1/2]°	2–1
428.82	3p[5/2]–12s[3/2]°	3–2	457.29	3p[5/2]–7d[5/2]°	2–2
428.97	3p[5/2]–13s[3/2]°	2–1	457.34	3p[5/2]–7d[3/2]°	2–1
429.25	3p[3/2]–10d'[5/2]°	2–2,3	457.50	3p[5/2]–7d[7/2]°	2–3
430.31	3p[1/2]–8s[3/2]°	1–1	458.24	3p[5/2]–8s[3/2]°	3–2
430.39	3p[3/2]–9d'[5/2]°	1–2	460.40	3p'[3/2]–9d[5/2]°	2–3
430.62	3p[1/2]–8s[3/2]°	1–2	460.48	3p'[3/2]–10s[3/2]°	2–3
431.00	3p[5/2]–11d[7/2]°	2–3	460.98	3p'[3/2]–7d'[3/2]°	1–2
431.46	3p[5/2]–10d[7/2]°	3–4,3	461.43	3p[5/2]–8s[3/2]°	2–1
436.19	3p[5/2]–9d[5/2]°	3–3	462.84	3p'[3/2]–7d'[5/2]°	2–2,3
436.01	3p[5/2]–10s[3/2]°	3–2	463.61	3p[3/2]–7d[5/2]°	1–2

Table 1 (continued)

Wavelength (nm)	Spectral transition		Wavelength (nm)	Spectral transition	
	JI coupling	*J–J*		*JI* coupling	*J–J*
463.66	3p[3/2]–7d[3/2]^0	1–1	500.52	3p[3/2]–5d'[5/2]^0	2–3
464.10	3p[1/2]–7d'[3/2]^0	0–1	503.13	3p[5/2]–5d[5/2]^0	3–3
464.63	3p[3/2]–6d'[3/2]^0	1–2	503.61	3p[5/2]–5d[3/2]^0	3–2
465.31	3p'[3/2]–8s'[1/2]^0	1–0	503.77	3p[5/2]–5d[7/2]^0	3–4
465.61	3p[1/2]–6s'[1/2]^0	1–1	504.28	3p'[1/2]–6d[3/2]^0	1–2
466.46	3p'[1/2]–10s[3/2]^0	1–2	507.42	3p[5/2]–5d[5/2]^0	2–2
	3p'[3/2]–8d[3/2]^0	1–1	507.87	3p[5/2]–5d[3/2]^0	2–2
466.72	3p'[1/2]–7d'[5/2]^0	1–2	508.05	3p[5/2]–5d[7/2]^0	2–3
467.13	3p'[3/2]–8s[1/2]^0	2–1	511.39	3p[1/2]–4d'[3/2]^0	1–1
467.88	3p[3/2]–7d[5/2]^0	2–3	511.73	3p[1/2]–4d'[5/2]^0	1–2
468.03	3p[3/2]–7d[7/2]^0	2–3	512.24	3p'[3/2]–5d'[5/2]^0	1–2
468.18	3p'[3/2]–8d[5/2]^0	2–3		3p'[3/2]–5d'[3/2]^0	1–2
468.70	3p[3/2]–6d'[5/2]^0	2–3	514.49	3p'[3/2]–5d'[5/2]^0	2–3
469.86				3p'[3/2]–5d'[3/2]^0	2–2
470.44	3p[1/2]–5d[3/2]^0	1–2	515.65	3p[3/2]–5d[3/2]^0	1–2
471.21	3p[5/2]–6d[5/2]^0	3–3	518.86	3p[5/2]–6s[3/2]^0	3–2
471.53	3p[5/2]–6d[7/2]^0	3–4	519.31	3p'[1/2]–5d'[3/2]^0	1–2
472.23	3p'[1/2]–8d[3/2]^0	1–2	520.35	3p[3/2]–5d[5/2]^0	2–3
472.56	3p[3/2]–8s[3/2]^0	2–2	520.83	3p[3/2]–5d[3/2]^0	2–2
474.27			523.36	3p[5/2]–6s[3/2]^0	2–2
475.25	3p'[1/2]–6d[7/2]^0	2–3	527.62	++	
475.82	3p[3/2]–7s'[7/2]^0	2–1	528.20	++	
477.13			529.82	3p'[3/2]–6s'[1/2]^0	2–1
477.52			530.45	3p[3/2]–6s[3/2]^0	1–1
477.93	3p'[3/2]–7d[5/2]^0	1–2	531.49	3p[1/2]–6s'[1/2]^0	0–1
478.92	3p[5/2]–7s[3/2]^0	3–2	532.32		
479.99	3p'[3/2]–7d[5/2]^0	2–3	532.66	3p[1/2]–4d[3/2]^0	1–1
481.02	3p'[3/2]–6d'[5/2]^0	2–3	533.09	3p[1/2]–4d[3/2]^0	1–2
481.39	3p[1/2]–7d[3/2]^0	0–1	533.35	3p'[3/2]–5d[3/2]^0	1–1
481.76	3p[3/2]–6d[5/2]^0	1–2	534.12	3p[1/2]–4d[1/2]^0	1–1
482.20	3p[5/2]–7s[3/2]^0	2–1	534.34	3p[1/2]–4d[1/2]^0	1–0
482.71	3p[1/2]–6s[3/2]^0	1–1	534.94	3p'[1/2]–6s'[1/2]^0	1–1
483.69	3p[1/2]–6s[3/2]^0	1–2	535.38	3p'[1/2]–6d'[3/2]^0	0–1
484.24	3p'[1/2]–7d[3/2]^0	1–1	535.56	3p'[1/2]–5d[5/2]^0	2–2
	3p'[1/2]–7d[3/2]^0	1–2		3p'[3/2]–5d[5/2]^0	2–3
485.22	3p'[1/2]–6d'[5/2]^0	1–2	536.07	3p[3/2]–6s[3/2]^0	2–1
486.30	3p[3/2]–6d[5/2]^0	2–3	536.22	3p'[3/2]–5d[7/2]^0	2–3
486.54	3p[3/2]–6d[3/2]^0	2–2	536.65	3p'[3/2]–5d[1/2]^0	2–1
488.49	3p'[3/2]–7s'[1/2]^0	2–1	537.23	3p[3/2]–6s[3/2]^0	2–2
	3p[5/2]–5d'[5/2]^0	2–3	537.50	3p[1/2]–5d[3/2]^0	0–1
492.80	3p'[1/2]–7s'[1/2]^0	1–1	538.34	3p[1/2]–5d[1/2]^0	0–1
493.91	3p[3/2]–7s[3/2]^0	2–1	539.41		
494.38	3p[3/2]–7s[3/2]^0	2–2	540.13	3s[3/2]–3p[1/2]^0	1–0
495.61	3p[3/2]–5d'[3/2]^0	1–2	541.02	3p[1/2]–5d[3/2]^0	1–1
496.23			541.26	3p'[1/2]–5d[3/2]^0	1–2
496.67			541.86	3p'[1/2]–5d[1/2]^0	1–1
497.40	3p'[3/2]–6d[5/2]^0	1–2	542.00	3p'[1/2]–5d[1/2]^0	1–0
	3p'[3/2]–6d[3/2]^0	1–1	542.68		
498.93			543.37	3p[1/2]–5s[1/2]^0	1–1
499.48	3p'[3/2]–6d[5/2]^0	2–3	544.14		
499.75	3p'[3/2]–6d[3/2]^0	2–2	545.40		
499.84	3p'[3/2]–6d[7/2]^0	2–3	546.10	Hg	

Table 1 (continued)

Wavelength (nm)	Spectral transition		Wavelength (nm)	Spectral transition	
	jl-coupling	*J*–*J*		*jl*-coupling	*J*–*J*
549.40	3p [3/2]–6s[3/2]^0	1–1	604.14	3p [1/2]–5d[3/2]^0	0–1
551.13	3p[5/2]–4d'[5/2]^0	3–3	606.38	3p[3/2]–5s [1/2]^0	1–0
553.34	3p [3/2]–6s[3/2]^0	2–2	606.91		
553.83	3p[1/2]–6s[3/2]^0	0–1	612.20		
555.61			612.85	3s[3/2]^0–3p [3/2]	1–1
555.89	3p[5/2]–4d'[3/2]^0	2–1	613.03	**	
556.28	3p[5/2]–4d'[5/2]^0	2–3	613.51		
	3p[5/2]–4d'[3/2]^0	2–2	613.78		
558.57	3p [1/2]–6d[3/2]^0	0–1	614.01	**	
558.93	3p [1/2]–6s[3/2]^0	1–2	614.31	3s[3/2]^0–3p[3/2]	2–2
565.25	3p[3/2]–4d'[3/2]^0	1–1	614.73		
565.65	3p[3/2]–4d'[5/2]^0	1–2	615.22		
566.26	3p[1/2]–5s[3/2]^0	1–1	615.55	3p [3/2]–4d[3/2]^0	1–2
568.50	3p [1/2]–7s[3/2]^0	0–1	616.05		
568.98	3p[1/2]–5s[3/2]^0	1–2	616.37	3s [1/2]–3p [1/2]^0	0–1
571.53	3p[3/2]–4d'[3/2]^0	2–1	616.59		
571.93	3p[3/2]–4d'[5/2]^0	2–3	617.18	+	
574.87	3p[5/2]–4d[5/2]^0	3–3	617.45	3p [3/2]–4d[5/2]^0	2–3
	3p[5/2]–4d[5/2]^0	3–2	617.54	3p [3/2]–4d[5/2]^0	2–2
576.05	3p[5/2]–4d[3/2]^0	3–2	618.22	3p[5/2]–5S[3/2]^0	3–2
576.47	3p[5/2]–4d[7/2]^0	3–4	618.31	3p [3/2]–4d[3/2]^0	2–1
577.04	3p [1/2]–5d'[3/2]^0	0–1	618.89	3p [3/2]–4d[3/2]^0	2–2
580.46	3p[5/2]–4d[5/2]^0	2–3	619.28	3p [3/2]–4d[7/2]^0	2–3
	3p[5/2]–4d[5/2]^0	2–2	620.30	3p [3/2]–4d[1/2]^0	2–1
581.17	3p[5/2]–4d[3/2]^0	2–1	620.41	**	
581.64	3p[5/2]–4d[3/2]^0	2–2	620.57	3p[1/2]–4d[3/2]^0	0–1
582.05	3p[5/2]–4d[7/2]^0	2–3	621.73	3s[3/2]^0–3p[3/2]	2–1
582.88	3p[5/2]–4d[1/2]^0	2–1	622.04		
585.24	3s'[1/2]^0–3p [1/2]	1–0	622.57	3p[1/2]–4d[1/2]^0	0–1
586.83	3p'[3/2]–4d'[3/2]^0	1–1	624.65	3p[5/2]–5s[3/2]^0	2–2
587.20	3p'[3/2]–4d'[3/2]^0	1–2	624.96	3p [1/2]–6s[3/2]^0	0–1
587.28	3p'[3/2]–4d'[5/2]^0	1–2	625.52		
588.23	3s[3/2]^0–3p'[1/2]	2–1	626.34		
589.85	3p [3/2]–4d'[3/2]^0	2–1	626.64	3s [1/2]–3p [3/2]^0	0–1
590.31	3p'[3/2]–4d'[5/2]^0	2–3	627.04		
590.64	3p[3/2]–4d[5/2]^0	1–2	627.59	3p [1/2]–4d[1/2]^0	1–0
591.37	3p[3/2]–4d[3/2]^0	1–1	629.01		
591.90	3p[1/2]–4d'[3/2]^0	0–1	629.38	3p [3/2]–5s [1/2]^0	1–1
592.12	3p[3/2]–4d[7/2]^0	1–3	630.19		
592.35	+		630.47	3s[3/2]^0–3p[3/2]	1–2
593.44	3p[3/2]–4d[3/2]^0	1–0	630.73		
593.94	3p[5/2]–5s'[1/2]^0	2–1	632.82	3p [3/2]–5s [1/2]^0	2–1
594.56	3s[3/2]^0–3p'[3/2]	2–2	633.12	3p[3/2]–3s[1/2]^0	1–1
596.17	3p [1/2]–4d'[3/2]^0	1–1	633.44	3s[3/2]^0–3p[5/2]	2–2
596.62	3p'[1/2]–4d'[5/2]^0	1–2	638.30	3s[3/2]^0–3p[3/2]	1–1
597.46	3p[3/2]–4d[5/2]^0	2–3	640.21	3s[3/2]^0–3p[5/2]	2–3
597.57	3s[3/2]–3p'[3/2]^0	2–1	650.70	3s[3/2]^0–3p[5/2]	1–2
598.23	3p[3/2]–4d[3/2]^0	2–1	653.29	3s [1/2]^0–3p [3/2]	0–1
598.79	3p[3/2]–4d[3/2]^0	2–2	659.97	3s [1/2]^0–3p [1/2]	1–1
599.16	3p[3/2]–4d[7/2]^0	2–3	671.82	3s [1/2]^0–3p [3/2]	1–1

a) Symbols: + neon wavelengths listed in ref. [20] but not identified. * wavelengths match with neon ionic transitions but they are not expected to occur. **Two photon absorption wavelengths reported in ref. [7]. + + closer to neon wavelengths but not very accurate.

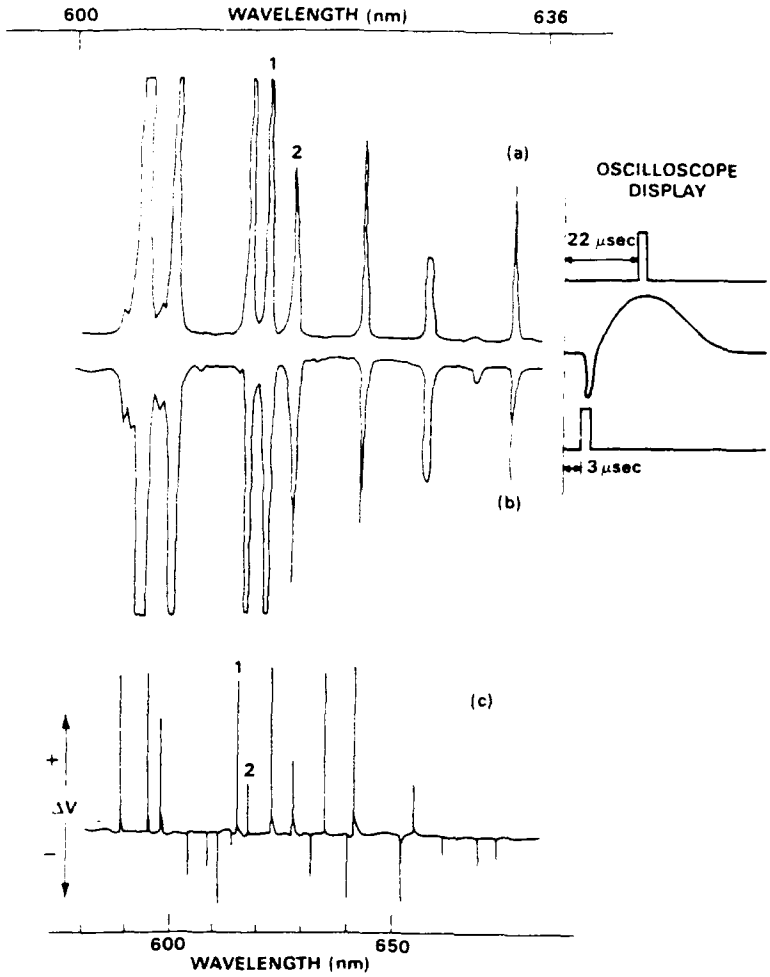

Fig. 1. Optogalvanic spectrum of neon in the wavelength region 610–640 nm obtained for a gate delay of (a) 22 μs and (b) 3 μs and (c) OG spectrum recorded by Nestor [8] in the same region. For comparison two peaks are identified with 1 and 2 in (a) and (c).

5. Energy transfer collisions

A major factor contributing to the discharge current is ionization of the buffer gas atoms by electron impact and collisions among the excited atoms. In addition some positively charged ions collide with the cathode surface and liberate atoms which form minor constituents of the discharge species. Some of the excited buffer gas atoms may collide with the sputtered atoms and cause further ionization [21] as

$$Ne^* + M \rightarrow Ne + M^+ + e^- ,$$

Penning ionization , (2)

where M represents the sputtered atoms. Penning ionization as well as buffer gas ionization take place at all currents. Since the electron concentration is much larger than that of sputtered atoms the effect of eq. (2) is not noticed in general at high discharge currents. An understanding of such phenomenon requires the study of temporal variation of OG signals. We have systematically recorded the temporal evolution of OG signals by tuning laser wavelength to excite several atomic transitions of Ne in Hg–Ne, U–Ne, B–Ne and Fe–Ne discharges. All the observed signals are in accordance with eq. (1). The signal at

428.97 nm exhibited unusual behaviour as shown in fig.2. This wavelength resonantly excites 3p[2 1/2]2→13s[1 1/2]1 transition of Ne (Racah's notation) and both the levels are radiatively coupled with the lower energy levels. Hence the temporal evolution of the signal is expected to be negative as was observed in Hg–Ne, U–Ne, and B–Ne discharges. However the signal in Fe–Ne discharge exhibited anomalous behaviour. The signal amplitude first decreases (negative) as expected and then rises above the steady state value (positive) and finally reaches the equilibrium value after 33 μs, whose explanation is given below. When a laser excites electrons to higher levels the ionization energy decreases and it is easier for a large number of electrons to ionize neon atoms. As a result momentarily the discharge current increases first or the voltage across the discharge tube decreases reaching the peak/minimum value at about 2 μs. At a later time the voltage across the discharge tube increases because of penning ionization effects. That is, in Fe–Ne discharge sputtered Fe atoms also contribute to the discharge current. A close examination of the energy levels of neon and iron [22] reveals a resonance in energy between the excited neon levels 3p[2 1/2]2 and the ionic levels of Fe (fig. 3). That is in the absence of laser radiation the excited neon atoms directly collide with ground state iron atoms and excited them to their ionic levels at 149 604 and 149 896 cm^{-1} of the configuration $3d^6(^5D)4d(J=7/2, 9/2)$. This process also contributes to the discharge current and is expressed as

$$Ne(3p[2\,1/2]2)+Fe(^5D_4)\rightarrow Ne(^1S_0)+Fe^+3d^6(^5D)4d(J=7/2, 9/2)+e^-+\Delta E, \quad (3)$$

where $\Delta E=(182, 110\ cm^{-1})$ is the mismatch in energy and is within the thermal energy kT which is ascribed to the translational energy of the colliding particles. Such energy transfer collisions are efficient whenever the mismatch in energy is less. We did not find such matching between this excited energy level of Ne and with that of any other atom B/U/Hg. The laser pulse of 428.97 nm resonantly excites electrons from 3p[2 1/2]2 level of neon to higher levels. When

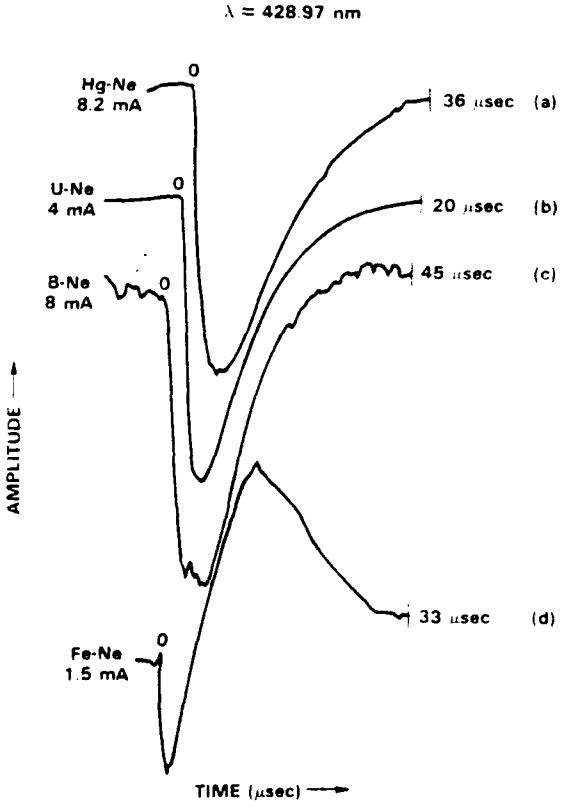

Fig. 2. Temporal evolution of neon optogalvanic signal at 428.97 nm obtained in different discharges.

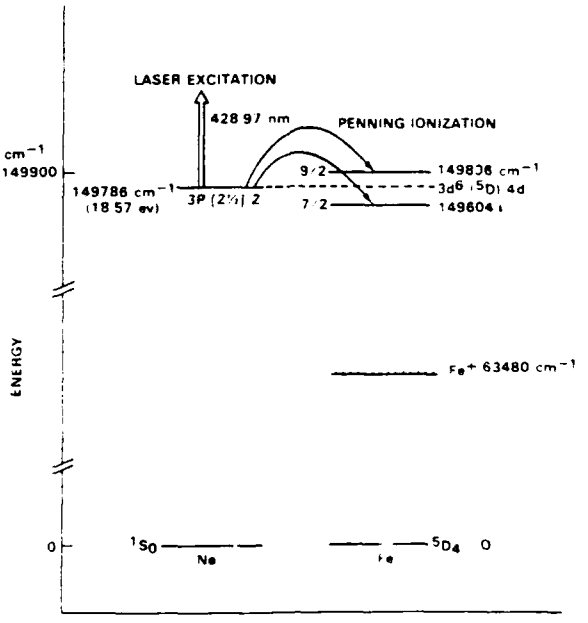

Fig. 3. Partial energy level diagram of Fe, Fe^+ and Ne atoms.

electrons from this level (which otherwise were used to ionize iron atoms) are excited to higher levels these electrons are no longer available to ionize iron atoms. Hence the discharge current decreases or the voltage across the discharge tube increases after 5 μs. This explains why the time dependence of OG signal in Fe–Ne discharge is different from that observed in Hg–Ne, U–Ne and B–Ne discharges. Our observation clearly suggests that penning ionization is not limited to metastable levels alone and in fact depends on the resonance in energy levels of the colliding particles. Similar interactions were observed in other systems also [23,24].

Acknowledgement

This work was supported by DOE grant No. DE-FG05-84ER13206, AIR FORCE grant No. AFOSR-90-0160 and NASA grant No. NAG8-107.

References

[1] D.S. King, P.K. Schenck, K.C. Smyth and J.C. Travis, Appl. Optics 16 (1977) 2617.
[2] B.A. Palmer, R. Engleman Jr. and R.A. Keller, An atlas of uranium emission intensities in a hollow cathode discharge, LASL report LA-8251-MS.
[3] F. Babin, P. Camus, J-M. Gagne, P. Pillet and J. Boulmer, Optics Lett. 12 (1987) 468.
[4] B.R. Reddy, P. Venkateswarlu and M.C. George, Optics Comm. 75 (1990) 267.
[5] M.G. Drouet and J.P. Novak, Phys. Lett. A 34 (1971) 199.
[6] E.F. Zalewski, R.A. Keller and R. Engleman Jr., J. Chem Phys. 70 (1979) 1015.
[7] G.A. Bickel and K.K. Innes, Appl. Optics 24 (1985) 3620.
[8] J.R. Nestor, Appl. Optics 21 (1982) 4154.
[9] W.B. Bridges, J. Opt. Soc. Am. 68 (1978) 352.
[10] R.A. Keller, R. Engleman Jr. and B.A. Palmer, Appl. Optics 19 (1980) 836.
[11] B.R. Reddy, P. Venkateswarlu, and M.C. George, Optics Comm. 73 (1989) 117.
[12] G. Racah, Phys. Rev. 61 (1942) 537.
[13] F.A. Sharpton, R.M. St. John, C.C. Lin and F.E. Fajen, Phys. Rev. A 2 (1970) 1305.
[14] N.E. Small-Warren and L.Y.C. Chiu, Phys. Rev. A 11 (1975) 1777.
[15] G. Erez, S. Lavi and E. Miron, IEEE J. Quant. Electron QE-15 (1979) 1328.
[16] A. Ben-Amar, G. Erez and R. Shuker, J. Appl. Phys. 54 (1983) 3688.
[17] A.R. Striganov and N.S. Sventitskii, Tables of spectral lines of neutral and ionized atoms (Plenum, New York, 1968).
[18] Wavelength by element, MIT Wavelength Tables, Vol. 2, (MIT Press, Cambridge 1982).
[19] B.R. Reddy, unpublished data.
[20] B.R. Reddy, P. Venkateswarlu and M.C. George, in Advances in laser science, Vol. 4, eds. J.L. Gole et al. (Am. Inst. Physics, New York, 1989) p. 731.
[21] K.C. Smith, B.L. Bentz, C.G. Bruhn and W.W. Harrison, J. Am. Chem. Soc. 101 (1979) 797.
[22] C. Corliss and J. Sugar, J. Phys. Chem. Ref. Data 11 (1982) 138.
[23] A. Ben-Amar, R. Shuker, G. Erez and E. Miron, Appl. Phys. Lett. 38 (1981) 763.
[24] A. Ben-Amar, G. Erez, S. Fastig and R. Shuker, Appl. Optics 24 (1984) 4529.